eman ta zabal zazu

Universidad del País Vasco

Euskal Herriko Unibertsitatea

Physics of Nanostructures and Advanced Materials

Nanoscale Engineering Omniphobic Surfaces

Ph D. Thesis

Marta Fenero Bisquer

San Sebastián-Donostia, 2020

Dr. Jesús Palenzuela

Prof. Mato Knez

eman ta zabal zazu

Universidad del País Vasco

Euskal Herriko Unibertsitatea

Physics of Nanostructures and Advanced Materials

Nanoscale Engineering Omniphobic Surfaces

Ph D. Thesis

Marta Fenero Bisquer

San Sebastián-Donostia, 2020

Dr. Jesús Palenzuela

Prof. Mato Knez

This PhD thesis has been carried out at:

CIDETEC Surface engineering

CIC nanoGUNE
Nanomaterials group

A mis padres.

A nene.

Agradecimientos

"Cualesquiera que hayan sido nuestros logros,
alguien nos ayudó siempre a alcanzarlos".
Althea Gibson.

Quiero aprovechar estas líneas para mostrar mi agradecimiento a todas aquellas personas e instituciones que de una forma u otra me han ayudado a lo largo de toda esta etapa.

En primer lugar, quiero agradecer a CIDETEC la oportunidad que me ofreció para desarrollar esta tesis en su organización. Jesús, Ramón, gracias por confiar en mí desde el inicio, cuando no me conocíais. Ver cómo levantabais desde abajo una línea nueva y hasta dónde habéis llevado las *superficies omnifóbicas* ha sido el aprendizaje que jamás imaginé. Gracias por hacerme partícipe de este proyecto.

A mis directores, Dr. Jesús Palenzuela y *Prof.* Mato Knez, les estaré siempre profundamente agradecida. Dos grandes científicos. Dos grandes personas que me han dado todo cuanto he necesitado en estos años.
Jesús, gracias por tu tiempo, dedicación e infinita paciencia. Gracias por tu guía, por tus valiosas enseñanzas, por tu apoyo constante. Este año ha sido muy complicado y, sin ti, no sé si habría llegado al final. Espero no haber consumido toda tu energía y seguir aprendiendo de ti cada día.
Mato, I am very grateful to you for your kind support. I appreciate the time you have dedicated to me. Some interesting ideas have fallen by the wayside. I hope that in the future we can do it.

Ramón, gracias por todo lo que me has aportado. Ha sido mucho. Es un privilegio que tu mano esté detrás de toda esta historia. En la sombra, pero esta tesis, también es tuya.

Quiero agradecer a nanoGUNE por haberme ofrecido sus instalaciones y equipamiento durante estos años. Gracias al grupo del *Prof.* Mato Knez, en especial a Itxasne Azpitarte y Oksana Yurkevich. Thank you for your work, dedication and valuable time spent on sheet resistance measurements.

I would like to thank *Prof.* Petravic and Iva Saric from University of Rijeka for the XPS measurements, and also for the invaluable discussion of the results.

Gracias a Ángel Alegría, director del programa, por resolver todas mis dudas administrativas.

A mis compañeros de CIDETEC. A los de ACNS y a los de otros ámbitos por todos los momentos compartidos. Especialmente a aquellos con los que he tenido la suerte de trabajar de forma más estrecha durante estos años. Eneko, gracias por tu simpatía y amabilidad guiando mis primeros pasos en la casa. Sandra, ¡cuántas tomas falsas compartidas cuando todo esto comenzaba! Iñaki, ¡cuánto nos unió la *fobicidad burgalesa*!, ¡qué paradoja! Gracias por aportar oxígeno a esos bidones, por compartir conmigo tu *visión industrial*, por romper parte de mis

ilusiones mostrándome la realidad y, por todo lo que me has dado fuera. Ivet, *¿qué es lo que tengo?* La suerte de conocerte. *¿Qué es lo que quiero?* Que estés siempre. Gracias por todo lo que me has enseñado. Tu conocimiento, dedicación y paciencia (que tantas veces he llevado al límite) me han permitido conocer mejor las superficies.
A las *calaveras poliméricas*, por hacer del trabajo diario algo más que una rutina.
Al grupo del café. Jesús, Ana (¡qué alegría me llevé al conocer que corría sangre maña por el grupo!), Virginia, Juanan, Estitxu, Yolanda, Yahira, Lorena, Antton, gracias por esos ratitos de desconexión. Espero el regreso de esas convocatorias estelares.
Aloña, Germán y Lorena, gracias por vuestras palabras de ánimo y vuestra ayuda cuando la he necesitado.

No me quiero olvidar de quiénes me formaron, la Universidad de Zaragoza y el Instituto de Nanociencia de Aragón. Gracias al grupo PLATON y sus PLATONES. Especialmente, a Nacho, Pilar y Santy por darme lo más difícil. La primera oportunidad. Y, por *anclar* los pilares sobre los que construir mi carrera. ¡Gracias, chicos!

Al pádel Drive OT y, a Saray y Nagore por hacer del tercer tiempo lo mejor de los martes.

A las chesas. A las mañas. Gracias por vuestra amistad. Lur, Sari, gracias por vuestro apoyo incondicional. Por tantos años juntas.

Calleji, esta aventura donostiarra no habría sido lo mismo sin ti. Gracias por todo lo que hemos compartido. Gracias por formar parte de mi vida.

Gracias a mi familia. Especialmente a mis padres y hermano, por su constante apoyo, comprensión y cariño. Gracias papá, gracias mamá, por el esfuerzo que habéis hecho siempre para que tuviéramos todas las oportunidades. Por creer siempre en los caminos que emprendemos. A vosotros os debemos todo lo que somos. Gracias, *nene*, por enseñarme desde tan pequeñito cómo se recorre el camino hacia los sueños.

Marta Fenero Bisquer
San Sebastián-Donostia, 2020

Table of contents

List of figures

List of tables

Glossary

Resumen

La primera interacción que un material establece con el entorno se produce a través de su superficie, confiriendo ésta la mayor parte de las propiedades del material. Dado que muchos procesos físico-químicos ocurren en la capa más externa de los materiales, las superficies tienen un gran impacto en nuestra vida diaria. Fenómenos tan cotidianos como la corrosión, la adhesión, la mojabilidad, la fricción o el desgaste tienen lugar en la superficie.[a] Además, las superficies desempeñan una función fundamental en muchos procesos catalíticos[b] y, un gran número de superficies biológicas están implicadas en procesos esenciales para la vida.[c] Todo esto es debido a la gran reactividad de algunas de estas superficies, capaces de desencadenar procesos complejos e incontrolables, a la vez que ofrecen un potencial enorme en el diseño de superficies a medida que den respuesta a las necesidades específicas de cada problema.

En general, la elección de un material u otro se basa en las propiedades internas de los mismos, independientemente de la aplicación que vaya a tener el producto final. Sin embargo, las propiedades superficiales con frecuencia no satisfacen el comportamiento requerido para la aplicación deseada. El recubrimiento de la superficie de un material mediante la fabricación de películas delgadas constituye una estrategia muy interesante para mejorar sus propiedades, así como para otorgar nuevas funcionalidades sin renunciar a las propiedades estructurales que aporta la naturaleza intrínseca del mismo. El diseño de superficies así como de sus propiedades superficiales, no sólo está desempeñando un papel fundamental en el desarrollo de nuevas tecnologías con gran impacto en numerosos sectores, sino que también se visualiza como un actor principal en tecnologías disruptivas del futuro.

Las superficies expuestas al ambiente presentan una gran tendencia a atraer y acumular suciedad suponiendo un impacto negativo en numerosas aplicaciones debido a que pueden generar importantes riesgos para la seguridad y la salud, así como, afectar negativamente al rendimiento, haciendo necesarias costosas operaciones de mantenimiento.[d] En este contexto, la industria tiene un gran interés en el desarrollo de

nuevas soluciones repelentes capaces de preservar limpias las superficies de los materiales, que permitan superar los problemas actuales asociados a la contaminación superficial mencionados anteriormente.

Dos de las fuentes de suciedad más relevantes involucradas en la contaminación superficial son los líquidos y las partículas sólidas. Por ello, en los últimos años se han dedicado muchos esfuerzos al desarrollo de superficies de baja adhesión capaces de repeler estas sustancias.

Las propiedades de mojabilidad de un material proporcionan información muy valiosa sobre la afinidad y las interacciones que se establecen entre un líquido y una superficie sólida, así como, acerca de la adhesión de partículas sólidas sobre la misma. La mojabilidad de una superficie viene determinada por su energía libre superficial y puede ser cuantificada mediante medidas del ángulo de contacto (AC) entre una gota de un líquido y una superficie. El AC se define como el ángulo formado entre la superficie del sólido y la interfase líquido-vapor de la gota (**Figura 1**).[e]

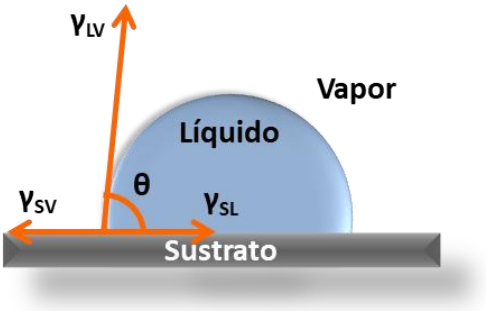

Figura 1. Ángulo de contacto (θ) de una gota de agua sobre la superficie de un sustrato sólido mostrando la tensión superficial de las tres interfases.

En función de su mojabilidad frente a agua o líquidos de baja tensión superficial (hexadecano, diiodometano, aceites,…), los materiales pueden clasificarse en cuatro estados representados en la **Figura 2**: 1). Superhidro(oleo)fílicos: con AC inferiores a 10°; 2). Hidro(oleo)fílicos: con AC entre 10° y 90°; 3). Hidro(oleo)fóbicos: con AC comprendidos entre 90° y 150° y, 4). Superhidro(oleo)fóbicos: con AC superiores a 150°. De igual forma, los materiales que presentan el mismo comportamiento tanto frente al agua, como a

líquidos de baja tensión superficial, se denominan: superomnifílicos, omnifílicos, omnifóbicos o superomnifóbicos, respectivamente.

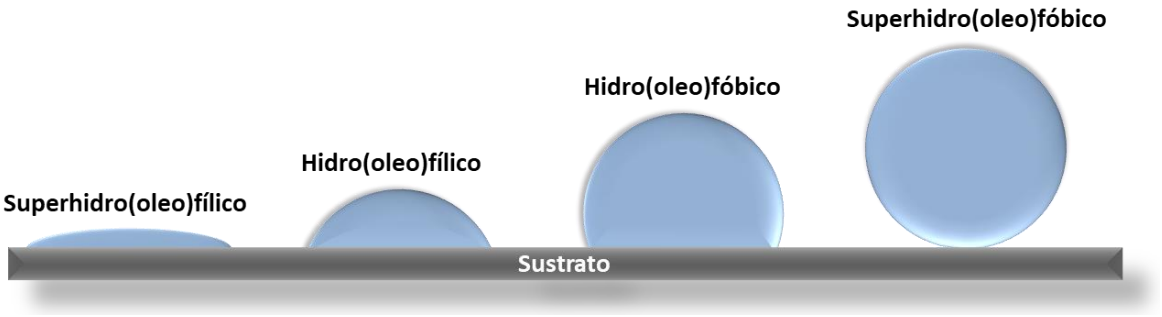

Figura 2. Representación de los distintos estados de mojabilidad.

Tradicionalmente, las superficies repelentes se han obtenido mediante el efecto de la superhidrofobicidad que combina superficies rugosas con motivos micro/nanoestructurados y compuestos de baja energía superficial. Esta aproximación está basada en el conocido efecto de la flor de loto,[f] en el que la repelencia surge del contacto mínimo que se establece entre una gota de agua y la superficie rugosa, disminuyendo así, la adhesión y permitiéndole rodar con facilidad sobre la superficie. A pesar de la gran capacidad de repelencia al agua que poseen, este tipo de superficies presentan una serie de problemas inherentes que limitan su aplicación, entre los que se encuentran la ineficacia para repeler líquidos de baja energía superficial, que pueden llegar a expandirse por toda la superficie y la fragilidad de las micro/nanoestructuras, cuya destrucción conlleva la pérdida de las propiedades de repelencia. Con el propósito de superar las limitaciones de las superficies superhidrofóbicas, el grupo de J. Aizenberg desarrolló en 2011 una nueva tecnología basada en superficies porosas impregnadas por un líquido lubricante (Slippery Liquid Infused Porous Surfaces, SLIPS).[g] En este caso, el efecto de repelencia está inspirado en la planta *Nephenthes*. En general, el uso de lubricantes líquidos estabilizados dentro de la estructura porosa del material mejora las prestaciones de repelencia del recubrimiento, alcanzando incluso la omnifobicidad, aunque también presenta otro problema importante como es la durabilidad debido a la evaporación de los líquidos lubricantes. Actualmente, una de las soluciones que se proponen para solventar la problemática de la evaporación es el uso de lubricantes anclados covalentemente a la superficie.[h]

En este contexto, el desarrollo de recubrimientos omnifóbicos de baja adhesión que sean durables ha despertado un enorme interés en los últimos años debido al gran impacto que presentan las superficies repelentes en la ciencia y la tecnología, con múltiples aplicaciones en sectores muy diversos.

Esta tesis nace con el propósito de desarrollar nuevas estrategias para la obtención de superficies repelentes, focalizando el trabajo en alcanzar soluciones robustas con buenas prestaciones de durabilidad que sean capaces de responder a varias fuentes de contaminación simultáneamente. Para ello, el potencial que ofrece la nanotecnología se utiliza desde dos aproximaciones diferentes: 1) a través de la estructuración de las superficies generando una morfología micro/nanoestructurada que proporciona las propiedades deseadas gracias al control en la nanoescala (**capítulo 3**) y, 2) mediante la incorporación de nanoobjetos como vehículos para introducir nuevas funcionalidades en una solución única (**capítulos 4** y **5**). El objetivo final de estas dos estrategias es el desarrollo de superficies omnifóbicas con propiedades diseñadas a medida que den respuesta a las necesidades de la industria y a las demandas del mercado.

Siguiendo la estrategia para obtener omnifobicidad utilizando el control de la morfología, en el **capítulo 3** se desarrollan superficies de aluminio omnifóbicas demostrando el potencial de la estructuración superficial en la obtención de propiedades de fácil limpieza y anti-hielo (**Figura 3**). Esta estrategia combina un ataque químico con la modificación superficial del aluminio. En una primera etapa, se crea una micro/nanoestructura jerárquica mediante un ataque químico utilizando cloruro férrico. Posteriormente, se ancla un perfluoropoliéter sobre la superficie, disminuyendo la energía libre superficial y proporcionando un sistema omnifóbico con baja afinidad hacia los líquidos. De hecho, la superficie muestra propiedades superhidrofóbicas con un AC al agua de 160° y notables propiedades oleofóbicas con un AC al hexadecano de 141°. Además, estas superficies omnifóbicas retrasan significativamente el tiempo de congelación de una gota de agua hasta los 5100 segundos, que es 20 veces superior al tiempo de congelación sobre el aluminio prístino (260 segundos) e inhiben la formación de hielo a partir de gotas individuales que llegan a la superficie repeliéndolas antes de

que se inicie el proceso de nucleación. Por otra parte, la capacidad para repeler líquidos de cualquier naturaleza revela el carácter de fácil limpieza que poseen estas superficies. Estos resultados alcanzados mediante un proceso económico y fácilmente escalable sitúan esta estrategia como una prometedora solución en aplicaciones que demanden propiedades de fácil limpieza y anti-hielo.

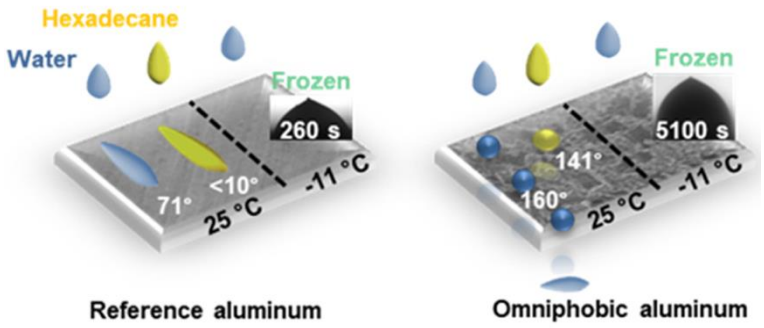

Figura 3. Representación de las superficies de aluminio prístino y omnifóbico mostrando sus propiedades de repelencia a líquidos y su capacidad anti-hielo.

En el **capítulo 4**, se reporta una estrategia novedosa para el desarrollo de superficies multifuncionales basada en la incorporación de nanopartículas como vectores para lograr superficies de fácil limpieza combinando propiedades omnifóbicas y antiestáticas. Nanopartículas de laponitas, cuya conductividad intrínseca tiene la capacidad de reducir las cargas electrostáticas de una superficie y, por tanto, evitar la acumulación de partículas de polvo, se funcionalizan con un compuesto perfluorado de baja energía superficial obteniendo una dispersión omnifóbica. La mezcla de laponitas funcionalizadas y sin funcionalizar en proporciones adecuadas permite obtener recubrimientos multifuncionales como solución holística de fácil limpieza evitando la contaminación superficial tanto por líquidos como por partículas sólidas (**Figura 4**). Esta estrategia supera la aproximación tradicional de las superficies omnifóbicas que sólo muestran propiedades de repelencia frente a líquidos.

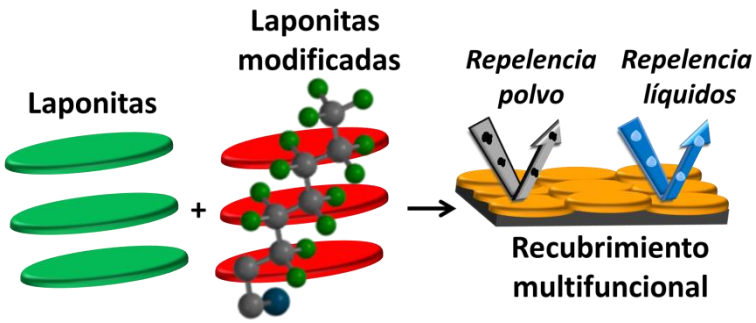

Figura 4. Esquema sobre el proceso de fabricación de recubrimientos multifuncionales combinando laponitas prístinas y laponitas modificadas con un compuesto perfluorado de baja energía superficial.

Inspirados por los recubrimientos multifuncionales desarrollados en el capítulo anterior, en el **capítulo 5**, se persigue mejorar la adhesión del recubrimiento al sustrato con el objetivo de alcanzar soluciones robustas que proporcionen buenas propiedades de durabilidad. Para ello, se aplica una nueva estrategia basada en la funcionalización de las nanopartículas de laponita utilizando un perfluoropoliéter, compuesto de baja energía superficial y que, en este caso particular, contiene un grupo funcional en cada uno de los extremos de su cadena. Esta doble funcionalización le confiere capacidad de anclaje tanto a las partículas de laponita como al sustrato de forma simultánea, mejorando la durabilidad y la resistencia mecánica de los recubrimientos obtenidos. La capacidad de esta nueva tecnología para repeler tanto líquidos como partículas sólidas permite mantener las superficies libres de contaminación reduciendo costes de mantenimiento y preservando el rendimiento óptimo de los materiales.

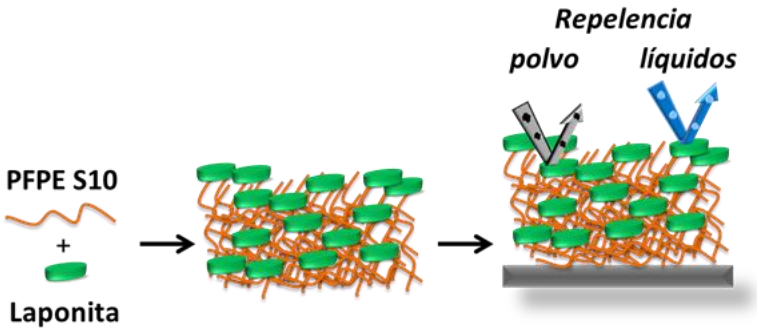

Figura 5. Representación de la estrategia propuesta para la obtención de recubrimientos multifuncionales basada en la funcionalización de laponitas utilizando un perfluoropoliéter con dos grupos funcionales en los extremos de su cadena.

En resumen, esta tesis constituye un avance en el ámbito de las superficies repelentes a través del desarrollo de superficies omnifóbicas novedosas que abren la puerta a la obtención de recubrimientos multifuncionales durables; contribuyendo a la transferencia de soluciones de baja adhesión hacia aplicaciones industriales.

(a) Marshall, S. J.; Bayne, S. C.; Baier, R.; Tomsia, A. P.; Marshall, G. W. A Review of Adhesion Science. *Dent. Mater.* **2010**, *26* (2), e11–e16. https://doi.org/10.1016/j.dental.2009.11.157.

(b) Tao, F. (Feng); Crozier, P. A. Atomic-Scale Observations of Catalyst Structures under Reaction Conditions and during Catalysis. *Chem. Rev.* **2016**, *116* (6), 3487–3539. https://doi.org/10.1021/cr5002657.

(c) Ahmad Khalili, A.; Ahmad, M. R. A Review of Cell Adhesion Studies for Biomedical and Biological Applications. *Int. J. Mol. Sci.* **2015**, *16* (8), 18149–18184. https://doi.org/10.3390/ijms160818149.

(d) Dalili, N.; Edrisy, A.; Carriveau, R. A Review of Surface Engineering Issues Critical to Wind Turbine Performance. *Renew. Sustain. Energy Rev.* **2009**, *13* (2), 428–438. https://doi.org/10.1016/j.rser.2007.11.009.

(e) Young, T. III. An Essay on the Cohesion of Fluids. *Philos. Trans. R. Soc. Lond.* **1805**, *95*, 65–87. https://doi.org/10.1098/rstl.1805.0005.

(f) Barthlott, W.; Neinhuis, C. Purity of the Sacred Lotus, or Escape from Contamination in Biological Surfaces. *Planta* **1997**, *202* (1), 1–8. https://doi.org/10.1007/s004250050096.

(g) Wong, T.-S.; Kang, S. H.; Tang, S. K. Y.; Smythe, E. J.; Hatton, B. D.; Grinthal, A.; Aizenberg, J. Bioinspired Self-Repairing Slippery Surfaces with Pressure-Stable Omniphobicity. *Nature* **2011**, *477* (7365), 443–447. https://doi.org/10.1038/nature10447.

(h) Wang, L.; McCarthy, T. J. Covalently Attached Liquids: Instant Omniphobic Surfaces with Unprecedented Repellency. *Angew. Chem. Int. Ed.* **2016**, *55* (1), 244–248. https://doi.org/10.1002/anie.201509385.

Chapter 1

Introduction

1.1 INTRODUCTION

1.1.1 General perspective of surfaces

Wherever we look, we are surrounded by solid matter. Each time we touch anything, we are interacting with a surface, which defines the boundary between a material and the outer world. Hence, the first interaction that a material establishes with the environment occurs through its surface. If we look in more depth, as far as to the atomic level, we can find that surface atoms have a different surrounding from those in the bulk. While inside of a solid each atom is interacting with neighbouring atoms in all directions, surface atoms are lacking neighbours in at least one direction, thereby exhibiting an excess of energy. This energy excess of the surface atoms of a material compared to that of atoms in the bulk is termed surface free energy (SFE) and it is related to both the strength of the interactions in the bulk, and the surface area exposed to the environment. In other words, surfaces possess a high reactivity as a consequence of their different environment, and this often provides them completely different properties. The great complexity of surfaces was termed by the Nobel Prize winner Wolfgang Pauli with his famous quote “God created solids, but the devil made their surfaces”.

Surfaces have a huge impact in our daily life because most of the physics and chemistry happens there. Common phenomena like corrosion, adhesion, wettability, friction, or wear occur on surfaces.[1,2,3] Catalytic processes happen on surfaces[4,5] and complex biological surfaces are involved in essential processes for human life.[6,7] All of this is due to their extremely high reactivity which, on one hand, triggers a chain of uncontrollable and complex events, and on the other hand, gives us a powerful tool to design surfaces suited to the needs of each specific problem, thereby opening the door to tailoring properties.

In general, materials are selected for their bulk and mechanical properties in view of the application of the end products. However, the surface properties of these materials often do not satisfy the demand by the final application. Surface modification provides an interesting method to protect or to improve the aesthetics of a material, but it also shows enormous potential to confer new functionalities without compromising the structural

properties derived from its intrinsic nature. Currently, engineering the surface properties is playing a key role in the development of new technologies relevant for various sectors ranging from energy conversion[8] to semiconductors[9] or biomedical implants[10,11,12] but also will become a key actor for disruptive technologies in future.

1.1.2 Impact of surface contamination

Surfaces show a great tendency to attract contamination when exposed to environment. Hence, taking into account that surfaces define most of the materials properties (aesthetics, haptics, functionality, etc.), it is not surprising that surface contamination has become a major issue in materials science with a significant economic impact on industry and society. Indeed, the presence and accumulation of fouling agents on solid surfaces implies a huge negative effect on a broad range of applications, as they could lead to significant safety and health risks, have a detrimental impact on performance and therefore high maintenance costs.[13]

The nature of the fouling may be quite different ranging from liquid contaminants to solid particles or biological matter (also known as biofouling). Depending on the environment and the working conditions in which the materials operate, they will be susceptible to one kind of contamination or another. Among liquid contaminants we can find oil residues or fluids like blood, creams and fingerprints, which concern different industrial sectors such as transport, textiles or electronic touch screens;[14,15] while solid fouling includes adhesion of dust particles, ice, clathrates or salts which negatively impact applications such as solar panels,[16] aircraft wings,[17] pipelines,[18,19] or heat exchangers.[20] Moreover, the adhesion of microorganisms, algae or other microscopic living beings is called biofouling and has an enormously negative impact on a broad range of sectors including medical devices,[21] food processing,[22,23] marine vessels[24] and water distribution systems.[25]

Nowadays, surface cleaning has become a routine activity for different sectors ranging from industrial applications to household activities and technological devices. The cleaning processes of surfaces are not only costly and time-consuming, but sometimes are essential to ensure optimum performance of materials. Accordingly, the development of new solutions to preserve clean surfaces has a significant industrial interest to

overcome the current drawbacks associated with surface contamination (i.e. need of maintenance - with consequent costs and loss of time and performance/efficiency).

1.2 REPELLENT SURFACES

Given the steadily rising demand of contamination-free surfaces by a broad range of industrial sectors, along the advent of nanotechnology and its fabrication and characterization techniques over the last decades, the development of repellent surfaces has become a promising strategy to achieve contamination resistant surfaces. The attainment of low adhesion solutions would provide a strong boost for emerging technologies which call for self-cleaning, anti-icing, anti-smudge, antifouling or anti-fingerprint properties.

In this context, enormous research efforts have been devoted over the last years to engineer repellent surfaces capable of reducing or even preventing the adhesion of fouling agents on materials surfaces.

1.2.1 Evolution of repellent surfaces

Repellent surfaces refer to their specific ability to remain uncontaminated by fouling agents. Liquids and solid particles are considered two of the most relevant soiling sources involved in surface contamination, and consequently several strategies have been explored to face the challenge of achieving non-stick surfaces.

In spite of the great amount of different repellent surfaces found in the nature like the leaves of numerous plants,[26,27] shark and springtail skin[28] or butterflies wings[29] and, whilst the concepts behind liquid repellent surfaces (those related to the influence of roughness on wettability properties) were established by Wenzel[30] and Cassie and Baxter[31] in 1936 and 1944 respectively, it was not until 1977 when Barthlott and Ehler, benefiting from the resolution offered by the nascent scanning electron microscopy, formulated the hypothesis that rough repellent surfaces might be providing "self-cleaning" functions.[32] In 1997 the *Lotus-effect* was reported for the first time by Barthlott and Neinhuis, who correlated the microscale papillae and the epicuticular wax on the Lotus leaves with their self-cleaning behaviour. They identified the low surface adhesion

of solid particles on rough surfaces and their water repellence being key aspects for the self-cleaning mechanism (**Figure 1.1**).[27] This discovery triggered the beginning of a relentless search for repellent surfaces. Indeed, much effort and resources have been devoted and currently, repellent surfaces still remain a very active field of research and innovation.

Figure 1.1. Fundamentals of self-cleaning in plants: a rough, hydrophobic surface (left) causes water to form droplets that don´t adhere to the leaf (middle), but remove solid particles while running off of the leaf (right).[33]

Prior to describing the evolution of the state-of-the-art on repellent surfaces, it is important to briefly introduce same definitions and concepts. First of all, it is important to point out that the wetting properties of the materials provide useful information about the affinity and the interactions of a liquid in contact with a solid surface. The wettability of a surface is characterized by the ability of a liquid to spread (or not) when it is placed on its top. This ability should be characterized in terms of the static and the dynamic behaviour of the liquid deposited on the surface. Two important parameters, the contact angle (CA, θ) and the hysteresis contact angle (CAH, θhys), are commonly used to evaluate the static and dynamic wetting properties, respectively. When a droplet of a liquid is resting on a solid surface, the CA is defined as the angle between the tangent to the solid-liquid interface and the solid surface at the three-phase contact line (i.e. where the three phases of the system: liquid, solid and vapor coexist) (**Figure 1.2a**).

On an ideal surface (i.e. completely smooth, rigid, chemically homogeneous and inert), the value of the CA for a contacting liquid is given by the Young equation[34] (**Equation 1.1**):

$$\cos\theta_Y = \frac{\gamma_{SV} - \gamma_{SL}}{\gamma_{LV}}, \qquad \text{(Eq. 1.1)}$$

where γ_{SV}, γ_{LV}, and γ_{SL} are the surface energy of the solid-vapor, liquid-vapor and solid-liquid interfaces, respectively. The surface energy of the solid-vapor interface and the surface energy of the liquid-vapor interface are often referred to as the solid SFE and the liquid surface tension, respectively. According to the Young equation, a droplet of a liquid tends to exhibit lower CA values on a solid with high SFE rather than on a solid with a low SFE.

In contrast to ideal surfaces, real surfaces usually show chemical heterogeneities and roughness, which has to be considered for real applications.[35] These defects result in different CAs from one point of the surface to another.[36] However, they are not observable macroscopically and therefore, the static CA (CA_s) concept, which is defined as the equilibrium CA that the liquid droplet establish with the projection of the surface (observed macroscopically), must be introduced. Owing to the above mentioned defects, real surfaces have a range of stable CAs (also known as hysteresis range). The highest and the lowest CA of the hysteresis range are the advancing CA (ACA, Θ_a) and the receding CA (RCA, Θ_r), respectively. For characterizing the wettability of surfaces, the CAH is defined as the difference between the ACA and the RCA. The CAH provides information about the mobility of a droplet on a surface, since the hysteresis is indicative of the adhesion of the liquid on the surface (i.e. a droplet slides easily on a surface if the CAH is small).[37] There are two commonly used methods for determining the CAH: sessile drop goniometry and tilting plate. With the former method, the ACA and the RCA are determined by increasing and decreasing the volume of the droplet, respectively. Initially, the CA increases as the droplet volume increases and the three-phase contact line remains pinned to the surface until the ACA is reached. A further increase of the droplet volume leads to the motion of the contact line. Similarly, by reducing the volume of the droplet, the CA decreases and the contact line remains pinned until the RCA is reached. A further reduction on the droplet volume results in the receding of the contact line.[38] In the latter method, a droplet is placed on the solid surface and the system is tilted. When the droplet starts sliding, the CA at the front (ACA) and at the back (RCA) of the droplet are determined (**Figure 1.2b**).[39]

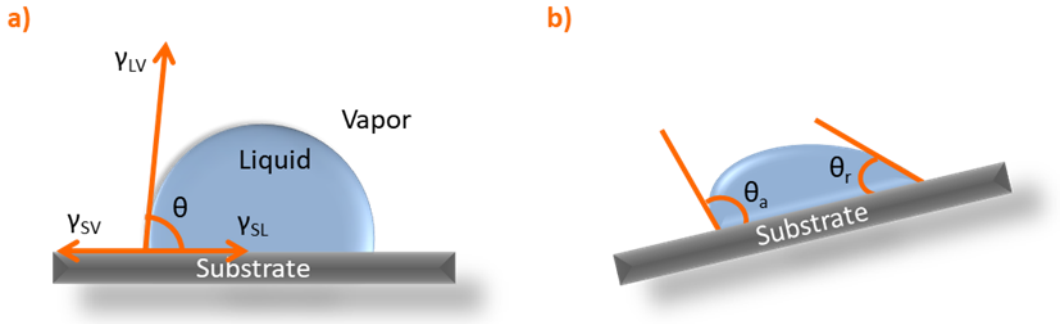

Figure 1.2. Scheme of a) contact angle (θ) of a drop of water on a solid substrate showing the three-phase boundary (adapted from reference [6]) and b) advancing and receding contact angles on a tilted substrate.

In this context and according to the nature of the measuring liquid, materials can be categorized by their wetting properties (defined by their CA_s and CAH) in four types. In the case of water, surfaces can be classified as superhydrophilic if their CA < 10°, hydrophilic if 10° < CA_s < 90°, hydrophobic if 90° < CA_s < 150° and superhydrophobic if CA_s > 150° and CAH < 10°. In the same way, for low surface tension liquids such as aprotic solvents or oils, surfaces are termed as superoleophilic, oleophilic, oleophobic or superoleophobic. And finally, surfaces that display the same behaviour against both, water and low surface tension liquids are called superomniphilic, omniphilic, omniphobic or superomniphobic.

It is important to note that on smooth surfaces the CA values reported for water droplets do not exceed 130°,[40,41] regardless of the chemical nature of the surface (i.e. there is a limit above which the SFE cannot further reduce the wettability of surfaces). Hence, an additional factor, surface roughness, is required for attaining higher CA values. There are two models to describe the influence of the roughness on the wetting behaviour of a liquid droplet onto a solid surface: Wenzel´s[42,43] and Cassie-Baxter´s[44] models, as illustrated in **Figure 1.3**.

The Wenzel´s model describes the wetting when a liquid droplet penetrates the cavities of a rough surface (i.e. there is no entrapped air between the solid and the liquid) (**Figure 1.3a**). In this way, the surface contact area is increased compared to a smooth surface by a factor (r), known as roughness factor and defined as the ratio of the specific area to the

projected area. According to this model, the experimental CA (θ_w) on a rough surface is given by **Equation 1.2**.

$$\cos\theta_w = r\cos\theta_Y \qquad \text{(Eq. 1.2)}$$

Based on this model, a smooth surface with CA greater than 90° will be more hydrophobic as the roughness factor is increased. In contrast, if the CA is less than 90° an increase of the roughness factor reduces the experimental CA, resulting in a more hydrophilic surface. It is noteworthy that a droplet in the Wenzel state is frequently recognized as sticky, since the adhesion between the droplet and the surface is significant, limiting the mobility of the droplet on the surface.

In contrast, in the Cassie-Baxter´s model the droplet does not fill the cavities of the rough surface. An air layer is trapped between the solid and the liquid, minimizing the contact between the liquid and the solid, thereby resulting in two interfaces: solid-liquid and solid-vapor. Thus, the droplet wets only the top of the asperities (**Figure 1.3b**). According to this model, the CA (θ_{CB}) is the result of the contribution of both phases and is given by **Equation 1.3**:

$$\cos\theta_{CB} = f(1+\cos\theta_Y) - 1 \qquad \text{(Eq. 1.3)}$$

where f represents the fraction of the solid surface in contact with the liquid.

It is noted that a droplet in Cassie-Baxter state establishes a minimum contact with the rough surface due to the presence of the air pocket between the solid and the liquid, allowing an easy movement of the droplet over the surface.

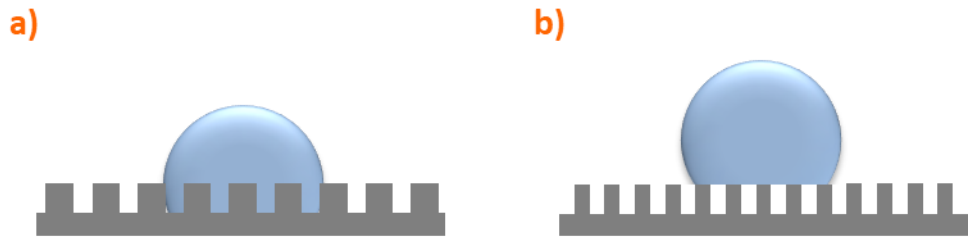

Figure 1.3. Schematic representation of the wetting behavior of rough surfaces according to a) Wenzel´s model and b) Cassie-Baxter´s model.

On the basis of these concepts, considerable research efforts have been devoted to designing and constructing repellent surfaces.

1.2.1.1 Liquid repellent surfaces

Over the last two decades, innovative concepts have been explored in three different directions, with the aim of obtaining liquid repellent surfaces.

1.2.1.1.1 Superhydrophobic surfaces (SHS)

Understanding the principles and mechanisms responsible for the singular wettability of Lotus leaves paved the way for mimicking the *Lotus effect* on synthetic surfaces. This milestone was the starting point for engineering a broad range of repellent surfaces based on hierarchical micro/nanostructures, capable of preserving a trapped air layer between the liquid and the solid, thus minimizing their contact area. Application of low SFE materials was necessary to reduce the chemical affinity between solid and liquid (**Figure 1.4**).

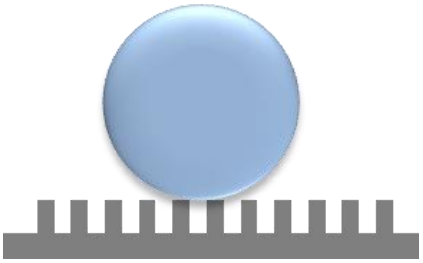

Figure 1.4. Schematics of structured SH surfaces.

Owing to the low contact area between the liquid and the surface, SHS show excellent water repellence as they display both high CA_s and very low CAH. (Note that in case of a high CA and high CAH, a droplet may remain stuck to the surface due to the *petal effect.*[45] Namely, a water droplet experiences strong adhesion on a rose petal surface, preventing its rolling off the surface even if the petal is turned upside down.) This ability to repel water has been largely explored and exploited for different applications including anti-icing,[46,47,48] self-cleaning,[49,50,51] oil-water separation,[52,53,54] anti-corrosion,[55,56] anti-fogging,[57,58] drag reduction[59,60] and anti-fouling.[61,62]

The fabrication of SHS involves creating a hierarchical micro/nanostructure on the material surface which is subsequently modified using a low SFE compound. Sometimes, when the starting material is hydrophobic or the surface roughness is induced by hydrophobic materials, chemical modification of the surface is not required. The desired micro/nanostructuring of the surface can be obtained by top-down or bottom-up approaches.[63] Top-down approaches involve etching (including chemical,[64,65] plasma[66,67] and laser[68,69]), lithography[70,71] and template-based[72] techniques. Bottom-up approaches include chemical, layer by layer[73] and nanoparticles (which could be modified before or during the deposition process)[74,75] deposition and sol-gel methods.[76,77,78] It is also possible to obtain SHS by combining the two approaches.

Currently, fabrication of SHS does not pose any technical problem because the technology is already well established and implemented. However, despite their excellent water repellence, these surfaces present significant inherent problems which restrict their practical application. The ability of SHS to repel liquids is ineffective against low surface tension liquids, which can easily spread along the surface, displacing the entrapped air. Furthermore, these surfaces cannot withstand pressure and liquids can sink into the structured surface, thereby losing its repellent properties. Additionally, the micro/nanostructured motifs required to achieve superhydrophobicity not only affect the material aesthetics, but also lower the mechanical resistance and their damages result in the loss of their repellence.

Several attempts to extend the singular behaviour of SHS to liquids dissimilar to water (i.e. low surface tension liquids such as oils, alcohols and aprotic solvents) have been carried out. It is noteworthy that a specific topography (re-entrant/overhanging structures) in addition to the hierarchical morphology required for SHS has been identified as the key parameter to achieve superomniphobicity.[79] However, these surfaces still suffer from the same drawbacks than SHS (i.e. fragility of morphological and topographical features).

1.2.1.1.2 Slippery Liquid Infused Porous Surfaces (SLIPS)

This liquid repellent technology emerged in 2011 as a new approach to fabricate non-stick surfaces. SLIPS are especially relevant for repelling low surface tension liquids, overcoming some of the limitations of SHS. Inspired by Pitcher plants, such as the Nepenthes plant, whose peristomes possess a micro/nanostructure impregnated by water or nectar that forms a lubricating layer, thereby enabling the slippage of insects into the inside and the bottom of the plant,[80] Aizenberg *et al.* developed the so-called *Slippery Liquid Infused Porous Surfaces.*[81] SLIPS involve a low surface tension lubricant liquid infiltrated into a textured or porous material (**Figure 1.5**). This technology benefits from the mobility of the lubricant phase and the thus obtained extremely smooth and defect free surfaces, resulting in excellent liquid repellent surfaces with very low CAH against low surface tension liquids. In this way, any liquid and fluid can be easily removed from the surface. To obtain a stable system, the lubricant should meet two requirements: 1) It must have a high affinity to the substrate, while repelling liquid or fluid contaminants and 2) it must be immiscible in the contaminant liquid.[81] In recent years, many surfaces with this singular repellence ability have been developed using various methods, because SLIPS have shown potential for omniphobic,[81] anti-icing,[82,83] anti-fouling[84,85,86] or biomedical[87,88] applications. Nevertheless, there are still some limitations on the SLIPS technology that are hindering their practical application at a large scale. The high liquid repellent performance of these surfaces relies on the mobility of their lubricant at the molecular scale, but this mobility has also become its major limitation since the lubricant can be depleted by evaporation processes and/or as a consequence of its interaction with the contaminants, causing a low durability.[89,90] Moreover, the textured or porous structures used to lock the lubricating agent are usually fragile, which restrict their mechanical robustness.

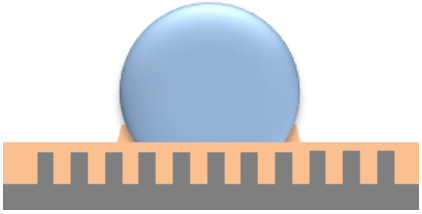

Figure 1.5. Schematics of structured lubricated surfaces (SLIPS).

1.2.1.1.3 Slippery Omniphobic Covalently Attached Liquid (SOCAL)

Recently, a novel type of liquid repellent surface, known as *Slippery Omniphobic Covalently Attached Liquid*, has been introduced by McCarthy´s group.[91] This strategy is based on minimising the hysteresis contact angle using smooth surfaces grafted with flexible molecular chains, which show a liquid-like behaviour due to their freedom to rotate (**Figure 1.6**).[92,93] Similarly to SLIPS, and despite showing only modest CA values, SOCAL surfaces have shown good slippery properties towards many liquids, including those with low surface tension, by taking advantage of the mobility of the grafted molecules which provide the low CAH.[94,95] It should be noted that this approach involves smooth surfaces (i.e. hierarchical structures, susceptible to damage, are not required) and a material providing slippery properties, which is covalently anchored to the substrate. These two aspects make this strategy a promising solution to develop repellent surfaces with enhanced mechanical robustness.

Figure 1.6. Schematics of flat surfaces grafted with liquid-like molecules (SOCAL surfaces).

The SOCAL approach has been studied on smooth surfaces and has not been yet explored in combination with nanostructures. In this way, covalently functionalizing nanostructured surfaces and nanomaterials by grafting molecules, capable of behaving like a liquid, will be one of the technical key aspects explored in this thesis.

1.2.1.2 Solid repellent surfaces

Materials exposed to ambient atmosphere or at their operational environment continuously suffer from contamination by solid particles originating from nature, human activities or the operating process itself in which the material is involved. However, resistance to solid fouling has not been explored so far as deeply as that against liquid contaminants.

To date, three strategies for repelling solid contaminants have been widely explored:

- SHS[96]: solid particles can easily be removed from SHS with rolling off water droplets benefiting from the low adhesion of water droplets to these surfaces.
- Superhydrophilic surfaces[97]: water spreads completely on these type of surfaces creating a thin layer, which can runs off the surface taking away the solid contaminants.
- Photocatalytic (mainly TiO_2-based) surfaces[98,99]: solid organic particles are decomposed by photocatalysis and a water layer formed from impacting water to the surface can wash away the solid debris.

Note, that in all three cases the presence of water is required for removing the contaminant solid particles from the surface.

1.2.2 Challenges of repellent surfaces

The great technological and economic importance of repelling surfaces and the promising results obtained during the last decades made the development of repellent surfaces a multidisciplinary research line of great interest for chemists, physicists, biologists and engineers. A clear indicator for this is the rapid and enormous growth of the number of publications in peer-reviewed journals (**Figure 1.7a**). In addition, it is worth highlighting that this interest is not limited to academic research, but also extends to technological and industrial levels, which is reflected in the increasing number of patents in recent years (**Figure 1.7b**).

However, in spite of the huge effort that has been devoted over the last years towards the development of highly repellent surfaces and the significant progress achieved in this field, current solutions are far from being perfect. Certain challenges still need to be overcome to finally reach the goal of transferring repellent surface technologies from laboratories to the market.

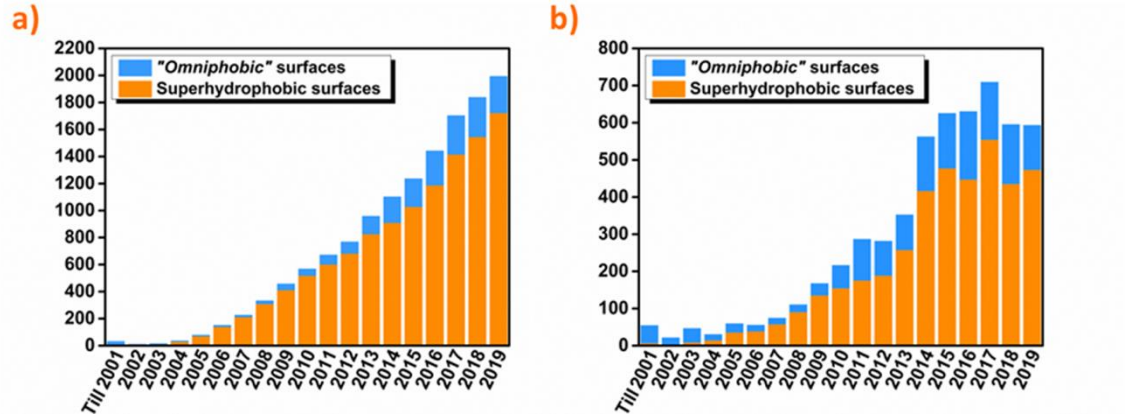

Figure 1.7. Scientific and technological evolution of the research on repellent surfaces. **a)** Number of published papers in scientific journals using "superhydrophobic surfaces" (orange) and "omniphobic surfaces" or "superomniphobic surfaces" or "oleophobic surfaces" or "superoleophobic surfaces" (pale blue) as key words. (Source: Web of Science) **b)** Number of published patents using "superhydrophobic surfaces" (orange) and "omniphobic surfaces" or "superomniphobic surfaces" or "oleophobic surfaces" or "superoleophobic surfaces" (pale blue) as key words. (Source: espacenet patent search)

Since the earliest SHS, inspired by the *Lotus effect*, until now, the highly repellent surfaces area has evolved so much, generating greater knowledge about the principles and mechanisms involved in surface contamination. Furthermore, their potential capabilities to play a key role in a wide range of applications have been demonstrated. It is for these reasons, together with the great industrial interest, and pushed mainly by the market needs, that a promising future for repellent surfaces can be envisaged. The market is waiting for contamination-free surfaces, but making this possible requires overcoming a series of scientific and technological challenges. Those challenges are:

- Durability: one of the main challenges facing repellent surfaces is their poor durability. The complex structures needed to obtain the morphology and the topography required for achieving highly repellent surfaces based on superhydrophobic or superomniphobic approaches suffer from the lack of mechanical robustness. Focusing on the most successful omniphobic technology in the state-of-the-art, SLIPS, the durability of low adhesion surfaces based on this technology is mainly determined by the stability of the lubricant layer, which is prone to depletion through leaking or evaporation processes. Furthermore, in some cases SLIPS also involve surface structuring to lock the lubricant and thus,

their robustness implies another limitation as mentioned above. Additionally, durability is also an important issue from the operating conditions point of view, because the surfaces need to withstand extreme temperatures, chemical environments or mechanical abrasion in dependence of their specific application. Hence, their poor durability is the major weakness of the currently available low adhesion solutions, which should be enhanced in order to allow practical applications with optimal performance.

- Multifunctionality: currently, highly repellent surfaces developments are mainly focused on the adhesion of certain fouling agents instead of focusing on a holistic look at all surface contaminant phenomena. A more universal technological solution, capable of responding to several contaminants, would have a huge impact on a wide range of applications. In this context, multifunctional surfaces are strongly emerging with the aim of integrating different functionalities into a single material.
- Lack of knowledge: the adhesion of liquids to solid surfaces has been widely investigated and the principles and mechanisms behind liquid repellent surfaces are well understood. However, the interaction of liquids with nanostructured surfaces, modified using liquid-like compounds, is still unexplored. In addition, regarding the interactions established between solid particles and surfaces, there is a lack of in-depth knowledge. It is important to advance this knowledge in order to be able to design the most effective surfaces repelling solid contaminants.

In order to meet the aforementioned challenges researchers keep on looking for new strategies to develop novel low adhesion solutions.

1.3 OBJECTIVE AND OUTLINE OF THE THESIS

The advent of nanotechnology has provided scientists and engineers a powerful tool for designing materials by taking advantage of their singular properties at the nanoscale. Indeed, advances in nanotechnology have given us the ability to tailor the properties of materials as well as the capacity to create completely new ones according to our specific

needs. Thanks to the potential provided by nanotechnology, the repellent surfaces field has experienced a great boost.

In this context, the aim of this thesis is to generate new knowledge and develop novel strategies which contribute to addressing the challenges discussed above, for advancing the repellent surfaces field. This work is focused on the development of robust repellent surfaces with enhanced durability. To achieve this, the potential of nanotechnology is exploited following two different ways:

1) Surface structuring.
2) Incorporation of nanoobjects to provide additional functionalities.

The first strategy pursues the fabrication of omniphobic surfaces by generating micro/nanostructured features with a singular morphology, capable of providing the desired properties by benefiting from the nanoscale control, whereas in the second strategy, nanoobjects are used as vehicles to introduce additional functionalities into a single omniphobic solution, thereby providing multifunctional surfaces. Both strategies are used with the aim of developing omniphobic surfaces with tailor-made properties seeking to give response for the industrial interest and the market needs.

The specific objectives of this work are the following:

- To develop omniphobic surfaces based on morphological effects, generating hierarchical micro/nanostructured surfaces.
- To study the performance of the structured omniphobic surfaces compared to the smooth ones at different applications.
- To develop a new strategy to obtain novel multifunctional surfaces designed on the nanoscale.
- To explore innovative approaches to provide low adhesion solutions from solid particles.
- To promote enhancements on the durability of the developed solutions by covalent anchoring.

- To provide omniphobic solutions compatible with current industrial manufacturing techniques.

This dissertation entitled "*Nanoscale engineering omniphobic surfaces*" has been structured in six chapters which are described below.

Chapter 1 provides an overview of repellent surfaces and their evolution over time. This chapter also includes the state-of-the-art of this topic, as well as a description of the most relevant technologies involved in developing low adhesion surfaces, resistant to contamination.

Chapter 2 introduces a description of the concepts, experimental methods and techniques used in this thesis for the fabrication and characterization of the omniphobic surfaces developed in the following chapters.

Chapter 3 reports the development of omniphobic aluminium surfaces showing the potential of surface structuring. The obtaining of self-cleaning and anti-icing properties by moving from smooth surfaces to structured ones and from one low SFE material to another is demonstrated in this chapter.

Chapter 4 reports a novel strategy to obtain multifunctional surfaces using nanoparticles as vectors to achieve self-cleaning surfaces by combining omniphobicity and antistatic properties. Conductive laponite nanoparticles are introduced into an omniphobic solution in order to confer an additional functionality, providing a singular holistic approach to the repellence against liquids and solid particles.

Chapter 5 reports the fabrication of robust omniphobic surfaces by covalently anchored nanoparticles. The use of an omniphobic precursor with two functional groups, which allow its simultaneous anchoring to both laponite nanoparticles and substrate, for the improvement of the abrasion resistance of the multifunctional coatings developed in **chapter 4**, is proposed.

Chapter 6 summarizes the most relevant conclusions and the impact of this work on the field of repellent surfaces.

1.4 References

(1) Landolt, D. *Corrosion and Surface Chemistry of Metals*; CRC Press, 2007.

(2) Marshall, S. J.; Bayne, S. C.; Baier, R.; Tomsia, A. P.; Marshall, G. W. A Review of Adhesion Science. *Dent. Mater.* **2010**, *26* (2), e11–e16. https://doi.org/10.1016/j.dental.2009.11.157.

(3) Kato, K. Wear in Relation to Friction — a Review. *Wear* **2000**, *241* (2), 151–157. https://doi.org/10.1016/S0043-1648(00)00382-3.

(4) Somorjai, G. A.; Li, Y. *Introduction to Surface Chemistry and Catalysis*; John Wiley & Sons, 2010.

(5) Tao, F. (Feng); Crozier, P. A. Atomic-Scale Observations of Catalyst Structures under Reaction Conditions and during Catalysis. *Chem. Rev.* **2016**, *116* (6), 3487–3539. https://doi.org/10.1021/cr5002657.

(6) Castner, D. G.; Ratner, B. D. Biomedical Surface Science: Foundations to Frontiers. *Surf. Sci.* **2002**, *500* (1), 28–60. https://doi.org/10.1016/S0039-6028(01)01587-4.

(7) Ahmad Khalili, A.; Ahmad, M. R. A Review of Cell Adhesion Studies for Biomedical and Biological Applications. *Int. J. Mol. Sci.* **2015**, *16* (8), 18149–18184. https://doi.org/10.3390/ijms160818149.

(8) Luo, J.; Zhang, S.; Sun, M.; Yang, L.; Luo, S.; Crittenden, J. C. A Critical Review on Energy Conversion and Environmental Remediation of Photocatalysts with Remodeling Crystal Lattice, Surface, and Interface. *ACS Nano* **2019**, *13* (9), 9811–9840. https://doi.org/10.1021/acsnano.9b03649.

(9) Vilan, A.; Cahen, D. Chemical Modification of Semiconductor Surfaces for Molecular Electronics. *Chem. Rev.* **2017**, *117* (5), 4624–4666. https://doi.org/10.1021/acs.chemrev.6b00746.

(10) Saini, M.; Singh, Y.; Arora, P.; Arora, V.; Jain, K. Implant Biomaterials: A Comprehensive Review. *World J. Clin. Cases WJCC* **2015**, *3* (1), 52–57. https://doi.org/10.12998/wjcc.v3.i1.52.

(11) Thevenot, P.; Hu, W.; Tang, L. SURFACE CHEMISTRY INFLUENCE IMPLANT BIOCOMPATIBILITY. *Curr. Top. Med. Chem.* **2008**, *8* (4), 270–280.

(12) Rupp, F.; Liang, L.; Geis-Gerstorfer, J.; Scheideler, L.; Hüttig, F. Surface Characteristics of Dental Implants: A Review. *Dent. Mater.* **2018**, *34* (1), 40–57. https://doi.org/10.1016/j.dental.2017.09.007.

(13) Dalili, N.; Edrisy, A.; Carriveau, R. A Review of Surface Engineering Issues Critical to Wind Turbine Performance. *Renew. Sustain. Energy Rev.* **2009**, *13* (2), 428–438. https://doi.org/10.1016/j.rser.2007.11.009.

(14) Blaszykowski, C.; Sheikh, S.; Thompson, M. Surface Chemistry to Minimize Fouling from Blood-Based Fluids. *Chem. Soc. Rev.* **2012**, *41* (17), 5599–5612. https://doi.org/10.1039/C2CS35170F.

(15) Belhadjamor, M.; Mansori, M. E.; Belghith, S.; Mezlini, S. Anti-Fingerprint Properties of Engineering Surfaces: A Review. *Surf. Eng.* **2018**, *34* (2), 85–120. https://doi.org/10.1080/02670844.2016.1258449.

(16) Sulaiman, S. A.; Hussain, H. H.; Leh, N. S. H. N.; Razali, M. S. I. Effects of Dust on the Performance of PV Panels. *Int. J. Mech. Mechatron. Eng.* **2011**, *5* (10), 2021–2026.

(17) Poots, G.; Gent, R. W.; Dart, N. P.; Cansdale, J. T. Aircraft Icing. *Philos. Trans. R. Soc. Lond. Ser. Math. Phys. Eng. Sci.* **2000**, *358* (1776), 2873–2911. https://doi.org/10.1098/rsta.2000.0689.

(18) Aiyejina, A.; Chakrabarti, D. P.; Pilgrim, A.; Sastry, M. K. S. Wax Formation in Oil Pipelines: A Critical Review. *Int. J. Multiph. Flow* **2011**, *37* (7), 671–694. https://doi.org/10.1016/j.ijmultiphaseflow.2011.02.007.

(19) Jr, E. D. S.; Koh, C. A.; Koh, C. *Clathrate Hydrates of Natural Gases*; CRC Press, 2007.

(20) Zhao, X.; Chen, X. D. A Critical Review of Basic Crystallography to Salt Crystallization Fouling in Heat Exchangers. *Heat Transf. Eng.* **2013**, *34* (8–9), 719–732. https://doi.org/10.1080/01457632.2012.739482.

(21) Percival, S. L.; Suleman, L.; Vuotto, C.; Donelli, G. Healthcare-Associated Infections, Medical Devices and Biofilms: Risk, Tolerance and Control. *J. Med. Microbiol.* **2015**, *64* (4), 323–334. https://doi.org/10.1099/jmm.0.000032.

(22) Verran, J. Biofouling in Food Processing: Biofilm or Biotransfer Potential? *Food Bioprod. Process.* **2002**, *80* (4), 292–298. https://doi.org/10.1205/096030802321154808.

(23) Goode, K. R.; Asteriadou, K.; Robbins, P. T.; Fryer, P. J. Fouling and Cleaning Studies in the Food and Beverage Industry Classified by Cleaning Type. *Compr. Rev. Food Sci. Food Saf.* **2013**, *2* (12), 121–143. https://doi.org/10.1111/1541-4337.12000.

(24) Callow, M. E.; Callow, J. E. Marine Biofouling: A Sticky Problem. *Biol. Lond. Engl.* **2002**, *49* (1), 10–14.

(25) Xiong, Y.; Liu, Y. Biological Control of Microbial Attachment: A Promising Alternative for Mitigating Membrane Biofouling. *Appl. Microbiol. Biotechnol.* **2010**, *86* (3), 825–837. https://doi.org/10.1007/s00253-010-2463-0.

(26) Neinhuis, C.; Barthlott, W. Characterization and Distribution of Water-Repellent, Self-Cleaning Plant Surfaces. *Ann. Bot.* **1997**, *79* (6), 667–677. https://doi.org/10.1006/anbo.1997.0400.

(27) Barthlott, W.; Neinhuis, C. Purity of the Sacred Lotus, or Escape from Contamination in Biological Surfaces. *Planta* **1997**, *202* (1), 1–8. https://doi.org/10.1007/s004250050096.

(28) Helbig, R.; Nickerl, J.; Neinhuis, C.; Werner, C. Smart Skin Patterns Protect Springtails. *PloS One* **2011**, *6* (9), e25105. https://doi.org/10.1371/journal.pone.0025105.

(29) Wagner, T.; Neinhuis, C.; Barthlott, W. Wettability and Contaminability of Insect Wings as a Function of Their Surface Sculptures. *Acta Zool.* **1996**, *77* (3), 213–225. https://doi.org/10.1111/j.1463-6395.1996.tb01265.x.

(30) Wenzel, R. N. RESISTANCE OF SOLID SURFACES TO WETTING BY WATER. *Ind. Eng. Chem.* **1936**, *28* (8), 988–994. https://doi.org/10.1021/ie50320a024.

(31) Cassie, A. B. D.; Baxter, S. Wettability of Porous Surfaces. *Trans. Faraday Soc.* **1944**, *40* (0), 546–551. https://doi.org/10.1039/TF9444000546.

(32) Barthlott, W.; Ehler, N. Raster-Elektronenmikroskopie Der Epidermis-Oberflächen von Spermatophyten. *Akad. Wiss. Lit.* **1977**, *19*, 367–467.

(33) Neinhuis, C. Innovations from the “Ivory Tower”: Wilhelm Barthlott and the Paradigm Shift in Surface Science. *Beilstein J. Nanotechnol.* **2017**, *8* (1), 394–402. https://doi.org/10.3762/bjnano.8.41.

(34) Young, T. III. An Essay on the Cohesion of Fluids. *Philos. Trans. R. Soc. Lond.* **1805**, *95*, 65–87. https://doi.org/10.1098/rstl.1805.0005.

(35) Gould, R. F. Contact Angle, Wettability, and Adhesion, Copyright, Advances in Chemistry Series. In *Contact Angle, Wettability, and Adhesion*; Robert F. Gould, Ed.; Advances in Chemistry; AMERICAN CHEMICAL SOCIETY, 1964; Vol. 43, pp i–iii. https://doi.org/10.1021/ba-1964-0043.fw001.

(36) Eick, J. D.; Good, R. J.; Neumann, A. W. Thermodynamics of Contact Angles. II. Rough Solid Surfaces. *J. Colloid Interface Sci.* **1975**, *53* (2), 235–248. https://doi.org/10.1016/0021-9797(75)90010-7.

(37) Furmidge, C. G. L. Studies at Phase Interfaces. I. The Sliding of Liquid Drops on Solid Surfaces and a Theory for Spray Retention. *J. Colloid Sci.* **1962**, *17* (4), 309–324. https://doi.org/10.1016/0095-8522(62)90011-9.

(38) Marmur, A. Solid-Surface Characterization by Wetting. *Annu. Rev. Mater. Res.* **2009**, *39* (1), 473–489. https://doi.org/10.1146/annurev.matsci.38.060407.132425.

(39) Pierce, E.; Carmona, F. J.; Amirfazli, A. Understanding of Sliding and Contact Angle Results in Tilted Plate Experiments. *Colloids Surf. Physicochem. Eng. Asp.* **2008**, *323* (1), 73–82. https://doi.org/10.1016/j.colsurfa.2007.09.032.

(40) Wang, S.; Liu, K.; Yao, X.; Jiang, L. Bioinspired Surfaces with Superwettability: New Insight on Theory, Design, and Applications. *Chem. Rev.* **2015**, *115* (16), 8230–8293. https://doi.org/10.1021/cr400083y.

(41) Bellanger, H.; Darmanin, T.; Taffin de Givenchy, E.; Guittard, F. Chemical and Physical Pathways for the Preparation of Superoleophobic Surfaces and Related Wetting Theories. *Chem. Rev.* **2014**, *114* (5), 2694–2716. https://doi.org/10.1021/cr400169m.

(42) Wenzel, R. N. RESISTANCE OF SOLID SURFACES TO WETTING BY WATER. *Ind. Eng. Chem.* **1936**, *28* (8), 988–994. https://doi.org/10.1021/ie50320a024.

(43) Wenzel, R. N. Surface Roughness and Contact Angle. *J. Phys. Colloid Chem.* **1949**, *53* (9), 1466–1467. https://doi.org/10.1021/j150474a015.

(44) Cassie, A. B. D.; Baxter, S. Wettability of Porous Surfaces. *Trans. Faraday Soc.* **1944**, *40* (0), 546–551. https://doi.org/10.1039/TF9444000546.

(45) Feng, L.; Zhang, Y.; Xi, J.; Zhu, Y.; Wang, N.; Xia, F.; Jiang, L. Petal Effect: A Superhydrophobic State with High Adhesive Force. *Langmuir* **2008**, *24* (8), 4114–4119. https://doi.org/10.1021/la703821h.

(46) Cao, L.; Jones, A. K.; Sikka, V. K.; Wu, J.; Gao, D. Anti-Icing Superhydrophobic Coatings. *Langmuir* **2009**, *25* (21), 12444–12448. https://doi.org/10.1021/la902882b.

(47) Wang, H.; He, M.; Liu, H.; Guan, Y. One-Step Fabrication of Robust Superhydrophobic Steel Surfaces with Mechanical Durability, Thermal Stability, and Anti-Icing Function. *ACS Appl. Mater. Interfaces* **2019**, *11* (28), 25586–25594. https://doi.org/10.1021/acsami.9b06865.

(48) Gao, L.; Liu, Y.; Ma, L.; Hu, H. A Hybrid Strategy Combining Minimized Leading-Edge Electric-Heating and Superhydro-/Ice-Phobic Surface Coating for Wind Turbine Icing Mitigation. *Renew. Energy* **2019**, *140*, 943–956. https://doi.org/10.1016/j.renene.2019.03.112.

(49) Latthe, S. S.; Sutar, R. S.; Kodag, V. S.; Bhosale, A. K.; Kumar, A. M.; Kumar Sadasivuni, K.; Xing, R.; Liu, S. Self – Cleaning Superhydrophobic Coatings: Potential Industrial Applications. *Prog. Org. Coat.* **2019**, *128*, 52–58. https://doi.org/10.1016/j.porgcoat.2018.12.008.

(50) Peng, J.; Zhao, X.; Wang, W.; Gong, X. Durable Self-Cleaning Surfaces with Superhydrophobic and Highly Oleophobic Properties. *Langmuir* **2019**, *35* (25), 8404–8412. https://doi.org/10.1021/acs.langmuir.9b01507.

(51) Manoj, T. P.; Rasitha, T. P.; Vanithakumari, S. C.; Anandkumar, B.; George, R. P.; Philip, J. A Simple, Rapid and Single Step Method for Fabricating Superhydrophobic Titanium Surfaces with Improved Water Bouncing and Self Cleaning Properties. *Appl. Surf. Sci.* **2020**, *512*, 145636. https://doi.org/10.1016/j.apsusc.2020.145636.

(52) Chu, Z.; Feng, Y.; Seeger, S. Oil/Water Separation with Selective Superantiwetting/Superwetting Surface Materials. *Angew. Chem. Int. Ed.* **2015**, *54* (8), 2328–2338. https://doi.org/10.1002/anie.201405785.

(53) Thasma Subramanian, B.; Alla, J. P.; Essomba, J. S.; Nishter, N. F. Non-Fluorinated Superhydrophobic Spray Coatings for Oil-Water Separation Applications: An Eco-Friendly Approach. *J. Clean. Prod.* **2020**, *256*, 120693. https://doi.org/10.1016/j.jclepro.2020.120693.

(54) Gu, J.; Fan, H.; Li, C.; Caro, J.; Meng, H. Robust Superhydrophobic/Superoleophilic Wrinkled Microspherical MOF@rGO Composites for Efficient Oil–Water Separation. *Angew. Chem.* **2019**, *131* (16), 5351–5355. https://doi.org/10.1002/ange.201814487.

(55) Vazirinasab, E.; Jafari, R.; Momen, G. Application of Superhydrophobic Coatings as a Corrosion Barrier: A Review. *Surf. Coat. Technol.* **2018**, *341*, 40–56. https://doi.org/10.1016/j.surfcoat.2017.11.053.

(56) Xie, J.; Hu, J.; Lin, X.; Fang, L.; Wu, F.; Liao, X.; Luo, H.; Shi, L. Robust and Anti-Corrosive PDMS/SiO2 Superhydrophobic Coatings Fabricated on Magnesium Alloys with Different-Sized SiO2 Nanoparticles. *Appl. Surf. Sci.* **2018**, *457*, 870–880. https://doi.org/10.1016/j.apsusc.2018.06.250.

(57) Anti-Fogging Performances of Liquid Metal Surface Modified by ZnO Nano-Petals. *J. Taiwan Inst. Chem. Eng.* **2019**, *95*, 65–70. https://doi.org/10.1016/j.jtice.2018.09.039.

(58) Durable and Regenerable Superhydrophobic Coatings for Aluminium Surfaces with Excellent Self-Cleaning and Anti-Fogging Properties. *Tribol. Int.* **2018**, *119*, 38–44. https://doi.org/10.1016/j.triboint.2017.10.033.

(59) Bhushan, B.; Jung, Y. C. Natural and Biomimetic Artificial Surfaces for Superhydrophobicity, Self-Cleaning, Low Adhesion, and Drag Reduction. *Prog. Mater. Sci.* **2011**, *56* (1), 1–108. https://doi.org/10.1016/j.pmatsci.2010.04.003.

(60) Rajappan, A.; Golovin, K.; Tobelmann, B.; Pillutla, V.; Abhijeet; Choi, W. (최원재); Tuteja, A.; McKinley, G. H. Influence of Textural Statistics on Drag Reduction by Scalable, Randomly Rough Superhydrophobic Surfaces in Turbulent Flow. *Phys. Fluids* **2019**, *31* (4), 042107. https://doi.org/10.1063/1.5090514.

(61) Bixler, G. D.; Theiss, A.; Bhushan, B.; Lee, S. C. Anti-Fouling Properties of Microstructured Surfaces Bio-Inspired by Rice Leaves and Butterfly Wings. *J. Colloid Interface Sci.* **2014**, *419*, 114–133. https://doi.org/10.1016/j.jcis.2013.12.019.

(62) Sun, Q.; Yang, Z.; Hu, C.; Li, C.; Yan, G.; Wang, Z. Facile Preparation of Superhydrophobic PVDF Microporous Membranes with Excellent Anti-Fouling Ability for Vacuum Membrane Distillation. *J. Membr. Sci.* **2020**, *605*, 118106. https://doi.org/10.1016/j.memsci.2020.118106.

(63) Li, X.-M.; Reinhoudt, D.; Crego-Calama, M. What Do We Need for a Superhydrophobic Surface? A Review on the Recent Progress in the Preparation of Superhydrophobic Surfaces. *Chem. Soc. Rev.* **2007**, *36* (8), 1350–1368. https://doi.org/10.1039/B602486F.

(64) Kim, J.-H.; Mirzaei, A.; Kim, H. W.; Kim, S. S. Facile Fabrication of Superhydrophobic Surfaces from Austenitic Stainless Steel (AISI 304) by Chemical Etching. *Appl. Surf. Sci.* **2018**, *439*, 598–604. https://doi.org/10.1016/j.apsusc.2017.12.211.

(65) Qian, B.; Shen, Z. Fabrication of Superhydrophobic Surfaces by Dislocation-Selective Chemical Etching on Aluminum, Copper, and Zinc Substrates. *Langmuir* **2005**, *21* (20), 9007–9009. https://doi.org/10.1021/la051308c.

(66) Dimitrakellis, P.; Gogolides, E. Hydrophobic and Superhydrophobic Surfaces Fabricated Using Atmospheric Pressure Cold Plasma Technology: A Review. *Adv. Colloid Interface Sci.* **2018**, *254*, 1–21. https://doi.org/10.1016/j.cis.2018.03.009.

(67) Kostal, E.; Stroj, S.; Kasemann, S.; Matylitsky, V.; Domke, M. Fabrication of Biomimetic Fog-Collecting Superhydrophilic–Superhydrophobic Surface Micropatterns Using Femtosecond Lasers. *Langmuir* **2018**, *34* (9), 2933–2941. https://doi.org/10.1021/acs.langmuir.7b03699.

(68) Boinovich, L. B.; Modin, E. B.; Sayfutdinova, A. R.; Emelyanenko, K. A.; Vasiliev, A. L.; Emelyanenko, A. M. Combination of Functional Nanoengineering and Nanosecond Laser Texturing for Design of Superhydrophobic Aluminum Alloy with Exceptional Mechanical and Chemical Properties. *ACS Nano* **2017**, *11* (10), 10113–10123. https://doi.org/10.1021/acsnano.7b04634.

(69) Yang, Z.; Liu, X.; Tian, Y. A Contrastive Investigation on Anticorrosive Performance of Laser-Induced Super-Hydrophobic and Oil-Infused Slippery Coatings. *Prog. Org. Coat.* **2020**, *138*, 105313. https://doi.org/10.1016/j.porgcoat.2019.105313.

(70) Rose, M. A.; Bowen, J. J.; Morin, S. A. Emergent Soft Lithographic Tools for the Fabrication of Functional Polymeric Microstructures. *ChemPhysChem* **2019**, *20* (7), 909–925. https://doi.org/10.1002/cphc.201801140.

(71) Gao, X.; Yan, X.; Yao, X.; Xu, L.; Zhang, K.; Zhang, J.; Yang, B.; Jiang, L. The Dry-Style Antifogging Properties of Mosquito Compound Eyes and Artificial Analogues Prepared by Soft Lithography. *Adv. Mater.* **2007**, *19* (17), 2213–2217. https://doi.org/10.1002/adma.200601946.

(72) Maghsoudi, K.; Momen, G.; Jafari, R.; Farzaneh, M. Direct Replication of Micro-Nanostructures in the Fabrication of Superhydrophobic Silicone Rubber Surfaces by Compression Molding. *Appl. Surf. Sci.* **2018**, *458*, 619–628. https://doi.org/10.1016/j.apsusc.2018.07.099.

(73) Lin, D.; Zeng, X.; Li, H.; Lai, X. Facile Fabrication of Superhydrophobic and Flame-Retardant Coatings on Cotton Fabrics via Layer-by-Layer Assembly. *Cellulose* **2018**, *25* (5), 3135–3149. https://doi.org/10.1007/s10570-018-1748-9.

(74) Karunakaran, R. G.; Lu, C.-H.; Zhang, Z.; Yang, S. Highly Transparent Superhydrophobic Surfaces from the Coassembly of Nanoparticles (≤100 Nm). *Langmuir* **2011**, *27* (8), 4594–4602. https://doi.org/10.1021/la104067c.

(75) Latthe, S. S.; Nakata, K.; Höfer, R.; Fujishima, A.; Terashima, C. CHAPTER 5:Lotus Effect-Based Superhydrophobic Surfaces: Candle Soot as a Promising Class of Nanoparticles for Self-Cleaning and Oil–Water Separation Applications. In *Green Chemistry for Surface Coatings, Inks and Adhesives*; 2019; pp 92–119. https://doi.org/10.1039/9781788012997-00092.

(76) Rao, A. V.; Latthe, S. S.; Mahadik, S. A.; Kappenstein, C. Mechanically Stable and Corrosion Resistant Superhydrophobic Sol–Gel Coatings on Copper Substrate. *Appl. Surf. Sci.* **2011**, *257* (13), 5772–5776. https://doi.org/10.1016/j.apsusc.2011.01.099.

(77) Mahadik, S. A.; Kavale, M. S.; Mukherjee, S. K.; Rao, A. V. Transparent Superhydrophobic Silica Coatings on Glass by Sol–Gel Method. *Appl. Surf. Sci.* **2010**, *257* (2), 333–339. https://doi.org/10.1016/j.apsusc.2010.06.062.

(78) Yang, M.; Liu, W.; Jiang, C.; He, S.; Xie, Y.; Wang, Z. Fabrication of Superhydrophobic Cotton Fabric with Fluorinated TiO2 Sol by a Green and One-Step Sol-Gel Process. *Carbohydr. Polym.* **2018**, *197*, 75–82. https://doi.org/10.1016/j.carbpol.2018.05.075.

(79) Tuteja, A.; Choi, W.; Ma, M.; Mabry, J. M.; Mazzella, S. A.; Rutledge, G. C.; McKinley, G. H.; Cohen, R. E. Designing Superoleophobic Surfaces. *Science* **2007**, *318* (5856), 1618–1622. https://doi.org/10.1126/science.1148326.

(80) Bohn, H. F.; Federle, W. Insect Aquaplaning: Nepenthes Pitcher Plants Capture Prey with the Peristome, a Fully Wettable Water-Lubricated Anisotropic Surface. *Proc. Natl. Acad. Sci.* **2004**, *101* (39), 14138–14143. https://doi.org/10.1073/pnas.0405885101.

(81) Wong, T.-S.; Kang, S. H.; Tang, S. K. Y.; Smythe, E. J.; Hatton, B. D.; Grinthal, A.; Aizenberg, J. Bioinspired Self-Repairing Slippery Surfaces with Pressure-Stable Omniphobicity. *Nature* **2011**, *477* (7365), 443–447. https://doi.org/10.1038/nature10447.

(82) Luo, H.; Yin, S.; Huang, S.; Chen, F.; Tang, Q.; Li, X. Fabrication of Slippery Zn Surface with Improved Water-Impellent, Condensation and Anti-Icing Properties. *Appl. Surf. Sci.* **2019**, *470*, 1139–1147. https://doi.org/10.1016/j.apsusc.2018.10.174.

(83) Sun, J.; Wang, C.; Song, J.; Huang, L.; Sun, Y.; Liu, Z.; Zhao, C.; Li, Y. Multi-Functional Application of Oil-Infused Slippery Al Surface: From Anti-Icing to Corrosion Resistance. *J. Mater. Sci.* **2018**, *53* (23), 16099–16109. https://doi.org/10.1007/s10853-018-2760-z.

(84) Zhang, M.; Yu, J.; Chen, R.; Liu, Q.; Liu, J.; Song, D.; Liu, P.; Gao, L.; Wang, J. Highly Transparent and Robust Slippery Lubricant-Infused Porous Surfaces with Anti-Icing and Anti-Fouling Performances. *J. Alloys Compd.* **2019**, *803*, 51–60. https://doi.org/10.1016/j.jallcom.2019.06.241.

(85) Manna, U.; Raman, N.; Welsh, M. A.; Zayas-Gonzalez, Y. M.; Blackwell, H. E.; Palecek, S. P.; Lynn, D. M. Slippery Liquid-Infused Porous Surfaces That Prevent Microbial Surface Fouling and Kill Non-Adherent Pathogens in Surrounding Media: A Controlled Release Approach. *Adv. Funct. Mater.* **2016**, *26* (21), 3599–3611. https://doi.org/10.1002/adfm.201505522.

(86) Basu, S.; Hanh, B. M.; Isaiah Chua, J. Q.; Daniel, D.; Ismail, M. H.; Marchioro, M.; Amini, S.; Rice, S. A.; Miserez, A. Green Biolubricant Infused Slippery Surfaces to Combat Marine Biofouling. *J. Colloid Interface Sci.* **2020**, *568*, 185–197. https://doi.org/10.1016/j.jcis.2020.02.049.

(87) Manna, U.; Lynn, D. M. Fabrication of Liquid-Infused Surfaces Using Reactive Polymer Multilayers: Principles for Manipulating the Behaviors and Mobilities of Aqueous Fluids on Slippery Liquid Interfaces. *Adv. Mater.* **2015**, *27* (19), 3007–3012. https://doi.org/10.1002/adma.201500893.

(88) Sunny, S.; Cheng, G.; Daniel, D.; Lo, P.; Ochoa, S.; Howell, C.; Vogel, N.; Majid, A.; Aizenberg, J. Transparent Antifouling Material for Improved Operative Field Visibility in Endoscopy. *Proc. Natl. Acad. Sci.* **2016**, *113* (42), 11676–11681. https://doi.org/10.1073/pnas.1605272113.

(89) Wexler, J. S.; Jacobi, I.; Stone, H. A. Shear-Driven Failure of Liquid-Infused Surfaces. *Phys. Rev. Lett.* **2015**, *114* (16), 168301. https://doi.org/10.1103/PhysRevLett.114.168301.

(90) Kreder, M. J.; Daniel, D.; Tetreault, A.; Cao, Z.; Lemaire, B.; Timonen, J. V. I.; Aizenberg, J. Film Dynamics and Lubricant Depletion by Droplets Moving on Lubricated Surfaces. *Phys. Rev. X* **2018**, *8* (3), 031053. https://doi.org/10.1103/PhysRevX.8.031053.

(91) Wang, L.; McCarthy, T. J. Covalently Attached Liquids: Instant Omniphobic Surfaces with Unprecedented Repellency. *Angew. Chem. Int. Ed.* **2016**, *55* (1), 244–248. https://doi.org/10.1002/anie.201509385.

(92) Krumpfer, J. W.; McCarthy, T. J. Contact Angle Hysteresis: A Different View and a Trivial Recipe for Low Hysteresis Hydrophobic Surfaces. *Faraday Discuss.* **2010**, *146* (0), 103–111. https://doi.org/10.1039/B925045J.

(93) Cheng, D. F.; Urata, C.; Yagihashi, M.; Hozumi, A. A Statically Oleophilic but Dynamically Oleophobic Smooth Nonperfluorinated Surface. *Angew. Chem. Int. Ed.* **2012**, *51* (12), 2956–2959. https://doi.org/10.1002/anie.201108800.

(94) Wang, X.; Wang, Z.; Heng, L.; Jiang, L. Stable Omniphobic Anisotropic Covalently Grafted Slippery Surfaces for Directional Transportation of Drops and Bubbles. *Adv. Funct. Mater.* **2020**, *30* (1), 1902686. https://doi.org/10.1002/adfm.201902686.

(95) Liu, P.; Zhang, H.; He, W.; Li, H.; Jiang, J.; Liu, M.; Sun, H.; He, M.; Cui, J.; Jiang, L.; Yao, X. Development of "Liquid-like" Copolymer Nanocoatings for Reactive Oil-Repellent Surface. *ACS Nano* **2017**, *11* (2), 2248–2256. https://doi.org/10.1021/acsnano.7b00046.

(96) Ragesh, P.; Ganesh, V. A.; Nair, S. V.; Nair, A. S. A Review on 'Self-Cleaning and Multifunctional Materials.' *J. Mater. Chem. A* **2014**, *2* (36), 14773–14797. https://doi.org/10.1039/C4TA02542C.

(97) Adachi, T.; Latthe, S. S.; Gosavi, S. W.; Roy, N.; Suzuki, N.; Ikari, H.; Kato, K.; Katsumata, K.; Nakata, K.; Furudate, M.; Inoue, T.; Kondo, T.; Yuasa, M.; Fujishima, A.; Terashima, C. Photocatalytic, Superhydrophilic, Self-Cleaning TiO2 Coating on Cheap, Light-Weight, Flexible Polycarbonate Substrates. *Appl. Surf. Sci.* **2018**, *458*, 917–923. https://doi.org/10.1016/j.apsusc.2018.07.172.

(98) Banerjee, S.; Dionysiou, D. D.; Pillai, S. C. Self-Cleaning Applications of TiO2 by Photo-Induced Hydrophilicity and Photocatalysis. *Appl. Catal. B Environ.* **2015**, *176–177*, 396–428. https://doi.org/10.1016/j.apcatb.2015.03.058.

(99) Arabatzis, I.; Todorova, N.; Fasaki, I.; Tsesmeli, C.; Peppas, A.; Li, W. X.; Zhao, Z. Photocatalytic, Self-Cleaning, Antireflective Coating for Photovoltaic Panels: Characterization and Monitoring in Real Conditions. *Sol. Energy* **2018**, *159*, 251–259. https://doi.org/10.1016/j.solener.2017.10.088.

Chapter 2

Concepts, materials and methods

2.1 INTRODUCTION

The objective of this chapter is to introduce the materials, concepts and methods used in this thesis. Firstly, the main materials that will be used in the next chapters for obtaining omniphobic surfaces are presented. Additionally, a summary of the methodologies of surface modification and coating deposition used in this work is included. Finally, the techniques used to characterize the omniphobic surfaces developed within this thesis are described.

2.1.1 Core materials

The main purpose of this thesis is the development of highly repellent surfaces based on omniphobic and antistatic properties; hence, the core materials employed in the following chapters can be divided in two main groups: low SFE and static dissipative precursors.

2.1.1.1 Low surface free energy materials

It is established that low SFE materials are necessary for achieving omniphobic surfaces, since they provide low adhesion properties and liquid repellence capabilities. When an omniphobic surface is designed, the SFE of the solid and the surface tension of the liquid must be taken into account. In this way, in order to promote low adhesion properties of the liquids, the SFE of the solid should be lower than the surface tension of the liquid. With this regard, in order to obtain hydrophobic surfaces, the SFE should be lower than 72.8 mN/m, since this value corresponds to the water surface tension. Conversely, owing to the low surface tension (20-30 mN/m)[1] of most aprotic solvents and oils, a SFE less than 20 mN/m is required for achieving oleophobic surfaces. Consequently, surfaces displaying a SFE lower than 20 mN/m are needed for obtaining omniphobic surfaces. In this context, fluorinated materials have proven to be very effective for lowering the SFE. Zisman *et al.* reported that the SFE of a material depends on its constituent groups, decreasing in following order: $-CH_2$ (36 mN/m) > $-CH_3$ (30 mN/m) > $-CF_2$ (23 mN/m) > $-CF_3$ (15 mN/m).[2] The singular properties of fluorinated surfaces arise from the unique characteristics of the fluorocarbon bond (C-F). The high electronegativity of fluorine (the most electronegative element) provides a strong C-F bond and a low

polarizability, which results in weak intermolecular forces and, therefore, in low SFE. In addition, owing to the strength and the nature of the C-F bond, fluorocarbons present a great stability exhibiting excellent durability and, high thermal and chemical resistance, making them especially interesting for a broad range of applications.

In this thesis, three different fluorinated compounds will be used as low SFE materials, which can be grouped into: perfluoroalkyl derivatives and perfluoropolymers, more specifically, perfluoropolyethers (PFPEs). All of them contain at least a triethoxysilane functional group, prone to hydrolyse, thereby losing the ethoxy groups and allowing a covalent silanol bond between the molecule and a hydroxylated surface.

In particular, the following perfluorinated compounds will be employed in the following chapters:

- **Perfluoroalkyl derivatives**:

  Perfluoroalkyl compounds are a type of synthetic fluorinated hydrocarbons and their alkoxysilane group containing derivatives have been widely employed to render hydroxylated surfaces omniphobic. The resulting modified surfaces exhibit high CA_s and CAH.

  In particular, 1H,1H,2H,2H-perfluorooctyltriethoxysilane (**Figure 2.1**) will be used in this thesis to functionalize silicon oxide-based nanoparticles to render omniphobic properties.

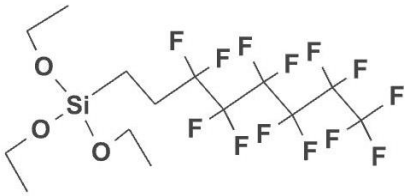

Figure 2.1. Scheme of the 1H,1H,2H,2H-perfluorooctyltriethoxysilane.

- **Perfluoropolyethers (PFPEs):**

  PFPEs compounds have typically been used as lubricant agents in the aerospace industry because of their high temperature resistance.

In the last years, the introduction of silane groups on the PFPE structure have been explored with the aim of allowing their grafting to hydroxylated surfaces. Benefiting from their long chain, based on (-CF_2CF_2O-) and/or (-CF_2O-), and their intrinsic flexibility (**Figure 2.2**), PFPE-modified surfaces can provide extremely low CAH compared to those obtained on perfluoroalkylsilane-modified surfaces.

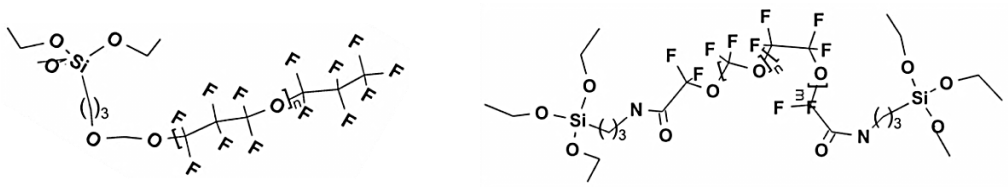

Figure 2.2. Scheme of the [perfluoro(polypropyleneoxy)]methoxypropyltrimethoxy silane (left) and Fluorolink S10 (right).

2.1.1.2 Static dissipative precursors

One of the strategies proposed for minimizing the dust accumulation on the surface of a material is by reducing the electrical resistance of the surface, which leads to antistatic characteristics. In this way, the attraction of dust by the surface is reduced by electrostatic charges.[3] Static electrical charges generally build up on the surface of insulators when they have been in contact with a material of a different nature. In processes of rubbing or during an air flow, an electron transfer takes place from one material to another, polarizing both of them.[4] Also a mosaic of localised positive and negative charges can occur over the insulator surface, able to attract dust particles. Facilitating the mobility of electrical charges along the surface by reducing the surface resistance will induce recombination of charge carriers and thus the attraction of dust to vanish.

In this thesis, laponite nanoparticles will be used as static dissipative precursors in coatings for reducing the surface resistance of materials. Benefiting from their intrinsic ionic and electrical conductivity, laponite nanoparticles appear to be an excellent candidate to provide antistatic (sheet resistance between 10^5 Ω/□ and 10^{12} Ω/□) and dust-repellent effects.

Laponite nanoparticles are a synthetic type of silicate nanoclay in the smectite family. Laponite has a layered structure formed by disc-shaped crystals (approximately 25 nm in

diameter and 0.92 nm thick, Figure 2.3) with an empirical formula of $Na^{+}_{0.7}[(Si_8Mg_{5.5}Li_{0.3})O_{20}(OH)_4]^{-0.7}$. Each single crystal is composed of a sheet of octahedrally coordinated magnesium oxide, sandwiched between two sheets of tetrahedrally coordinated silica.[5] The presence of lithium cations, randomly replacing some of those of magnesium in the octahedral sheet, induces a negative charge on the crystal face, which is neutralized by sodium cations in the interlayer space. Consequently, electrostatic interactions appear, promoting the formation of crystals arranged into stacks. Conversely, the edges of the crystals have small localised positive charges, since the exposed hydroxyl groups can be protonated.[6]

In addition to the expected antistatic properties of the resulting laponite coatings, the hydroxyl groups on the edges of the laponite nanocrystals can be functionalised by silanisation reactions using alkoxysilane derivatives. In this way, organic and/or omniphobic chains can be covalently grafted onto the laponite edges. This potential for functionalizing the laponite nanoparticles for obtaining multifunctional coatings with omniphobic and antistatic properties will be explored in this thesis.

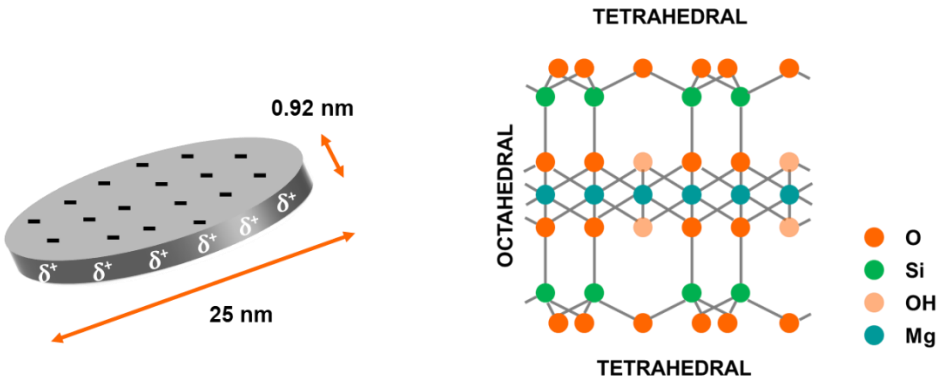

Figure 2.3. Schematic representation of a laponite nanocrystal and its chemical structure.

2.1.2 Methods

2.1.2.1 Surface modification

Surface modification by chemisorption processes requires compounds with specific anchoring groups compatible with the chemical nature of the material to be modified. There are several experimental methods for the deposition of both, organic thin solid films and polymeric coatings. In general, the nature of the substrate that will be

modified, determines the modification methods that can be used. In this thesis, self-assembly and bar-coating have been chosen as deposition techniques to modify the surface properties of different types of materials. These methods are simple and inexpensive (complex equipment's are not required), they allow high quality film depositions and industrial up-scaling would be a simple process.

2.1.2.1.1 Self-assembly technique: thin film deposition

The attachment of self-assembled monolayers (SAMs) is a powerful tool for surface modification.[7] This technique provides high control of the density and orientation of the organic molecules on the surface, resulting in an attractive way to design surfaces with specific properties. SAMs are molecular assemblies spontaneously formed upon immersion of an appropriate substrate into a solution of an active surfactant in an organic solvent.[8] Since the first report of formation of ordered monolayers by spontaneous adsorption on solid substrates published in 1983 by Sagiv,[9] the self-assembly technique has been widely applied using several types of molecules and different substrates. The most studied systems have been alkanethiols on metals, especially gold[10,11] and organosilicon derivatives on hydroxylated surfaces.[12]

The deposition of SAMs requires a clean substrate that is immersed into a solution, typically in the 1-10 mM range, of the compound for a certain time that can vary from minutes to days, depending on different factors such as, the nature of the substrate, the nature of the molecule, and the solution concentration. Immediately after deposition, rinsing of the substrate is required to remove weakly physisorbed molecules from the surface.

As mentioned above, in this thesis the self-assembly of organosilanes derivatives will be carried out. Particularly, the surface modification with organosilanes is one of the most used methods to form monolayers on hydroxylated materials. Reactions of organosilanes (containing chlorine-, methoxy- or ethoxy- as hydrolysable groups) with hydroxylated surfaces result in monolayers covalently attached to the substrate with considerable chemical and mechanical stability. The typical formation of monolayers from silanes involves three basic steps, as illustrated in **Figure 2.4**: 1) organosilanes are

hydrolysed by neighbouring water molecules (stemming from adsorbed water on the substrate surface, from the formulation, or from the atmosphere moisture) to form the corresponding hydroxysilane; 2) formation of hydrogen bonds between hydroxysilane molecules and hydroxyl groups of a hydroxylated surface; 3) a condensation reaction between silanol groups and the hydroxylated surface occurs forming (Si-O-Surface) bonds. This condensation reaction may also take place between neighbouring silanol groups to form a cross linked silica network.[13] It is important to note that the initial hydrolysis of silanes, to generate silanol, is the critical step of this process and controls the quality of the obtained SAM. The amount of water in the system has fundamental importance.[14] A lack of water involves the incomplete formation of the monolayer, whereas an excess of water results in polycondensation of silane molecules prior to the adsorption onto the substrate surface.[15]

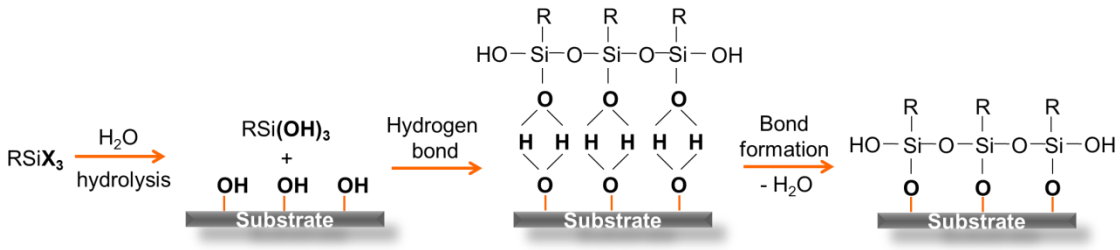

Figure 2.4. Formation of a self-assembled monolayer onto a hydroxylated surface. Adapted from reference [16].

2.1.2.1.2 Bar-coating technique: fabrication of coatings

The bar-coating is a simple technique for obtaining high quality coatings. It allows a fast deposition rate over a large area, while producing a minimal waste of the applied material. This technique involves a rolling bar over a substrate. An excess of the coating precursor material is placed on the substrate and it is spread over the surface of the latter by the bar, forming a flat uniform coating (**Figure 2.5**).

Typically, the bar is a cylindrical rod with a wire spiral around it. The thickness of the coating is determined by the amount of the material allowed to pass through the gaps created between the wire and the substrate. Indeed, the coating thickness provided by a rod is approximately 10% of the wire diameter. This technique offers the potential to tailor the coating thickness just by changing the bar applicator. It should be taken into

account that the viscosity of the material to be applied is an important parameter for obtaining high quality coatings and it must be within the range 10-200 centipoise.

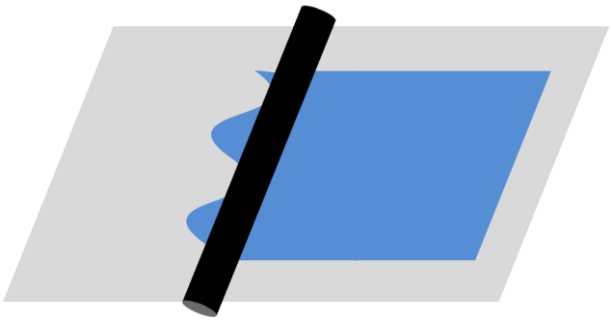

Figure 2.5. Scheme of the coating process by the bar-coating technique.

2.2 CHARACTERIZATION TECHNIQUES

2.2.1 Materials

2.2.1.1 Attenuated Total Reflectance Fourier Transform Infrared Spectroscopy (ATR-FTIR)

Infrared spectroscopy provides information about the nature of chemical bonds present in a molecule. This technique involves the interaction of infrared (IR) radiation with matter and absorption of photons with a specific energy, which is characteristic of each functional group present in a molecule, thereby allowing the identification of its chemical nature.

The attenuated total reflectance accessory allows analysing the surface region of a sample instead of the bulk, since the infrared radiation only penetrates to a depth of 0.5-5 µm of the sample. In ATR-FTIR, an IR beam is directed at a certain angle into a crystal with a high refractive index and multiple internal reflections of the beam occur, creating an evanescent wave atop the crystal, which upon physical contact penetrate into a sample (**Figure 2.6**). Some of the energy of the evanescent wave is absorbed by the sample and the reflected radiation is collected by the detector, thus enabling the system to generate an infrared spectrum, providing information about the functional groups present in the most external region of the sample.

ATR-FTIR is used in this thesis to verify both the successful functionalization of laponite particles by grafting the omniphobic compounds mentioned in section 2.1.1 and the deposition of the thin films on different substrates.

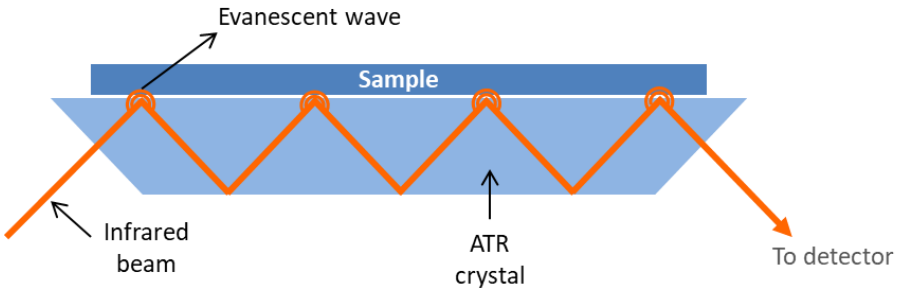

Figure 2.6. Schematic diagram of the attenuated total reflectance FTIR principle.

2.2.1.2 Thermogravimetric analysis (TGA)

Thermogravimetric analysis is a quantitative technique in which the mass of a sample is measured over time as it is subjected to a thermal treatment. These measurements provide information about physical (i.e. phase transitions, absorption, adsorption and desorption) and chemical (i.e. chemisorption, thermal decomposition, and solid-gas reactions) phenomena.[17] The thermal treatment may include heating, cooling, isothermal holds, or a combination of some or even all of these. The thermogravimetric analysis is conducted in a thermogravimetric analyser, which is based on a precision microbalance connected to a sample pan inside a furnace with a programmable control temperature. A purge gas controls the sample atmosphere and the mass of the sample is monitored during the experiment. In this thesis, the mass loss of a sample produced by thermal decomposition of organic matter during a heating experiment is used to determine the degree of surface functionalization by grafted molecules.

2.2.2 Surfaces and coatings

2.2.2.1 Ultraviolet visible spectroscopy (UV-vis)

UV-vis is a powerful technique to characterize the optical properties (i.e. absorbance, transmittance and reflectance) of liquids and solids. This technique is based on the processes that a beam of ultraviolet and visible radiation undergoes when it interacts with matter. The beam may be absorbed, reflected, transmitted, refracted,

diffused, or polarized and UV-vis spectroscopy allows to determine the light absorbed, reflected, and transmitted by a sample. In order to accurately determine the transmittance and the reflectance of a sample (i.e. all the transmitted and reflected beam reaches the detector whilst diffusion, refraction or polarization phenomena occurs) an integrating sphere must be used instead of a standard detector as it allows to collect all the scattered beams.

2.2.2.2 Field Emission Scanning Electron Microscopy (FESEM)

The FESEM provides information about the morphology and the chemical composition of a sample by acquisition of high resolution images (< 2 nm). This technique involves an electron gun in which the electrons are accelerated by applying an electric field. The beam of the accelerated electrons is then focused on the sample using electromagnetic lenses. When a sample is exposed to an accelerated electron beam, different kinds of interactions occur, producing various types of radiation that is collected from specific detectors. The radiation emitted from the sample contains low energy secondary electrons, high energy backscattered electrons, X-ray or Auger electrons. Analysing each of these types of radiation provides different information. Secondary electrons allow constructing the surface morphology image, since they are produced in the most external part of the sample (to around 2 nm depth). In contrast, backscattered electrons enable images of the chemical composition of the sample, because these electrons are generated from the elastic dispersion of incident electrons impacting the atomic nucleus. X-ray and Auger electrons provide spectroscopic information, thus allowing the elemental analysis of the sample.

In this thesis, FESEM is used to characterize the surface morphology of the developed coatings. Furthermore, this technique is also employed to determine the thickness of the coatings by analysing the cross section of the samples.

2.2.2.3 X-ray photoelectron spectroscopy (XPS)

XPS is a qualitative and quantitative technique for analysing the elemental composition of a surface or near-surface region of a sample. Furthermore, it provides information about the different chemical environments surrounding the same element,

differentiating oxidation states. Depth and image profiles can also be obtained according to the variation in the lateral composition.[18] When a high energy photon is absorbed by an atom, an electron can be ejected (**Figure 2.7**). Even though X-rays are deeply penetrating radiation, the photoemitted electron can only be detected if the atom from which it originates is located in the top 1-10 nm of the sample. In this process, the kinetic energy (E_K) of the ejected electron is given by **equation 2.1**:

$$E_K = h\nu - E_B - \Phi \qquad \text{(Eq 2.1)}$$

where hν is the energy of the X-rays photons used, E_B refers to the binding energy of the electron within the atom (i.e. the energy required to remove the electron from the atom) and Φ is the value of the work function of the spectrophotometer. Since the energy of the incident photon and the work function are known, the binding energy (which is characteristic of each chemical element, since it depends on the atomic number) of the ejected electron can be determined by measuring it´s kinetic energy, thereby allowing to identify the elemental composition of the surface.

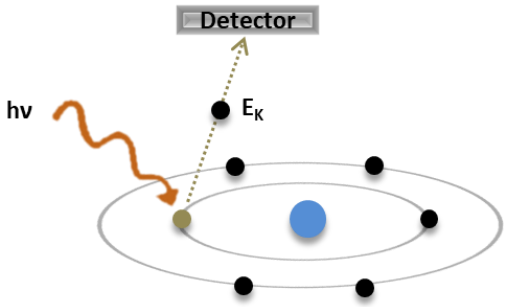

Figure 2.7. Scheme of the fundamental principle of the XPS technique.

2.2.2.4 Optical tensiometer

A tensiometer is an instrument which allows the measurement of the CA of a droplet in contact with a solid. As was introduced in **Chapter 1**, the CA provides highly valuable information of the wetting properties of a material and enables the SFE to be determined. The equipment involves a simple system in which a liquid droplet is placed onto the surface of a sample and a high resolution camera records the droplet profile using monochromatic LED light. The captured image is then analysed with a profile fitting method to accurately determine the CA (**Figure 2.8**).

In this thesis, the static CAs are measured by the sessile droplet method, while the hysteresis CAs are determined through the tilting plate method (explained in **Chapter 1**). In both cases, the Young-Laplace fitting method is used to calculate the CA.

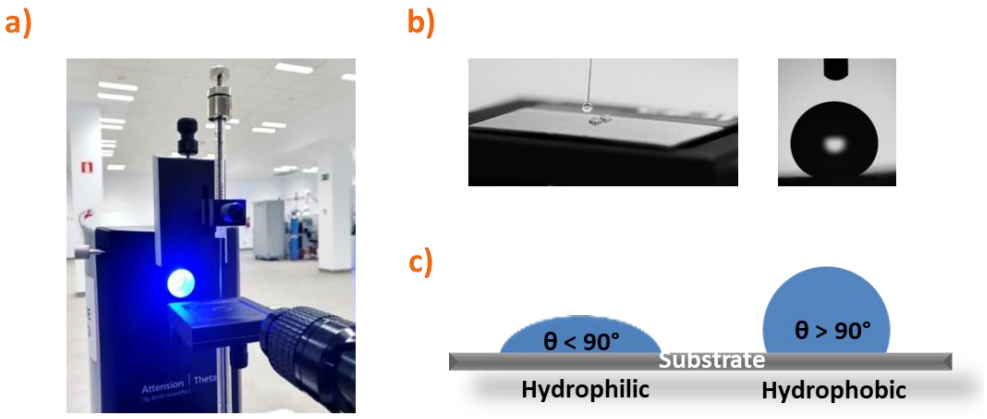

Figure 2.8. a) Optical tensiometer. b) Droplet deposition process on a substrate (left) and the droplet profile image provided by the software (right). c) CA of a droplet of water onto a hydrophilic surface (left) and a hydrophobic surface (right).

The SFE (i.e. the surface tension of a solid-vapor interface, γ_{SV}) is a characteristic property of a solid and it is related to the energy excess of the surface atoms of a material compared to that on the bulk (as was explained in **Chapter 1**). Hence, the SFE determines how a liquid will interact with a surface. While the SFE of a solid cannot be measured directly, it can be easily calculated from CA measurements. According to Young´s equation (**Equation 1.1**), the SFE depends on the CA (θ), the liquid surface tension (γ_{LV}) and the surface tension of the solid-liquid interface (γ_{SL}) (**Equation 2.2**):

$$\gamma_{SV} = \gamma_{SL} + \gamma_{LV} \cos\theta \qquad \text{(Eq. 2.2)}$$

Although the CA is measured using a probe liquid of known surface tension, two factors remain unknown in the Young´s equation. Consequently, in order to determine the SFE, another equation, allowing the calculation of the surface tension of the solid-liquid interface, is required. A number of models have been reported to determine the SFE (e.g. Fowkes,[19] Owens-Wendt-Rabel-Kaelble (OWRK),[20,21,22] Van Oss-Good,[23] Wu,[24]…), which differ mainly in their theoretical approach (in particular, the type of the interactions) used to calculate this solid-liquid surface tension. Most of these models rely on the assumption that the solid-liquid surface tension is a sum of different contributions related to specific

interactions (dispersive, polar, hydrogen, induction and acid-base). The OWRK model is one of the most widely applied for determining the SFE of a solid. This model assumes that solid-liquid surface tension is the sum of the surface tensions (which can be separated in two main contributions: polar and dispersive) of the individual phases (**Equation 2.3**). The polar component involves the sum of the polar, hydrogen, induction and acid-base interactions, while the dispersive component contains the dispersive interactions.

$$\gamma_{SL} = \gamma_{SV} + \gamma_{LV} - 2\left(\sqrt{\gamma_{SV}^{p}\,\gamma_{LV}^{p}} + \sqrt{\gamma_{SV}^{d}\,\gamma_{LV}^{d}}\right) \qquad \textbf{(Eq. 2.3)}$$

By combining **Equation 2.3** with the Young´s equation results in **Equation 2.4**:

$$\gamma_{LV}(1 + \cos\theta) = 2\left(\sqrt{\gamma_{SV}^{p}\,\gamma_{LV}^{p}} + \sqrt{\gamma_{SV}^{d}\,\gamma_{LV}^{d}}\right) \qquad \textbf{(Eq. 2.4)}$$

In this way, the polar (γ_{SV}^{p}) and the dispersive (γ_{SV}^{d}) contributions of the surface energy can be determined by CA measurements using at least two measuring liquids of which both, their surface tension and their polar and dispersive contributions are known. In one of the liquids the polar contribution should be the dominant component, while the other liquid should have a dominant dispersive contribution. Typically, distilled water is used as the polar liquid (glycerol and formamide can also be used) and diiodomethane as the dispersive one (bromonaphtalene can also be used). **Table 2.1** contains the surface tension and the polar and the dispersive contributions of the most widely used liquids for SFE determination.

Table 2.1. The surface tension (γ_{LV}) and the polar (γ_{LV}^{p}) and the dispersive (γ_{LV}^{d}) contributions of selected measuring liquids for the SFE determination.[25]

Measuring liquid	γ_{LV} (mN/m)	γ_{LV}^{p} (mN/m)	γ_{LV}^{d} (mN/m)
Distilled water	72.8	51.0	21.8
Diiodomethane	50.8	2.3	48.5

The Zisman model[2] is also often used to determine the SFE of a solid. In this case, the model assumes that the SFE of a solid corresponds to the surface tension of the liquid

needed to fully wet the surface (CA = 0°), also referred as the critical surface tension. Since this model focuses only on Van-der-Waals interactions (the influence of the polar ones is not considered), it is only useful for characterizing non-polar surfaces.

In this thesis, the SFE of the samples is determined using the OWRK model. Since the separation of the SFE into its polar and dispersive components allows predictions about how a liquid behaves on a surface according to its polar or non-polar nature.

2.2.2.5 Sheet resistance

The sheet resistance is a measure of the opposition of thin films, which are uniform in thickness, to the flow of electrical current through it. For measuring, a four-point probe is used in order to avoid the contact resistance. Typically, a constant current is applied between two of the electrodes and the potential difference between the other two electrodes is measured using a high impedance voltmeter.
According to the Ohm´s Law, the resistance (R) of a material is given by **Equation 2.5**:

$$V = I \cdot R \qquad \text{(Eq. 2.5)}$$

where, V is the voltage and I is the current.

The resistance can also be written as:

$$R = \rho \frac{L}{W \cdot t} = R_s \frac{L}{W} \qquad \text{(Eq. 2.6)}$$

where, ρ is the resistivity, L is the length, W is the weight, t is the thickness and R_s is the sheet resistance of the sample.

The sheet resistance is commonly defined as the resistivity of a material divided by its thickness:

$$R_s = \frac{\rho}{t} \qquad \text{(Eq. 2.7)}$$

In this thesis, sheet resistance measurements will be used to characterize the antistatic behaviour of different coatings. One of the advantages of this electrical

property is that it is independent of the size of the sample, allowing an easy comparison between different samples.

2.3 References

(1) James Speight, P. D. *Lange's Handbook of Chemistry, Sixteenth Edition*; McGraw-Hill Education, 2005.

(2) ZISMAN, W. A. Relation of the Equilibrium Contact Angle to Liquid and Solid Constitution. In *Contact Angle, Wettability, and Adhesion*; Advances in Chemistry; AMERICAN CHEMICAL SOCIETY, 1964; Vol. 43, pp 1–51. https://doi.org/10.1021/ba-1964-0043.ch001.

(3) Narushima, D.; Takanohashi, H.; Hirose, J.; Ogawa, S. Antistatic Effect of Power-Enhancement Coating for Photovoltaic Modules. **2011**, *8112*, 811208. https://doi.org/10.1117/12.892440.

(4) Baytekin, H. T.; Baytekin, B.; Hermans, T. M.; Kowalczyk, B.; Grzybowski, B. A. Control of Surface Charges by Radicals as a Principle of Antistatic Polymers Protecting Electronic Circuitry. *Science* **2013**, *341* (6152), 1368–1371. https://doi.org/10.1126/science.1241326.

(5) Manning, D. a. C. Handbook of Clay Science (Developments in Clay Science, 1) - Edited by F. Bergaya, B.K.G. Theng & G. Lagaly. *Eur. J. Soil Sci.* **2007**, *58* (2), 518–519. https://doi.org/10.1111/j.1365-2389.2007.00898_4.x.

(6) Tawari, S. L.; Koch, D. L.; Cohen, C. Electrical Double-Layer Effects on the Brownian Diffusivity and Aggregation Rate of Laponite Clay Particles. *J. Colloid Interface Sci.* **2001**, *240* (1), 54–66. https://doi.org/10.1006/jcis.2001.7646.

(7) Ariga, K. *Organized Organic Ultrathin Films: Fundamentals and Applications*; John Wiley & Sons, 2012.

(8) Ulman, A. Formation and Structure of Self-Assembled Monolayers. *Chem. Rev.* **1996**, *96* (4), 1533–1554. https://doi.org/10.1021/cr9502357.

(9) Sagiv, J. Organized Monolayers by Adsorption. 1. Formation and Structure of Oleophobic Mixed Monolayers on Solid Surfaces. *J. Am. Chem. Soc.* **1980**, *102* (1), 92–98. https://doi.org/10.1021/ja00521a016.

(10) Love, J. C.; Estroff, L. A.; Kriebel, J. K.; Nuzzo, R. G.; Whitesides, G. M. Self-Assembled Monolayers of Thiolates on Metals as a Form of Nanotechnology. *Chem. Rev.* **2005**, *105* (4), 1103–1170. https://doi.org/10.1021/cr0300789.

(11) Vericat, C.; Vela, M. E.; Benitez, G.; Carro, P.; Salvarezza, R. C. Self-Assembled Monolayers of Thiols and Dithiols on Gold: New Challenges for a Well-Known System. *Chem. Soc. Rev.* **2010**, *39* (5), 1805–1834. https://doi.org/10.1039/B907301A.

(12) Haensch, C.; Hoeppener, S.; Schubert, U. S. Chemical Modification of Self-Assembled Silane Based Monolayers by Surface Reactions. *Chem. Soc. Rev.* **2010**, *39* (6), 2323–2334. https://doi.org/10.1039/B920491A.

(13) Ulman, A. *An Introduction to Ultrathin Organic Films: From Langmuir--Blodgett to Self--Assembly*; Academic Press, 2013.

(14) McGovern, M. E.; Kallury, K. M. R.; Thompson, M. Role of Solvent on the Silanization of Glass with Octadecyltrichlorosilane. *Langmuir* **1994**, *10* (10), 3607–3614. https://doi.org/10.1021/la00022a038.

(15) Fadeev, A. Y.; McCarthy, T. J. Self-Assembly Is Not the Only Reaction Possible between Alkyltrichlorosilanes and Surfaces: Monomolecular and Oligomeric Covalently Attached Layers of Dichloro- and Trichloroalkylsilanes on Silicon. *Langmuir* **2000**, *16* (18), 7268–7274. https://doi.org/10.1021/la000471z.

(16) ARKLES, B.; B, A. TAILORING SURFACES WITH SILANES. *TAILORING Surf. SILANES* **1977**.

(17) Coats, A. W.; Redfern, J. P. Thermogravimetric Analysis. A Review. *Analyst* **1963**, *88* (1053), 906–924. https://doi.org/10.1039/AN9638800906.

(18) Engelhard, M. H.; Droubay, T. C.; Du, Y. X-Ray Photoelectron Spectroscopy Applications. In *Encyclopedia of Spectroscopy and Spectrometry (Third Edition)*; Lindon, J. C., Tranter, G. E., Koppenaal, D. W., Eds.; Academic Press: Oxford, 2017; pp 716–724. https://doi.org/10.1016/B978-0-12-409547-2.12102-X.

(19) Fowkes, F. M. ATTRACTIVE FORCES AT INTERFACES. *Ind. Eng. Chem.* **1964**, *56* (12), 40–52. https://doi.org/10.1021/ie50660a008.

(20) Owens, D. K.; Wendt, R. C. Estimation of the Surface Free Energy of Polymers. *J. Appl. Polym. Sci.* **1969**, *13* (8), 1741–1747. https://doi.org/10.1002/app.1969.070130815.

(21) Rabel, W. Einige Aspekte Der Benetzungstheorie Und Ihre Anwendung Auf Die Untersuchung Und Veränderung Der Oberflächeneigenschaften von Polymeren. *Farbe Lack* **1971**, *77* (10), 997–1005.

(22) Kaelble, D. H. Dispersion-Polar Surface Tension Properties of Organic Solids. *J. Adhes.* **1970**, *2* (2), 66–81. https://doi.org/10.1080/0021846708544582.

(23) Good, R. J.; van Oss, C. J. The Modern Theory of Contact Angles and the Hydrogen Bond Components of Surface Energies. In *Modern Approaches to Wettability: Theory and Applications*; Schrader, M. E., Loeb, G. I., Eds.; Springer US: Boston, MA, 1992; pp 1–27. https://doi.org/10.1007/978-1-4899-1176-6_1.

(24) Wu, S. Calculation of Interfacial Tension in Polymer Systems. *J. Polym. Sci. Part C Polym. Symp.* **1971**, *34* (1), 19–30. https://doi.org/10.1002/polc.5070340105.

(25) Rudawska, A. *Surface Treatment in Bonding Technology*; Academic Press, 2019.

Chapter 3

From smooth to nanostructured omniphobic surfaces

A glance to anti-icing and self-cleaning properties

Based on the article: Fenero et al. Omniphobic etched aluminum surfaces with anti-icing ability. Langmuir 2020, 36 (37), 10916–10922.

3.1 INTRODUCTION

As previously introduced, the wetting properties of materials depend on a variety of surface characteristics, of which the surface morphology (together with low SFE materials) has a major influence. Since the modification of the surface morphology allows tuning the wettability properties of the materials, surface structuration has been extensively investigated as a powerful strategy to create singular functionalities such as self-cleaning,[1] antireflective,[2] low-friction[3] or enhanced adhesion.[4] Benefiting from the potential of nanotechnology to construct tailor-made structures, a large amount of surfaces with morphologies designed at the nanoscale level have been developed. A broad range of micro- and nanostructure fabrication techniques, including lithography,[5,6,7] etching[8] and deposition,[9,10] have been used for this purposes. Among them, etching has proven to be a fast and effective way to obtain rough surfaces with a structured morphology through either plasma,[11] laser,[12] chemical,[13,14] or electrochemical[15] methods.

Water repellent surfaces that base on morphological effects are prone to contamination by oils or dust particles that may adversely affect their performance. As described in **Chapter 1**, omniphobic surfaces offer the potential to repel high and low surface tension liquids, including water, oils and alcohols.[16,17] Designing omniphobic surfaces has attracted interest in recent years due to their broad impact on industrial applications, including self-cleaning,[18,19,20] anti-fouling,[21] water-oil separation[22] and anti-icing.[23,24,25] An interesting strategy to engineer such surfaces involves the generation of structures and their subsequent chemical modification by applying a low SFE material to render omniphobic properties. To achieve this, perfluorocarbon compounds are among the most widely used materials due to the presence of CF_2 and CF_3 groups, which show the lowest possible surface energy.

Ice formation and accretion on solid surfaces is a complex phenomenon causing serious problems in so many aspects of the daily life including, driving safety, aircrafts, power lines, or wind turbines. The impact of the surface on safety risks and the economy is huge. According to the United States National Highway Traffic Safety Administration

(NHTS) data, approximately 21% of vehicle accidents are related to weather conditions and average statics show that annually more than 150,000 accidents occur because of icy roads.[26] Electrical power lines often suffer failures due to excessive ice loading[27] and ice accumulated on wings of aircrafts induces negatively or even catastrophically affects the aerodynamic performance disrupting laminar airflows and decreasing the lift force.[28] Additionally, icing of wind turbine blades can reduce the annual wind energy conversion by 50%.[29]

Functionalizing surfaces to prevent icing (anti-icing) and to repel ice (ice-phobic) (also referred to as *passive methods*) became greatly interesting for both fundamental research and industrial applications to reduce the machinery and energy consumptions associated with traditional de-icing strategies (also known as *active methods*). *Passive methods* delay icing formation and accretion and lower the ice adhesion. To address this icing challenge, research efforts are mainly focused on three technologies: 1) low SFE coatings, which includes superhydrophobic (associated to surface structuration) or omni(hydro)phobic surfaces, based on their extraordinary water repellent ability,[30] 2) SLIPS, based on low SFE and mostly on the reduction of the ice adhesion strength by the presence of a thin lubricant film on the surface[31] and 3) Low Interfacial Toughness (LIT) materials based on crack formation between ice and the surface, allowing its easy detachment.[32]

The low SFE of omniphobic surfaces may benefit anti-icing behaviour by delaying the freezing time of water droplets and/or repelling water droplets from the surface before freezing starts. The use of perfluorinated compounds is widely proposed for obtaining such low SFE surfaces. However, this family of compounds causes a number of environmental issues.[33] Indeed, the use of perfluorinated molecules with chains longer than eight carbon atoms has been limited for several applications due to their toxicity, high persistence and bioaccumulation.[34] Therefore, to achieve persistent liquid repellence for various applications, omniphobic surfaces, based on alternative low SFE compounds, are sought for.[34]

Omniphobic surfaces with covalently anchored PFPEs, able to repel any type of liquids, including water droplets, appear to be excellent candidates to address the above-mentioned issues.[35] Indeed, the use of PFPEs has been investigated as an environmentally safe substitute for the traditional perfluorinated molecules on smooth surfaces[36,37] or forming hybrid sol-gel coatings.[38,39] However, a direct covalent anchoring of PFPE molecules on tailor-made nanostructured surfaces is still unexplored.

Encouraged by the scenario described above, in this chapter, a method to develop omniphobic aluminum surfaces with anti-icing and self-cleaning properties, combining chemical etching and surface modification, is reported. Aluminum has been selected as substrate for this development for its relevance for the current and future industrial products. Its low specific weight, excellent thermal and electrical conductivity and its low cost made aluminum one of the most used metals in materials engineering. Examples can be found as structural component in aircraft and automotive industries, in electrical conductivity applications like overhead electrical wires and electronic components, or machinery tools with moving parts. During the development of this work, a hierarchical micro/nanostructuring of the aluminum surface was carried out through chemical etching with ferric chloride. Subsequently, the surface was modified with perfluoro(polypropyleneoxy)methoxypropyltrimethoxysilane, an environmentally safe and non-toxic low SFE compound, in order to provide the omniphobic properties to the system. The wetting behaviour of the developed surfaces and their relation to the surface roughness and chemical composition is discussed in this work. The obtained omniphobic surfaces are tested against various liquids in order to characterize their omniphobicity. More importantly, we show for the first time that a PFPE, directly attached to the substrate, provides anti-icing properties. The freezing delay of water droplets and the ice formation process are analyzed to assess the anti-icing performance. In the same way, the anti-icing performance of perfluorinated-grafted aluminum using a standard perfluorinated molecule (perfluorooctyltriethoxysilane, PF) is included at the end of **section 1.3.4.1** for comparative purposes.

3.2 EXPERIMENTAL SECTION

3.2.1 Materials

The used substrate was a 1050 aluminum alloy (provided by Alu stock) with a chemical composition of Al: 99.08 % min, Mg: ≤ 0.05 %, Mn: ≤ 0.05 %, Fe: ≤ 0.40 %, Si: ≤ 0.25 %, Cu: ≤ 0.05 %, Zn: ≤ 0.07 %, Ti: ≤ 0.05 %. Ferric chloride hexahydrate (98%) and hexadecane (98%) were purchased from Sigma-Aldrich. Hydrochloric acid (37%), ethanol (96%) and acetone (96%) were purchased from Scharlab. Perfluoro(polypropyleneoxy)methoxypropyltrimethoxysilane (PFPE, 20% in fluorinated hydrocarbon) was purchased from Gelest. Perfluorotripentylamine (FC-70, 85%) was acquired from Apollo Scientific. Millipore water with a conductivity of 0.054 µS/cm was used in all experiments. All reagents were used as received.

3.2.2 Methods

3.2.2.1 Chemical etching

Before the chemical etching, the aluminum substrates were washed with soap and thoroughly rinsed with millipore water, followed by sonication in acetone, ethanol and deionized water for 10 minutes each at room temperature. Subsequently, chemical etching of the cleaned substrates was performed by immersion into a 14 wt. % aqueous ferric chloride solution at 50 °C for various periods of time.[40] After etching, the samples were cleaned by sonication in isopropyl alcohol for 10 minutes and dried in a nitrogen gas stream.

3.2.2.2 Surface modification

Functionalization of pristine substrates and etched aluminum samples with PFPE was performed by drop-casting a 0.1 wt. % PFPE dispersion in FC-70. Special care has been taken that the surface of the sample was completely covered by the dispersion. After that, the samples were stored in an oven with saturated humidity conditions at 60 °C during 3 hours to promote the hydrolysis of the PFPE molecules. Finally, an additional thermal treatment at 100 °C was carried out for 3 hours.

3.2.3 Surface characterization

The surface morphology of the samples was analysed using an ULTRA plus FESEM from ZEISS. The examinations were carried out at 7 kV accelerating voltage. Topographical surface images were captured using a Leica DCM 3D confocal microscope. The surface roughness of the samples was examined using a Talysur 50 mm Intra Taylor Hobson profilometer. The average of the surface roughness values was obtained by measuring at ten different positions.

FTIR spectra of the samples were obtained with a PerkinElmer Frontier spectrometer equipped with an ATR sampling stage. The spectra were acquired from 20 scans from 800 cm^{-1} to 4000 cm^{-1} and a resolution of 4 cm^{-1}.

The surface composition of pristine and treated surfaces was analysed by XPS. The experiments were performed using a SPECS instrument equipped with a hemispherical electron analyser and a monochromatized source of Al K_α X-rays. The calibration of the energy scale in all spectra was done by positioning the binding energy of the characteristic C 1*s* peak at 284.5 eV. The XPS spectra were deconvoluted into several sets of mixed Gaussian-Lorentzian (G-L) functions with Shirley background subtraction.[41]

An Attension Theta Lite optical tensiometer was used to determine the CAs of the films. Droplets of solvents were placed on a minimum of three different areas of the surface. The CA_s were recorded using the Laplace-Young fitting method. The total SFE of the coatings was determined according to the Fowkes model using water and ethylene glycol as polar liquids and diiodomethane as non-polar liquid.

The anti-icing experiments were carried out with an optical tensiometer. A fluid circulating cooling stage and the measuring chamber accessories were coupled to the equipment for temperature control and environmental protection, respectively. To determine the freezing delay time, the cooling stage temperature was decreased from room temperature to -11 °C and the sample was placed over it. Once this temperature was reached, the sample was preconditioned for 10 minutes. Afterwards, a 5 µL droplet of deionized water was placed on the cooled aluminum surface. The time at which the

water droplet started to freeze was considered as freezing delay time. To evaluate the ice formation and accretion process, the substrates were fixed to the cooling stage with a tilted angle of 10° and allowed to cool down to -10 °C. A 5 µL droplet of deionized water was placed onto the aluminum surface. All experiments were monitored through the images obtained from the high-speed camera of the optical tensiometer equipment.

The omniphobic performance of the surfaces was evaluated by testing their ability to repel methylene blue-dyed water and olive oil droplets. The self-cleaning performance of the omniphobic surfaces was evaluated by testing their ability to repel water tinted with methylene blue and olive oil droplets, as well as, by immersion in a tank containing motor oil with molybdenum disulphide nanoparticles.

3.3 RESULTS AND DISCUSSION

3.3.1 Surface morphology

As a first step, the etching time was optimized in order to induce superhydrophobicity by the generation of micro-nanoscale roughness on the aluminum surface. This was achieved by immersion in a ferric chloride solution as described in **section 1.2.2.1**. After proceeding with a systematic study by varying the immersion time and the bath temperature, the optimal experimental conditions were identified to be 20 minutes etching at 50 °C, as shown in **Figure 3.1**.

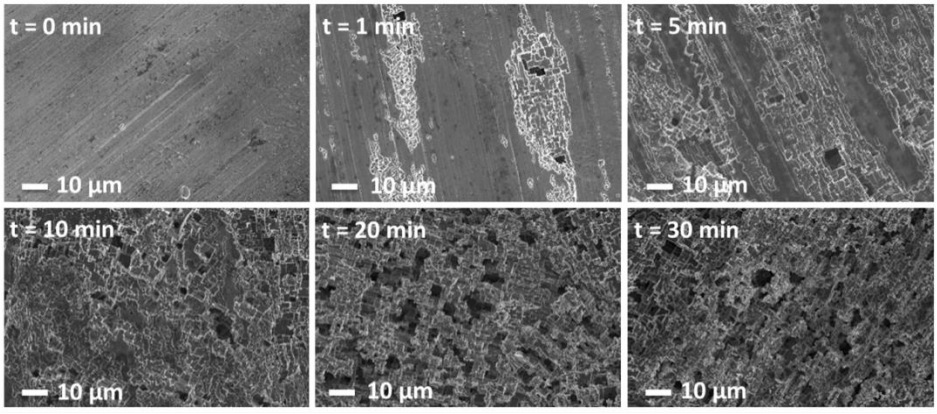

Figure 3.1. FESEM micrographs of pristine aluminum and aluminum surfaces after chemical etching with 14 wt. % aqueous ferric chloride solution at 50 °C during different periods of time as indicated in the images.

The surface morphology of the aluminum samples was analysed by FESEM images at different magnifications (**Figure 3.2**). A relatively smooth surface (R_a = 0.401 ± 0.036 µm and R_z = 2.639 ± 0.707 µm determined by profilometer) without the presence of significant structured motifs was observed for the pristine aluminum (**Figure 3.2a**,**b**). In contrast, rectangular micro- and nanoscale features, uniformly distributed over the surface, were observed on the samples etched under optimal etching conditions (**Figure 3.2c**). At higher magnification (**Figure 3.2d**) the formation of iron spherulites could be observed, which increased the surface roughness (R_a = 1.084 ± 0.347 µm and R_z = 8.071 ± 2.498 µm) and generated a hierarchical structure, as previously reported by Maitra *et al.*[40]

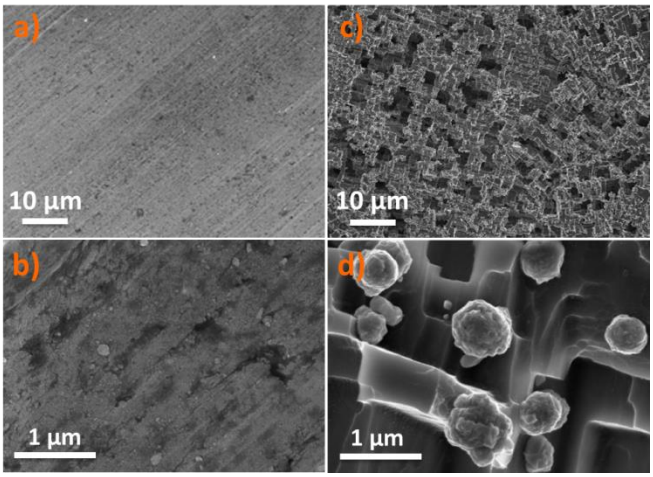

Figure 3.2. a) Low and b) high magnification FESEM micrographs of pristine aluminum substrate. c) Low and b) high magnification FESEM micrographs of the aluminum surface after chemical etching using 14 wt. % ferric chloride aqueous solution for 20 minutes at 50 °C.

In addition to FESEM micrographs, 3D topographical images (**Figure 3.3**) and the roughness analysis in terms of R_a and R_z shown in **Table 3.1** confirmed the increase of the surface roughness with the etching time, up to 20 minutes. Note that a further increase in etching time (30 min) leads to a reduction of the surface roughness which is attributed to a greater content of spherulites.

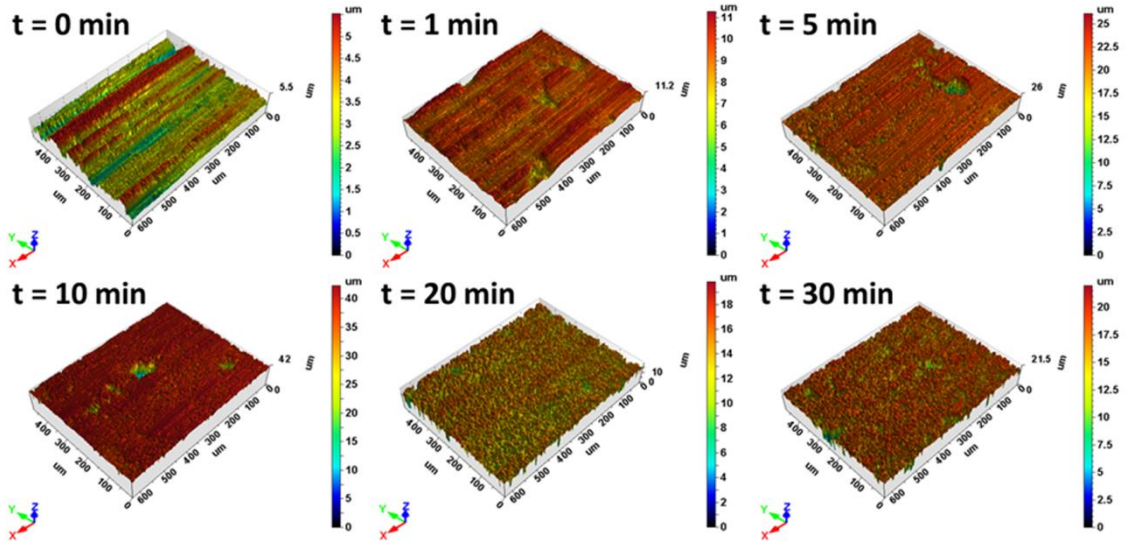

Figure 3.3. 3D topographical images of pristine aluminum and aluminum surfaces after chemical etching with 14 wt. % aqueous ferric chloride solution at 50 °C during different periods of time.

Table 3.1. Surface roughness (Ra and Rz) of pristine aluminum and aluminum surfaces after chemical etching with 14 wt. % aqueous ferric chloride solution at 50 °C during different periods of time.

	Etching time (min)					
	0	**1**	**5**	**10**	**20**	**30**
R_a (µm)	0.401 ± 0.036	0.407 ± 0.050	0.498 ± 0.121	0.646 ± 0.149	1.084 ± 0.347	0.742 ± 0.085
R_z (µm)	2.639 ± 0.707	2.980 ± 0.763	4.066 ± 1.174	6.749 ± 2.292	8.071 ± 2.498	6.771 ± 2.054

3.3.2 Chemical modification

As the next step, the corrugated surface was subjected to chemical modification with PFPE in order to reduce the SFE. The grafting of PFPE to the aluminum surface was evaluated by ATR-FTIR and XPS. ATR-FTIR spectra of a pristine aluminum substrate and a PFPE film grafted onto a rough aluminum substrate are shown in **Figure 3.4a**. Characteristic absorption peaks of CF_2 and CF_3 groups, corresponding to the stretching vibration of C-F bonds, were observed between 1150 cm^{-1} and 1200 cm^{-1}.[37] The peak at 1006 cm^{-1} can be assigned to the etheric C-O-C bond. The presence of these characteristic bands is in agreement with those of pure PFPE and confirm the presence of PFPE molecules on the surface of the rough aluminum substrate. Similar absorption bands were obtained for the PFPE deposited on smooth aluminum (**Figure 3.4c**), which confirms the successful surface functionalization. However, the observed sloping down of the

baseline on the rough sample indicates a difference to the smooth substrate. This sloping was attributed to the scattering of the light on the rough surface.

In addition to the ATR-FTIR analysis, XPS spectroscopy was used in order to gain more insight into the chemical surface composition. **Figure 3.4b** shows the photoemission spectra of the PFPE film, grown on the etched aluminum substrate, around the C 1*s* core level. The C 1*s* emission exhibits a number of components originating from different carbon bonds of different relative concentrations. Eight contributions were employed for the Gaussian-Lorentzian (G-L) deconvolution to obtain a good fit of the experimental spectra. The photoemission from the PFPE-modified surface is dominated by the set of bonds related to the C-F complexes characteristic for PFPE. We assign the three peaks (peaks 2, 3, and 4), at the binding energy (BE) of 293.3eV, 291.0 eV and 289.05 eV, to the characteristic C-F_3, C-F_2 and O-CH_2-O bonds, respectively, in good agreement with the literature.[42,43] Peak 1, at 292.4 eV, can be assigned to the C 1*s* emission from carbon F_2C-O bonds, while the feature on the lower BE side (peak 8) corresponds to the C-Si bonds.[44,45] Besides, three carbon-related components characteristic for contaminated surfaces, were also detected: C-C/C-H, C-O and C=O bonds at 284.5 eV, 285.95 eV and 287.75 eV, respectively (peaks 7, 6 and 5). The major contribution of these peaks (especially peaks 5 and 7) in the spectrum obtained from smooth surfaces (that is from non-etched and, consequently, more polluted surface) (**Figure 3.4d**) supports the hypothesis of surface carbon contamination as the main origin of the peaks 5-7. The presence of CF_3, CF_2, CF_2-CH_2 or O-CF_2 bonding combinations reveals the functionalization of aluminum surfaces with fully grown PFPE films.

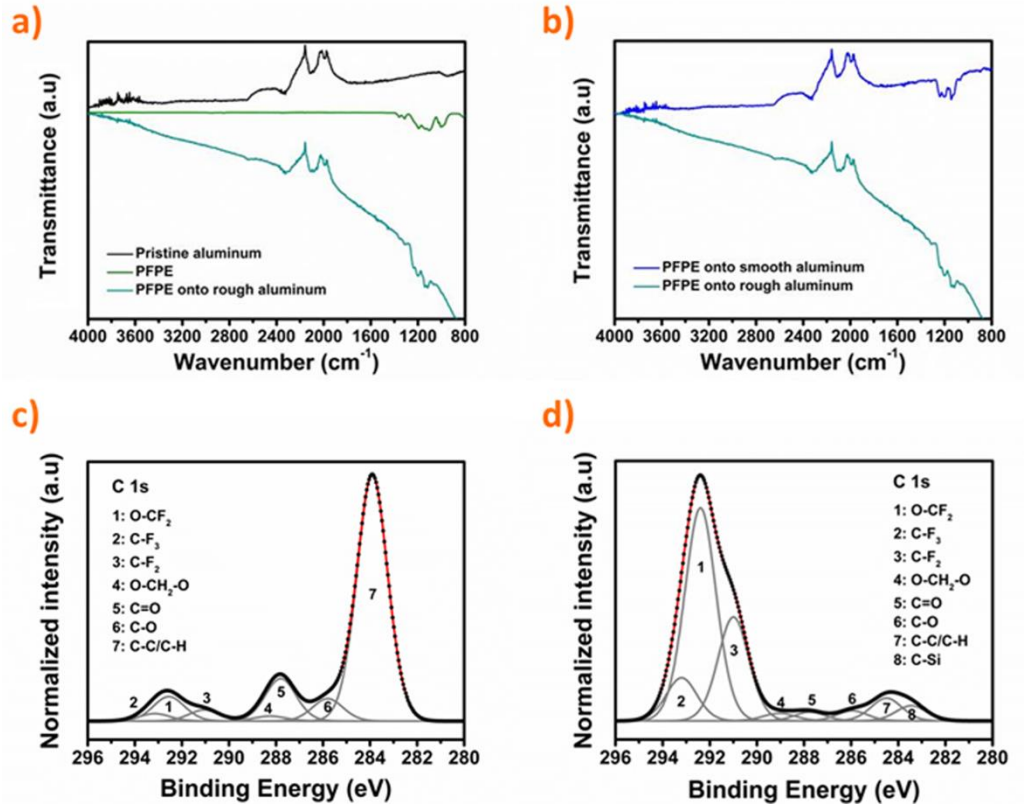

Figure 3.4. a) ATR-FTIR spectra of unmodified aluminum substrate (black), PFPE deposited onto a rough aluminum substrate (cyan) and pure PFPE (green). b) XPS spectrum around C 1*s* core levels of PFPE film deposited onto a rough aluminum substrate. c) ATR-FTIR spectra of PFPE deposited onto smooth (blue) and rough (cyan) aluminum surfaces. d) XPS spectrum around C 1*s* core levels of PFPE film deposited onto smooth aluminum substrate.

3.3.3 Wetting properties

It is well known that the wettability of materials depends on both, the chemical composition, and the surface roughness. The effect of the PFPE surface grafting to aluminum substrates and the chemical etching modification to induce the surface roughness, was evaluated through CA measurements. **Figure 3.5a** and **Table 3.2** show the results obtained using water and hexadecane as liquid probes in order to evaluate the wetting and omniphobicity of the prepared surfaces. Pristine and PFPE-modified aluminum substrates were subjected to water and oil repellence tests. As expected, the water and hexadecane CA for the pristine aluminum significantly increased from 70° to 116° and from <10° to 68°, respectively, after PFPE grafting. Therefore, the wetting properties of aluminum changed from superomniphilic to omniphobic. This was attributed to the presence of -CF_2 and -CF_3 groups from the PFPE, which again confirms

the surface functionalization. In addition, a strong relationship between the surface roughness and the CA was observed. The influence of the structuring of the aluminum surfaces was studied by chemical etching during different periods of time (**Figure 3.1**). After PFPE grafting of the etched substrates, short etching times (1 minute) did not show any influence on the CA values. This fact is consistent with the observed surface morphology of the sample (**Figure 3.1**), which was rather smooth with only small regions with structural motifs. Increasing the etching time progressively increased the CA, reaching considerably high values, such as 160° in the case of water and 141° for hexadecane, for samples which underwent 20 minutes of etching treatment. In order to gain further insight into the liquid-solid interactions, the SFE of the various surfaces was determined. In general, the wettability of a solid by a liquid is reduced by lowering its SFE. Besides, it is important to take into account the nature of the SFE components, because they strongly affect the liquid-solid interactions.[46] According to the Fowkes model, the SFE can be defined as a sum of its polar and dispersive components and the contribution of each of them to the total SFE determines the affinity of a surface to liquids, depending on their polar or non-polar nature.[47] **Figure 3.5b** and **Table 3.3** display the determined SFE of the different surfaces and the contribution of their polar and non-polar components. As expected, the SFE of the pristine aluminum (39.22 mN/m) was reduced after the PFPE modification (10.80 mN/m). A further reduction in SFE was observed from the etched samples, proving a direct correlation between the reduction of the SFE and the increased surface roughness, monitored by the etching time. Note the extremely low SFE of samples etched during 20 and 30 min., reaching values as low as 1.8 mN/m and 0.3 mN/m, respectively. An important observation is that, after modification, the contribution of the polar component to the total SFE is very low, almost negligible, as can be seen in **Figure 3.5b**. This means that lowering the affinity of a surface to a liquid is more strongly expressed with polar liquids like, for example, water. This insight consequently suggests the potential of the developed samples as an efficient anti-icing substrate.

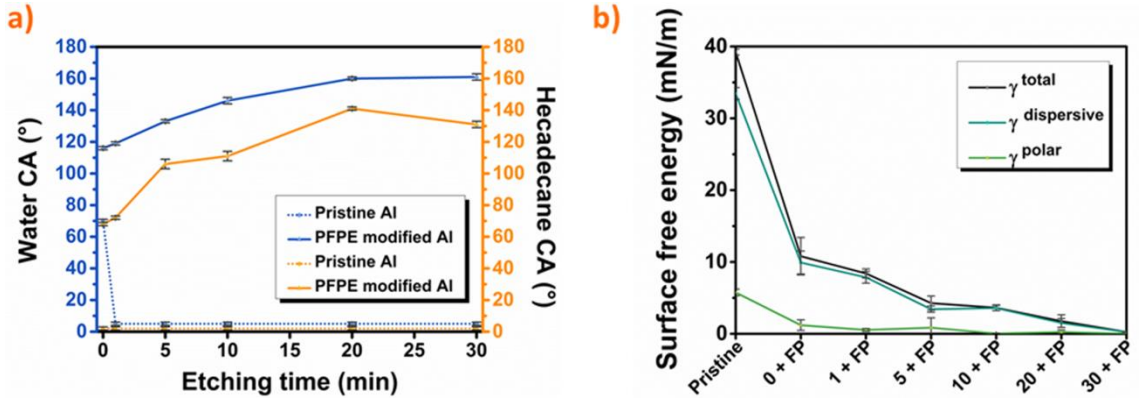

Figure 3.5. a) Static contact angles observed for pristine aluminum and PFPE-modified aluminum before and after chemical etching during different etching times. b) Total surface free energy and its dispersive (non-polar) and polar components determined using the Fowkes model for pristine aluminum, PFPE-modified aluminum and PFPE-modified aluminum after chemical etching treatment during different etching times. The numbers x + PFPE indicate the etching times (in minutes).

Table 3.2. Static contact angle values observed for pristine aluminum and PFPE-modified aluminum before and after chemical etching during different etching times.

	Pristine aluminum		PFPE-modified aluminum	
Etching time (min)	**CA_{water} (°)**	**$CA_{hexadecane}$ (°)**	**CA_{water} (°)**	**$CA_{hexadecane}$ (°)**
0	70 ± 1	< 10	116 ± 1	68 ± 1
1	< 10	< 10	119 ± 1	72 ± 1
5	< 10	< 10	133 ± 1	106 ± 3
10	< 10	< 10	146 ± 2	111 ± 3
20	< 10	< 10	160 ± 1	141 ± 1
30	< 10	< 10	161 ± 2	131 ± 2

Table 3.3. Total surface free energy and its dispersive (non-polar) and polar components determined using the Fowkes model for pristine aluminum, PFPE-modified aluminum and PFPE-modified aluminum after chemical etching treatment during different etching times.

	Surface energy (mN/m)		
Sample	**Υ^{total} (mN/m)**	**$\Upsilon^{dispersive}$ (mN/m)**	**Υ^{polar} (mN/m)**
Reference	39.22 ± 0.40	33.46 ± 0.82	5.76 ± 0.46
0	10.80 ± 2.61	9.91 ± 1.60	1.20 ± 0.74
1	8.40 ± 0.63	7.87 ± 0.81	0.53 ± 0.19
5	4.27 ± 0.99	3.42 ± 0.43	0.85 ± 1.37
10	3.63 ± 0.40	3.59 ± 0.36	0.04 ± 0.02
20	1.76 ± 0.88	1.50 ± 0.63	0.26 ± 0.25
30	0.26 ± 0.02	0.25 ± 0.02	0.01 ± 0.00

3.3.4 Potential applications

3.3.4.1 Anti-icing performance of omniphobic coatings

The weak interaction of the surface and polar liquids, such as water, may benefit the anti-icing performance of the developed omniphobic surfaces. Therefore, the freezing delay time and the ice formation from impinging droplets were evaluated, as depicted in **Figure 3.6**. The freezing delay time of water droplets was determined on both smooth and rough aluminum substrates, modified by PFPE, along with the pristine aluminum substrate, in order to evaluate the influence of the surface roughness on the freezing time. **Figure 3.6b** shows the evolution of a 5 µL water droplet, placed onto the three different samples, from the liquid state to the frozen state. In all three samples, the water droplet showed similar behaviour. In liquid state the droplet was transparent. The start of the freezing process was identified by the reduction of the transparency of the droplet. After freezing, the shape of the droplet changed showing a tip on the top of the droplet (**Figure 3.6a**). The time needed for the droplet to freeze was significantly different for each surface (**Figure 3.6b** and **Table 3.4**). In the case of the pristine aluminum substrate, the droplet became completely frozen in 260 seconds, while on the smooth PFPE-functionalized aluminum surface it took 780 seconds. In contrast, for the rough PFPE-modified aluminum, the time until freezing of the droplet was 5100 seconds, considerably more than with the other two samples. The significant increase in the freezing time can be related to two different effects. On the one hand, the SFE of the pristine aluminum was reduced from 39.22 mN/m to 10.80 mN/m after modification with PFPE (smooth aluminum functionalized with PFPE). This SFE reduction, together with the low contribution of the polar component to the total SFE, lowered the affinity between the water droplet and the material surface, giving rise to an increase in the freezing delay time. The time required for a water droplet to freeze on the low SFE sample was 780 seconds, thereby 3-fold that on pristine aluminum (260 seconds). On the other hand, the surface morphology also played an important role in the increase of freezing time. With 5100 seconds, the freezing time on rough and PFPE-modified aluminum outperformed the freezing times on the other investigated surfaces. This remarkable increase of the freezing time by a factor of more than 6 was achieved by corrugation when compared to

the smooth PFPE-modified. Furthermore, an almost 20-fold delay in the freezing time was achieved versus the pristine aluminum substrate by combining the surface structuring and PFPE-modification. This behaviour is attributed to the thermal conductivity. The thermal conductivity is related to the contact area between two phases, in this case, between the substrate surface and the droplet surface.[48] On smooth surfaces, the contact area is maximized, in dependence on the wettability, thus the thermal conduction is also maximized. Consequently, the droplet freezes quickly on smooth surfaces. In contrast, if the droplet is placed onto a surface with a structured morphology in the Cassie-Baxter wetting regime, air will be trapped below the water droplet, thereby minimizing the contact area between the surfaces of the substrate and water droplet. The air trapped in the surface cavities is a poor thermal conductor and together with the reduction of the contact area, will considerably hinder the heat transfer between the substrate and the liquid, significantly delaying the freezing time of the droplet. Furthermore, ice formation from impacting droplets was evaluated on the three different samples, as shown in **Figure 3.6c**. The experiment was carried out by tilting the substrates to 10° at a temperature of -10 °C and dropping one water droplet on the surface of each sample. As expected from the wettability, and according to the literature,[49] the hydrophilic nature of the pristine aluminum substrate allowed the incoming water droplet to rest in contact with the surface, promoting the ice nucleation and the subsequent droplet freezing (**Figure 3.6c i**). On the PFPE-modified smooth aluminum (**Figure 3.6c ii**), despite reduced interaction, the water droplet remains in contact with the surface and the freezing process occurs in a short period of time. However, on the rough PFPE-modified aluminium (**Figure 3.6c iii**), the impinging droplet fully bounced off of the surface before the ice nucleation started, thus preventing the ice formation. The above results verify the significantly greater efficiency of the rough, PFPE-modified aluminum surface in the prevention of the ice formation than the pristine aluminum. Hence, the freezing delay time and the ice formation experiments shown in **Figure 3.6** confirm the great potential of the developed omniphobic surface as an anti-icing solution.

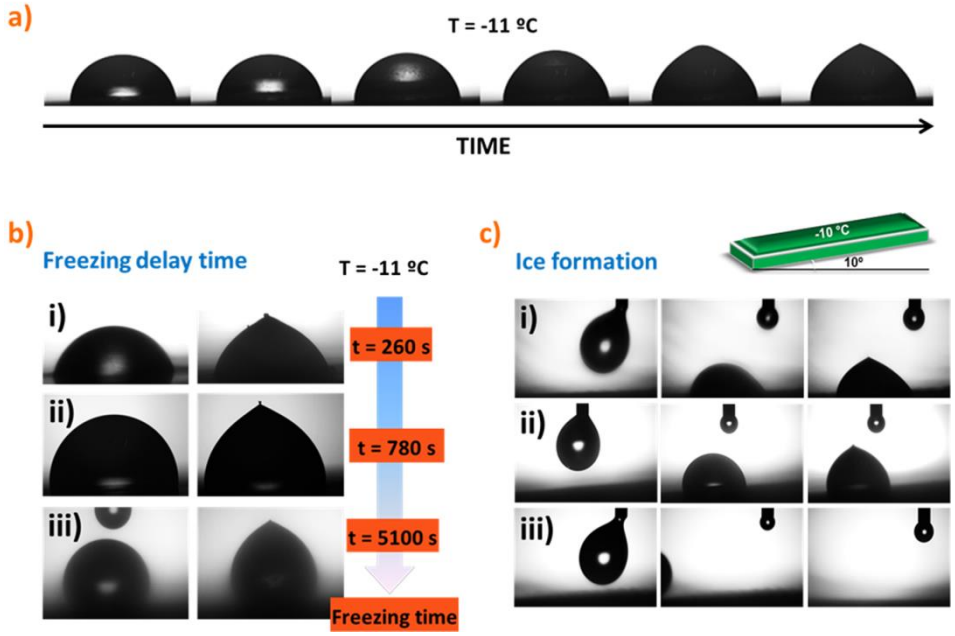

Figure 3.6. Anti-icing properties. a) Time-sequential images showing the freezing process of a water droplet. b) Freezing delay time and c) ice formation on: i) Pristine aluminum, ii) PFPE-grafted smooth aluminum, iii) PFPE-grafted rough aluminum.

To evaluate the effectiveness of this novel anti-icing system based on an environmentally safe and PFPE-grafted aluminum, another anti-icing system, employing a traditional perfluorinated compound (perfluorooctyltriethoxysilane, PF), was developed and compared to the PFPE anti-icing system. The PF system was anchored to the aluminium substrate in a similar morphological strategy as PFPE. Hereafter, its anti-icing performance was evaluated. The freezing delay time was determined for PF grafted on smooth and rough aluminium (**Figure 3.7a** and **Table 3.4**). The same trend in the freezing delay time as observed for PFPE-grafted aluminium was obtained for the PF-grafted aluminium system, increasing the freezing time from 260 s to 729 s after grafting the perfluorooctylsilane to a smooth aluminum substrate, and to 4800 s after combination of hierarchical micro/nanostructuring and PF grafting. Furthermore, incoming water droplets on PF-grafted rough aluminium bounced off of the surface preventing water accumulation before freezing (**Figure 3.7b**). These results demonstrate the excellent anti-icing behaviour of PFPE-grafted and PF-grafted aluminium. It is worth noting that PFPE-grafted even slightly improved the performance of the traditional perfluorinated-based solutions, proving that PFPE could be a promising candidate to substitute the traditional PF molecules.

Figure 3.7. Freezing delay time (a) and ice formation (b) on PF-grafted rough aluminum.

Table 3.4. Freezing delay times determined for pristine aluminum, PFPE-grafted, and PF-grafted smooth and rough aluminum.

Sample	Freezing delay time (s)
Pristine Al	260 ± 15
PFPE-grafted smooth Al	780 ± 60
PFPE-grafted rough Al	5100 ± 125
PF-grafted smooth Al	729 ± 58
PF-grafted rough Al	4800 ± 100

In addition to assessing the anti-icing performance of the omniphobic surfaces against impinging water droplets, the frost formation from condensed droplets was also examined. The low-temperature icing experiments were carried out on the cooling stage at -5 °C with a RH of 60% ± 5%. As shown in **Figure 3.8**, condensed droplets start to appear within 10 minutes on the pristine aluminum, completely covering the surface after 20 minutes. The aluminum surface was completely covered by ice within 30 minutes. The same behavior was observed for PFPE-grafted smooth aluminum, however, the times required for the water droplets to condensate (30 minutes) and completely freeze (61 minutes) on the surface, were significantly higher. This fact was attributed to the lower SFE (i.e. less affinity for water) of these surfaces compared to that of the pristine aluminum. In contrast, tiny condensed droplets were observed on PFPE-grafted rough aluminum only after 60 minutes after beginning the essay. After 85 minutes, a layer of ice completely covered the surface. Note that this time is notably higher than observed from pristine aluminum (30 minutes) and PFPE-grafted smooth aluminum (61 minutes) surfaces. This significant delay in the ice formation is attributed to the low thermal conductivity derived from the low contact area between the droplet and the surface as consequence of the trapped air pockets on its hierarchical micro/nanostructuring.[50] Note that tinier droplets than those observed on both the pristine aluminum and PFPE-grafted smooth aluminum were noticed on PFPE-grafted rough aluminum. This finding suggests

the significant influence of the surface structure in hindering the coalescence process. This result reveals that the PFPE-grafted rough aluminum exhibits an increase in the icing delay time by almost 3-fold compared to pristine aluminum.

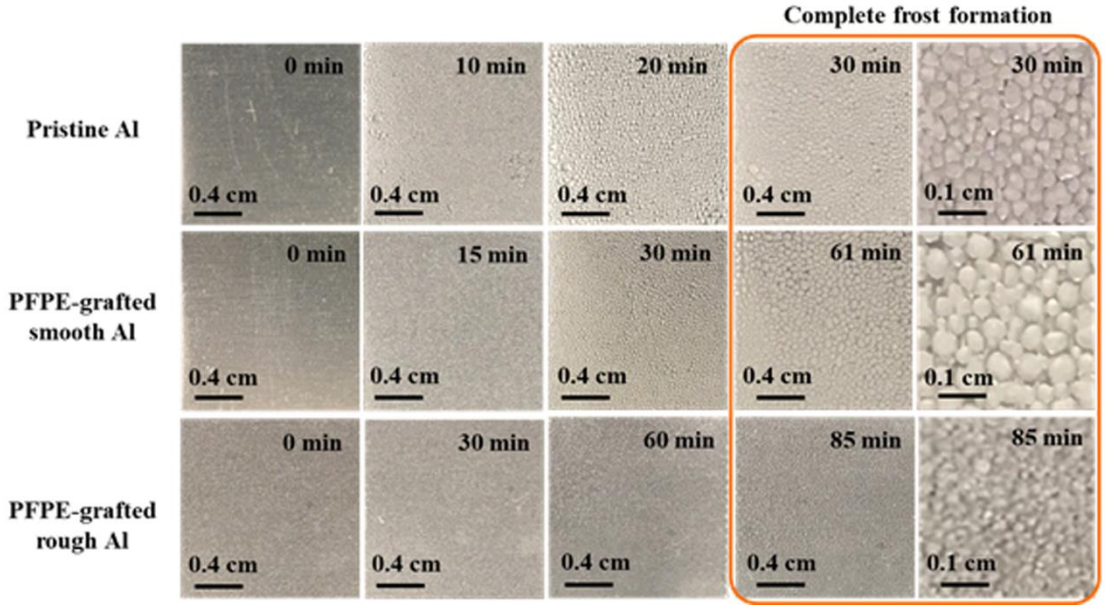

Figure 3.8. Time-lapse photographs showing the frost formation process on the different surfaces at a temperature of -5 ºC.

Nowadays, the durability of engineered surfaces is a challenging issue, in order to satisfy their industrial application requiring highly efficient and durable surfaces. In view of this, the durability of the anti-icing properties of the surfaces was evaluated by monitoring the evolution of their wetting properties through contact angle measurements after being subject to various freeze-thaw cycles, as depicted in **Table 3.5**. Contact angle values similar to those in the initial samples (prior to performing the freeze-thaw essay) were obtained.

Table 3.5. Water contact angles observed for PFPE-grafted rough aluminum after a series of freeze-thaw cycles.

	Number of freeze-thaw cycles					
	0	**1**	**2**	**3**	**4**	**5**
CA_{water} (°)	160 ± 2	157± 3	158 ± 2	156 ± 2	159 ± 2	158 ± 2

In addition, the freezing delay time of a droplet on the PFPE-modified aluminum surface has been determined three times on the same sample (**Table 3.6**), displaying a similar freezing delay time in all the essays.

Table 3.6. Freezing delay time determined for PFPE-grafted rough aluminum after a series of freeze-thaw cycles.

	Number of freeze-thaw cycles		
	0	**1**	**2**
Freezing delay time (s)	5210	4960	5050

These results demonstrate that the anti-icing performance is also maintained after several freeze-thaw cycles, proving the repeatability of the omniphobic samples.

3.3.4.2 Self-cleaning performance of omniphobic coatings

In addition to the anti-icing properties, the self-cleaning performance was also evaluated. In particular, the repelling ability against water and oils was verified (**Figure 3.9**). Omniphobic rough aluminum and pristine aluminium samples were tilted to an angle of 20° and water (**Figure 3.9a1**), olive oil (**Figure 3.9a2**) and Liqui Moly® 10W-40 motor oil, containing MoS_2 particles (**Figure 3.9a3**), droplets were deposited on the surface. In all three cases, the contaminant liquid easily slid down from the omniphobic coating without adhesion and without leaving a trace behind. In contrast, the liquid droplets remained well adhered to the pristine aluminium under identical conditions, demonstrating the well-expressed self-cleaning capability of the omniphobic surfaces. In addition, **Figure 3.9b** shows the self-cleaning ability of the omniphobic rough surface compared to the pristine aluminum substrate in more demanding conditions, like immersion, using Liqui Moly® 10W-40 motor oil additive, with MoS_2 particles, as contaminant. It is noteworthy that the omniphobic coating remained completely clean after the immersion in a tank with the motor oil. Nevertheless, the pristine aluminum substrate left the tank with its entire surface impregnated by the oil. Once again, this performance exhibited a great self-cleaning ability for the omniphobic surface.

Figure 3.9. a) Self-cleaning ability of omniphobic surfaces against: a1) methylene blue-tinted water, a2) olive oil and a3) Liqui Moly 10W-40 motor oil with MoS_2 particles. b) Oil self-cleaning test by immersion in Liqui Moly 10W-40 motor oil additive with MoS_2 particles tanks. Being i) pristine aluminum and ii) omniphobic aluminum.

3.4 CONCLUSIONS

The development of omniphobic aluminum surfaces by a simple 2-step method, which involves the fabrication of rough surfaces containing micro/nanostructures by chemical etching and further functionalization of the surface by grafting PFPE, was reported in this chapter.

This unique combination of tailored hierarchical nanostructured surfaces and chemical modification allowed to obtain low SFE surfaces with outstanding omniphobic

behaviour, including anti-icing (freezing delay time and ice formation) and self-cleaning properties. Excellent anti-icing capabilities have been proven for the optimized sample, which achieved a 20-fold delay in the water droplet freezing time, if compared to pristine aluminum, and showed the ability to repel incoming water droplets before ice nucleation occurs. The better performance achieved by the rough omniphobic surfaces, compared to the smooth omniphobic ones, highlights the beneficial effect of surface structuration. Moreover, the anti-icing capabilities exhibited by the PFPE-grafted rough aluminium are similar or even better than the similarly PF-grafted rough aluminum, proving the potential of the PFPE molecules (environmentally safe and non-toxic) to substitute the traditional PF compounds used for this purpose. Furthermore, the ability of these surfaces to repel any type of liquid reveals their great self-cleaning performance.

The experimental results, achieved with a low-cost and easily up-scalable process, make the reported approach a very promising solution for applications where anti-icing and self-cleaning are required or desired.

3.5 References

(1) Bhushan, B.; Koch, K.; Jung, Y. C. Biomimetic Hierarchical Structure for Self-Cleaning. *Appl. Phys. Lett.* **2008**, *93* (9), 093101. https://doi.org/10.1063/1.2976635.

(2) Nishijima, Y.; Komatsu, R.; Ota, S.; Seniutinas, G.; Balčytis, A.; Juodkazis, S. Anti-Reflective Surfaces: Cascading Nano/Microstructuring. *APL Photonics* **2016**, *1* (7), 076104. https://doi.org/10.1063/1.4964851.

(3) Ball, P. Engineering Shark Skin and Other Solutions. *Nature* **1999**, *400* (6744), 507–509. https://doi.org/10.1038/22883.

(4) Murphy, M. P.; Kim, S.; Sitti, M. Enhanced Adhesion by Gecko-Inspired Hierarchical Fibrillar Adhesives. *ACS Appl. Mater. Interfaces* **2009**, *1* (4), 849–855. https://doi.org/10.1021/am8002439.

(5) Wang, G.; Shen, Y.; Tao, J.; Luo, X.; Zhang, L.; Xia, Y. Fabrication of a Superhydrophobic Surface with a Hierarchical Nanoflake–Micropit Structure and Its Anti-Icing Properties. *RSC Adv.* **2017**, *7* (16), 9981–9988. https://doi.org/10.1039/C6RA28298A.

(6) Lin, Y.; Zhou, R.; Xu, J. Superhydrophobic Surfaces Based on Fractal and Hierarchical Microstructures Using Two-Photon Polymerization: Toward Flexible Superhydrophobic Films. *Adv. Mater. Interfaces* **2018**, *5* (21), 1801126. https://doi.org/10.1002/admi.201801126.

(7) Berwind, M. F.; Hashibon, A.; Fromm, A.; Gurr, M.; Burmeister, F.; Eberl, C. Rapidly Prototyping Biocompatible Surfaces with Designed Wetting Properties via Photolithography and Plasma

Polymerization. *Microfluid. Nanofluidics* **2017**, *21* (9), 144. https://doi.org/10.1007/s10404-017-1984-6.

(8) Xiu, Y.; Zhu, L.; Hess, D. W.; Wong, C. P. Hierarchical Silicon Etched Structures for Controlled Hydrophobicity/Superhydrophobicity. *Nano Lett.* **2007**, *7* (11), 3388–3393. https://doi.org/10.1021/nl0717457.

(9) Lin, D.; Zeng, X.; Li, H.; Lai, X.; Wu, T. One-Pot Fabrication of Superhydrophobic and Flame-Retardant Coatings on Cotton Fabrics via Sol-Gel Reaction. *J. Colloid Interface Sci.* **2019**, *533*, 198–206. https://doi.org/10.1016/j.jcis.2018.08.060.

(10) Huang, Z.; Gurney, R. S.; Wang, T.; Liu, D. Environmentally Durable Superhydrophobic Surfaces with Robust Photocatalytic Self-Cleaning and Self-Healing Properties Prepared via Versatile Film Deposition Methods. *J. Colloid Interface Sci.* **2018**, *527*, 107–116. https://doi.org/10.1016/j.jcis.2018.05.004.

(11) Dimitrakellis, P.; Gogolides, E. Hydrophobic and Superhydrophobic Surfaces Fabricated Using Atmospheric Pressure Cold Plasma Technology: A Review. *Adv. Colloid Interface Sci.* **2018**, *254*, 1–21. https://doi.org/10.1016/j.cis.2018.03.009.

(12) Huerta-Murillo, D.; García-Girón, A.; Romano, J. M.; Cardoso, J. T.; Cordovilla, F.; Walker, M.; Dimov, S. S.; Ocaña, J. L. Wettability Modification of Laser-Fabricated Hierarchical Surface Structures in Ti-6Al-4V Titanium Alloy. *Appl. Surf. Sci.* **2019**, *463*, 838–846. https://doi.org/10.1016/j.apsusc.2018.09.012.

(13) Safarpour, M.; Hosseini, S. A.; Ahadani-Targhi, F.; Vašina, P.; Alishahi, M. A Transition from Petal-State to Lotus-State in AZ91 Magnesium Surface by Tailoring the Microstructure. *Surf. Coat. Technol.* **2020**, *383*, 125239. https://doi.org/10.1016/j.surfcoat.2019.125239.

(14) Qian, X.; Tang, T.; Wang, H.; Chen, C.; Luo, J.; Luo, D. Fabrication of Hydrophobic Ni Surface by Chemical Etching. *Mater. Basel Switz.* **2019**, *12* (21). https://doi.org/10.3390/ma12213546.

(15) Ma, N.; Chen, Y.; Zhao, S.; Li, J.; Shan, B.; Sun, J. Preparation of Super-Hydrophobic Surface on Al–Mg Alloy Substrate by Electrochemical Etching. *Surf. Eng.* **2019**, *35* (5), 394–402. https://doi.org/10.1080/02670844.2017.1421883.

(16) Tuteja, A.; Choi, W.; Mabry, J. M.; McKinley, G. H.; Cohen, R. E. Robust Omniphobic Surfaces. *Proc. Natl. Acad. Sci. U. S. A.* **2008**, *105* (47), 18200–18205. https://doi.org/10.1073/pnas.0804872105.

(17) Hensel, R.; Neinhuis, C.; Werner, C. The Springtail Cuticle as a Blueprint for Omniphobic Surfaces. *Chem. Soc. Rev.* **2016**, *45* (2), 323–341. https://doi.org/10.1039/C5CS00438A.

(18) Lu, Y.; Sathasivam, S.; Song, J.; Crick, C. R.; Carmalt, C. J.; Parkin, I. P. Repellent Materials. Robust Self-Cleaning Surfaces That Function When Exposed to Either Air or Oil. *Science* **2015**, *347* (6226), 1132–1135. https://doi.org/10.1126/science.aaa0946.

(19) Ganesh, V. A.; Raut, H. K.; Nair, A. S.; Ramakrishna, S. A Review on Self-Cleaning Coatings. *J. Mater. Chem.* **2011**, *21* (41), 16304–16322. https://doi.org/10.1039/C1JM12523K.

(20) Fenero, M.; Palenzuela, J.; Azpitarte, I.; Knez, M.; Rodríguez, J.; Tena-Zaera, R. Laponite-Based Surfaces with Holistic Self-Cleaning Functionality by Combining Antistatics and Omniphobicity. *ACS Appl. Mater. Interfaces* **2017**, *9* (44), 39078–39085. https://doi.org/10.1021/acsami.7b13535.

(21) Zhang, P.; Lin, L.; Zang, D.; Guo, X.; Liu, M. Designing Bioinspired Anti-Biofouling Surfaces Based on a Superwettability Strategy. *Small Weinh. Bergstr. Ger.* **2017**, *13* (4). https://doi.org/10.1002/smll.201503334.

(22) Lee, J.; Boo, C.; Ryu, W.-H.; Taylor, A. D.; Elimelech, M. Development of Omniphobic Desalination Membranes Using a Charged Electrospun Nanofiber Scaffold. *ACS Appl. Mater. Interfaces* **2016**, *8* (17), 11154–11161. https://doi.org/10.1021/acsami.6b02419.

(23) Kreder, M. J.; Alvarenga, J.; Kim, P.; Aizenberg, J. Design of Anti-Icing Surfaces: Smooth, Textured or Slippery? *Nat. Rev. Mater.* **2016**, *1* (1), 1–15. https://doi.org/10.1038/natrevmats.2015.3.

(24) Zhang, S.; Huang, J.; Cheng, Y.; Yang, H.; Chen, Z.; Lai, Y. Bioinspired Surfaces with Superwettability for Anti-Icing and Ice-Phobic Application: Concept, Mechanism, and Design. *Small Weinh. Bergstr. Ger.* **2017**, *13* (48). https://doi.org/10.1002/smll.201701867.

(25) Wu, X.; Chen, Z. A Mechanically Robust Transparent Coating for Anti-Icing and Self-Cleaning Applications. *J. Mater. Chem. A* **2018**, *6* (33), 16043–16052. https://doi.org/10.1039/C8TA05692G.

(26) How Do Weather Events Impact Roads? - FHWA Road Weather Management https://ops.fhwa.dot.gov/weather/q1_roadimpact.htm (accessed May 4, 2020).

(27) Merrill, H. M.; Feltes, J. W. Transmission Icing: A Physical Risk with a Physical Hedge. In *2006 IEEE Power Engineering Society General Meeting*; 2006; pp 7 pp.-. https://doi.org/10.1109/PES.2006.1709619.

(28) Cao, Y.; Tan, W.; Wu, Z. Aircraft Icing: An Ongoing Threat to Aviation Safety. *Aerosp. Sci. Technol.* **2018**, *75*, 353–385. https://doi.org/10.1016/j.ast.2017.12.028.

(29) Lamraoui, F.; Fortin, G.; Benoit, R.; Perron, J.; Masson, C. Atmospheric Icing Impact on Wind Turbine Production. *Cold Reg. Sci. Technol.* **2014**, *100*, 36–49. https://doi.org/10.1016/j.coldregions.2013.12.008.

(30) Meuler, A. J.; McKinley, G. H.; Cohen, R. E. Exploiting Topographical Texture To Impart Icephobicity. *ACS Nano* **2010**, *4* (12), 7048–7052. https://doi.org/10.1021/nn103214q.

(31) Kim, P.; Wong, T.-S.; Alvarenga, J.; Kreder, M. J.; Adorno-Martinez, W. E.; Aizenberg, J. Liquid-Infused Nanostructured Surfaces with Extreme Anti-Ice and Anti-Frost Performance. *ACS Nano* **2012**, *6* (8), 6569–6577. https://doi.org/10.1021/nn302310q.

(32) Golovin, K.; Dhyani, A.; Thouless, M. D.; Tuteja, A. Low–Interfacial Toughness Materials for Effective Large-Scale Deicing. *Science* **2019**, *364* (6438), 371–375. https://doi.org/10.1126/science.aav1266.

(33) Lindstrom, A. B.; Strynar, M. J.; Libelo, E. L. Polyfluorinated Compounds: Past, Present, and Future. *Environ. Sci. Technol.* **2011**, *45* (19), 7954–7961. https://doi.org/10.1021/es2011622.

(34) Buck, R. C.; Franklin, J.; Berger, U.; Conder, J. M.; Cousins, I. T.; de Voogt, P.; Jensen, A. A.; Kannan, K.; Mabury, S. A.; van Leeuwen, S. P. J. Perfluoroalkyl and Polyfluoroalkyl Substances in the Environment: Terminology, Classification, and Origins. *Integr. Environ. Assess. Manag.* **2011**, *7* (4), 513–541. https://doi.org/10.1002/ieam.258.

(35) Janjic, J. M.; Srinivas, M.; Kadayakkara, D. K. K.; Ahrens, E. T. Self-Delivering Nanoemulsions for Dual Fluorine-19 MRI and Fluorescence Detection. *J. Am. Chem. Soc.* **2008**, *130* (9), 2832–2841. https://doi.org/10.1021/ja077388j.

(36) Masuko, M.; Ikushima, F.; Aoki, S.; Suzuki, A. Preliminary Study on the Tribology of an Organic-Molecule-Coated Touch Panel Display Surface. *Tribol. Int.* **2013**, *65*, 314–325. https://doi.org/10.1016/j.triboint.2013.01.019.

(37) Liu, Q.; Sun, Y.; Li, Z. Terminal Silanization of Perfluoropolyether, Polydimethylsiloxane, Their Block Polymer and the Self-Assembled Films on Plasma-Treated Silicon Surfaces. *Chem. Pap.* **2019**, *73* (1), 105–117. https://doi.org/10.1007/s11696-018-0547-y.

(38) Oldani, V.; Sergi, G.; Pirola, C.; Sacchi, B.; Bianchi, C. L. Sol-Gel Hybrid Coatings Containing Silica and a Perfluoropolyether Derivative with High Resistance and Anti-Fouling Properties in Liquid Media. *J. Fluor. Chem.* **2016**, *188*, 43–49. https://doi.org/10.1016/j.jfluchem.2016.06.005.

(39) Susoff, M.; Siegmann, K.; Pfaffenroth, C.; Hirayama, M. Evaluation of Icephobic Coatings—Screening of Different Coatings and Influence of Roughness. *Appl. Surf. Sci.* **2013**, *282*, 870–879. https://doi.org/10.1016/j.apsusc.2013.06.073.

(40) Maitra, T.; Antonini, C.; Mauer, M. A. der; Stamatopoulos, C.; Tiwari, M. K.; Poulikakos, D. Hierarchically Nanotextured Surfaces Maintaining Superhydrophobicity under Severely Adverse Conditions. *Nanoscale* **2014**, *6* (15), 8710–8719. https://doi.org/10.1039/C4NR01368A.

(41) Hesse, R.; Chassé, T.; Szargan, R. Peak Shape Analysis of Core Level Photoelectron Spectra Using UNIFIT for WINDOWS. *Fresenius J. Anal. Chem.* **1999**, *365* (1), 48–54. https://doi.org/10.1007/s002160051443.

(42) Kaynak, B.; Spoerk, M.; Shirole, A.; Ziegler, W.; Sapkota, J. Polypropylene/Cellulose Composites for Material Extrusion Additive Manufacturing. *Macromol. Mater. Eng.* **2018**, *303* (5), 1800037. https://doi.org/10.1002/mame.201800037.

(43) Wang, D.; Goel, V.; Oleschuk, R. D.; Horton, J. H. Surface Modification of Poly(Dimethylsiloxane) with a Perfluorinated Alkoxysilane for Selectivity toward Fluorous Tagged Peptides. *Langmuir ACS J. Surf. Colloids* **2008**, *24* (3), 1080–1086. https://doi.org/10.1021/la702038t.

(44) Gurav, A. B.; Guo, Q.; Tao, Y.; Mei, T.; Wang, Y.; Wang, D. Durable, Robust and Free-Standing Superhydrophobic Poly(Vinyl Alcohol-Co-Ethylene) Nanofiber Membrane. *Mater. Lett.* **2016**, *182*, 106–109. https://doi.org/10.1016/j.matlet.2016.06.086.

(45) Sansotera, M.; Navarrini, W.; Magagnin, L.; Bianchi, C. L.; Sanguineti, A.; Metrangolo, P.; Resnati, G. Hydrophobic Carbonaceous Materials Obtained by Covalent Bonding of Perfluorocarbon and Perfluoropolyether Chains. *J. Mater. Chem.* **2010**, *20* (39), 8607–8616. https://doi.org/10.1039/C0JM02077J.

(46) Song, K.; Lee, J.; Choi, S.-O.; Kim, J. Interaction of Surface Energy Components between Solid and Liquid on Wettability, and Its Application to Textile Anti-Wetting Finish. *Polymers* **2019**, *11* (3). https://doi.org/10.3390/polym11030498.

(47) Fowkes, F. M. ATTRACTIVE FORCES AT INTERFACES. *Ind. Eng. Chem.* **1964**, *56* (12), 40–52. https://doi.org/10.1021/ie50660a008.

(48) Tang, Y.; Zhang, Q.; Zhan, X.; Chen, F. Superhydrophobic and Anti-Icing Properties at Overcooled Temperature of a Fluorinated Hybrid Surface Prepared via a Sol-Gel Process. *Soft Matter* **2015**, *11* (22), 4540–4550. https://doi.org/10.1039/c5sm00674k.

(49) Mishchenko, L.; Hatton, B.; Bahadur, V.; Taylor, J. A.; Krupenkin, T.; Aizenberg, J. Design of Ice-Free Nanostructured Surfaces Based on Repulsion of Impacting Water Droplets. *ACS Nano* **2010**, *4* (12), 7699–7707. https://doi.org/10.1021/nn102557p.

(50) Barthwal, S.; Lim, S.-H. Rapid Fabrication of a Dual-Scale Micro-Nanostructured Superhydrophobic Aluminum Surface with Delayed Condensation and Ice Formation Properties. *Soft Matter* **2019**, *15* (39), 7945–7955. https://doi.org/10.1039/C9SM01256G.

Chapter 4

Nanoobjects as vectors to achieve omniphobicity

Towards multifunctional developments for a full self-cleaning

Based on the article: Fenero et al. Laponite-Based Surfaces with Holistic Self-Cleaning Functionality by Combining Antistatics and Omniphobicity. ACS Appl. Mater. Interfaces 2017, 9 (44), 39078–39085.

4.1 INTRODUCTION

On its natural pathway towards the reduction of their SFE, materials tend to attract and adhere contaminant matter from the environment. As it was introduced in **Chapter 1,** the contamination of the material surfaces has a negative impact on a broad range of applications leading to significant safety and health risks, detrimental impact on performance and/or high maintenance costs. Liquids and solid particles have been identified as two of the most relevant soiling sources involved in surface contamination, since any fouling agent with a specific SFE (or surface tension for liquids) can be deposited on top of a material with a higher SFE. The chemical composition and the physicochemical properties of surfaces and fouling agents significantly determine the interactions between them and consequently the soiling/anti-soiling capacity of the system. In this regard, and from the surface point of view, chemical composition and elastic modulus of surfaces have been identified as the two main aspects involved on the adhesion of fouling agents.[1] Therefore, chemical functionalization and tailoring the elastic modulus of surfaces could be used as strategies to lower the surface contamination. The surface chemical functionalization comprises two different approaches:

1) The first one involves low SFE solutions decreasing the affinity and, therefore, the interactions between the fouling agent and the surface. Indeed, lowering the SFE of the substrate can benefit the repellent behaviour by two ways. Firstly, it might prevent surfaces from solid particles adhesion and secondly, removal of adhered particles can be easier. Owing to their low SFE, silicones and perfluoropolymers are commonly used for designing low adhesion solutions based on this approach.[2,3,4]
2) The second approach is related to induce specific particle-surface interactions like the established between biofouling or proteins and zwitterionic polymers repelling them.[5,6]

On the other hand, designing surfaces with low elastic modulus coatings reduce the adhesion of fouling agents capable of deforming the surface (i.e. soft surfaces) since, the strength of the adhesion (σ) is proportional to the elastic modulus (E) according to

Equation 4.1 (**Eq. 4.1**). Therefore, less energy is required for the particle to be detached from the elastic surface.[7]

$$\sigma = \sqrt{\frac{W_a \cdot E}{t}} \qquad \text{(Eq. 4.1)}$$

Where W_a is the work of adhesion (which is related to the SFEs) and t is the thickness of the coating.

Hence, in order to design the most effective solution to lower the adhesion of solid contaminants to a surface, it is important to understand how the physical properties of the fouling agent affect to their adhesion onto surfaces. Tuteja´s group[1] has classified the fouling agents according to two relevant parameters: their elastic modulus (as soft or hard contaminants) and their length scale. Based on these critical parameters, it is possible to predict the best strategy to minimize the surface contamination. Hence, Tutejas's group identified that for soft and small particles, the reduction of the SFE by chemical functionalization of the surfaces will be the most effective strategy in order to reduce the adhesion, while in the case of hard and large particles, the reduction of the E of the surface will provide the best low adhesion solutions.

Focusing on the particular case of dust particles as fouling agents (which are soft and small particles, attending to the Tuteja´s mentioned classification), two main mechanisms have been identified to promote its adhesion on material surfaces: van der Waals and electrostatic forces.[8] Van der Waals interactions between dust particles and material surfaces can be reduced by decreasing the SFE of the latter,[9] while the electrostatics forces can be avoided by means of surface conductivity which prevents the electrostatic charge build-up, and hence inhibiting the electrostatic interactions with particles.[10]

In this context, self-cleaning coatings have attracted recently a great recognition in research and industry, due to their wide range of commercial applications, facilitating the daily life of human societies and saving time and money by enabling novel and improved products and technologies.[11,12,13] The concept of self-cleaning surfaces has been inspired

by nature, where numerous self-cleaning examples in animals and plants can be found.[14] In these examples and also in lab engineered systems, the presence of water is essential, since dirt particles are picked up by water droplets, rolling-off along a non-wetting surface and therefore cleaning the surface along the droplet path.[15,16,17] However, non-wetting surfaces based on hydrophobic and SHS solutions do not provide an effective response in dry conditions or when the liquid to be repelled out the surface is of another nature different from water. As a consequence, in the latter case, droplets from low surface tension liquids, such as oils or organic solvents, remain pinned onto the surfaces, causing an unsightly and stained appearance. Engineered omniphobic surfaces may be able to repel any kind of liquid and capable to remain cleaner than just hydrophobic or oleophobic surfaces on their own; nevertheless, for omniphobic surfaces, the self-cleaning concept can only be partially asserted, since it is limited to surfaces with rolling droplets effects and do not provide any self-cleaning response when the surfaces are covered by dust in dry conditions.

On the other hand, one of the strategies proposed in order to avoid dust accumulation is by reducing the electrical surface resistance, leading to antistatic characteristics and diminishing the dust attraction on the coating by avoiding the formation of electrostatic charges.[18,19] Big efforts of antistatic dust-repellent coatings are being made for application in industrial sectors such as automotive, construction or photovoltaics. Antistatic coatings are also implemented by the industry to elude charge accumulation and dramatic discharges producing dangerous sparks, which may cause equipment failures or fires.[20,21]

However, dust-repellent surfaces have been very little studied in combination with omniphobicity in order to provide full self-cleaning characteristics to avoid accumulation of dust and liquids. Indeed, up to our best knowledge, there are no reports on holistic self-cleaning approaches based on that unique combination. Laponite nanoparticles may be an excellent candidate to achieve this holistic approach for several reasons: 1) laponite particles have intrinsic ionic and electrical conductivity, which could provide antistatic and dust-repellent effects; 2) like other clays, laponites can be flexibly modified through the

unhindered hydroxyl groups,[22] and are able to be silanised with omniphobic and fluorinated groups; 3) laponite nanoparticles are easily dispersed in solvents, such as water,[22,23] and processed to homogeneous and continuous films by conventional coating methods such as casting, bar-coating, dip-coating, or blade-coating[24] and finally 4) laponite films are normally highly transparent.[25,26] Other properties shown by laponite coatings include minimization of the corrosion effect of metal works by preventing or reducing the movement of species, such as water and ions into the metal substrate.[27,28]

In the work presented in the current chapter, laponite nanoparticles are modified with perfluorinated pendant groups. The physico-chemical properties of the modified laponites are characterized and correlated to the electrical sheet resistance and omniphobic response. Furthermore, innovative coatings (i.e. based on a controlled mixture of unmodified and modified laponites) with dual-action, anti-dust accumulation and liquid repellence, are proposed for a holistic approach with a triple active self-cleaning response against liquids, solids and liquid-solid mixtures. This will be achieved through the following pathways:

1) Reducing the SFE, using a perfluorinated system, will provide liquid repellent surfaces, as well as, will contribute to reduce the van der Walls interactions and consequently, the dust accumulation.
2) Reducing the electrostatic charges through means of intrinsically charged laponites will minimized the accumulation of dust particles.

4.2 EXPERIMENTAL SECTION

4.2.1 Materials

Laponite grades XLG and JS from Rockwood Additives Ltd. were generously donated by Azelis and Comindex respectively. 1H,1H,2H,2H-perfluorooctyltriethoxysilane 97% was acquired from abcr GmbH. Ethanol absolute was purchased from Sigma-Aldrich. All chemical were used as received. Deionized water used in all experiments had a conductivity < 1 µS. Glass substrates with 1 mm thickness were obtained from Deltalab S.L. with reference D100001 and cut into 25 x 25 mm size. PVC substrates with a thickness of 180 µm was acquired from Fellowes and cut into 25 x 25 mm size.

4.2.2 Methods

4.2.2.1 Synthesis of perfluoalkylsilanized-modified laponites

General silanisation of laponites has been described previously by other authors;[29,30] however, the methodology was modified according to our materials and targeted product. To a 100 mL round-bottomed flask with 25 mL of deionized water, Laponite XLG (1 g) was added in small portions under vigorous stirring until full dispersion of the solid. After 1 h of stirring, 25 mL of absolute ethanol was added to the clear dispersion, followed by 1H,1H,2H,2H-perfluorooctyltriethoxysilane (1.77 mL). Upon silane addition, the solution turned cloudy and it was allowed to stir at 50 °C for 16 h. The cloudy white dispersion was collected in centrifuge tubes and centrifuged at 3500 rpm for 20 min. The supernatant was decanted and the remaining gel collected and dispersed again in a mixture of 50% ethanol/water. The centrifuge procedure was repeated to remove all unbound material. Finally, the collected gelled clay was redispersed in a total volume of 25 mL of a mixture 50% ethanol/water, leading to a 4% (w/v) dispersion based on the initial laponite amount.

4.2.2.2 Substrates preparation

Glass substrates were cleaned with warm acetone in a first stage, followed by soap and rinsed with deionized water before being used. PVC substrates were cleaned with soap, rinsed with deionized water and activated using a nano Dieder plasma system, consisting in a RF signal generator (40 kHz, 200 W). Initially, a vacuum generation stage was run at 0.3 mbar before the surface activation stage. The PVC substrates were treated with oxygen plasma to promote adhesion during 60 s at 90% power.

4.2.2.3 General procedure for the film fabrication

Films were prepared by processing the corresponding solution through a bar-coating methodology according to the methodology depicted in **Figure 4.1**. The films were prepared by placing the substrates in the bar-coating equipment (Sheen 1137-G-MAN automatic film applicator) and applying the corresponding solution using a rod-shaped 100 µm size wire coil bar at a speed of 50 mm/s at room temperature. After the

solution was spread over the substrate coating, the obtained films were dried in an oven for 80 °C during 1 h.

4.2.2.4 Fabrication of unmodified-laponite films with antistatic functionality

In a 50 mL flask with 25 mL of deionized water, 700 mg of laponite XLG were added in small portions under vigorous stirring. When the solid was completely dispersed, 300 mg of laponite JS were added in the same manner. The solution turned cloudy. After stirring for 3 h, the solution became clear and collected, obtaining a XLG:JS (7:3), 4% (w/v) laponite dispersion based on the total weight of laponite. The aqueous laponite dispersion was aged for 2 weeks before being used for the film preparation, when it reached a suitable viscosity to be processed through a bar-coating technique, following the general procedure.

4.2.2.5 Fabrication of holistic multifunctional laponite films

For the preparation of multifunctional laponite films with self-cleaning synergetic functionalities, a multifunctional laponite mixture 4% (w/v) was firstly prepared. Hence, 7 g from the laponite XLG:JS (7:3) 4% (w/v) dispersion from the unmodified-laponite film preparation with antistatic functionality were taken and mixed with 3 g of the 4% (w/v) perfluoroalkylsilanised-modified laponite solution. The obtained mixture was used through a bar-coating technique following the general procedure. For convenience, the films obtained from the latter mixture are named as multifunctional in the rest of the manuscript.

4.2.3 Modified laponites and thin film characterization

FTIR spectra of the solids were obtained by Attenuated Total Reflectance (ATR) technique with a Jasco 4100 FTIR, from 400 cm^{-1} to 4000 cm^{-1}.

TGA was carried out on a TA instruments Q500 thermobalance. Samples were heated at a rate of 10 °C/min from ambient temperature to 700 °C under a nitrogen flow of 60 mL/min.

Morphological properties of the film were analysed using ULTRA plus ZEISS FESEM.

UV−vis spectra were obtained in transmission/absorption mode on a Jasco V-570 spectrophotometer using air as the background. The spectra were registered using a film holder accessory for solid samples from 300 nm to 800 nm. Reflectance was measured using an integrating sphere Jasco ISN-470 at the same range of wavelength.

Sheet resistance of the films was measured at atmospheric pressure and room temperature conditions using a Keithley Semiconductor Characterization System 4200-SC with a four-point probe.

KSV CAM 200 Optical contact angle meter was used to determine the CA_s of the films. Solvents droplets were placed, at least, on three different areas of the surface. The static contact angles were recorded using the Laplace-Young fitting method.

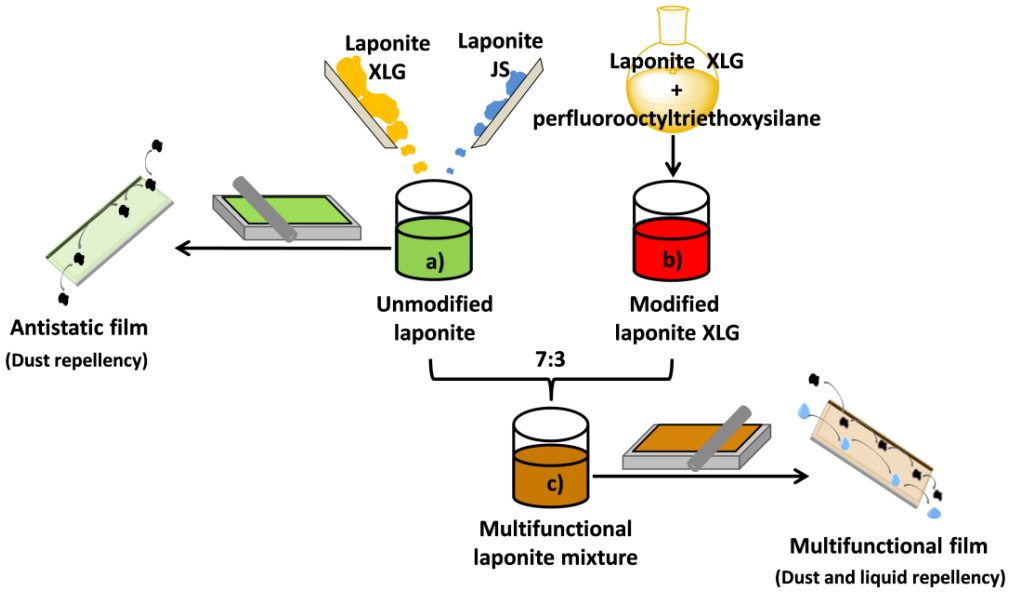

Figure 4.1. Schematic illustration of preparation of multifunctional films with self-cleaning response repelling liquids and dust particles.

4.3 RESULTS AND DISCUSSION

4.3.1 Perfluoroalkylsilanized-modified Laponites

In this work, covalent modification of Laponite with 1H, 1H, 2H, 2H-perfluorooctyltriethoxysilane was achieved in order to render omniphobic functionality to the laponite nanodisks. As described by other authors, each laponite nanodisk may have an overall negative charge with approximately 700 electron charges,[31] which facilitate

very effectively the nuclear substitution at the silane position to generate new O-Si bonds during the silanisation process. Qualitative evidence of the modification was provided by FTIR. The FTIR spectra of bare and modified XLG laponites are shown in **Figure 4.2a**. It is worth noting that FTIR-recorded signals for modified laponites show a clear overlapping with the bare laponites and the silanising reagent peaks. As similar assignment already pointed out at another studies,[32] vibrations for the modified laponite XLG at 651 cm^{-1} and 963 cm^{-1} can be attributed to bending and asymmetric stretching of Si-O-Si bonds. Bands between 1000 - 600 cm^{-1} are likely due to C-C stretching modes. The presence of C-F group is detected on the intense absorption around 1058 cm^{-1}. The adsorption bands for CF_2 and CF_3 were found at 1193 cm^{-1} and 1142 cm^{-1}. Furthermore, similar conclusions were found from the FTIR analysis of modified laponite JS (**Figure 4.2b**).

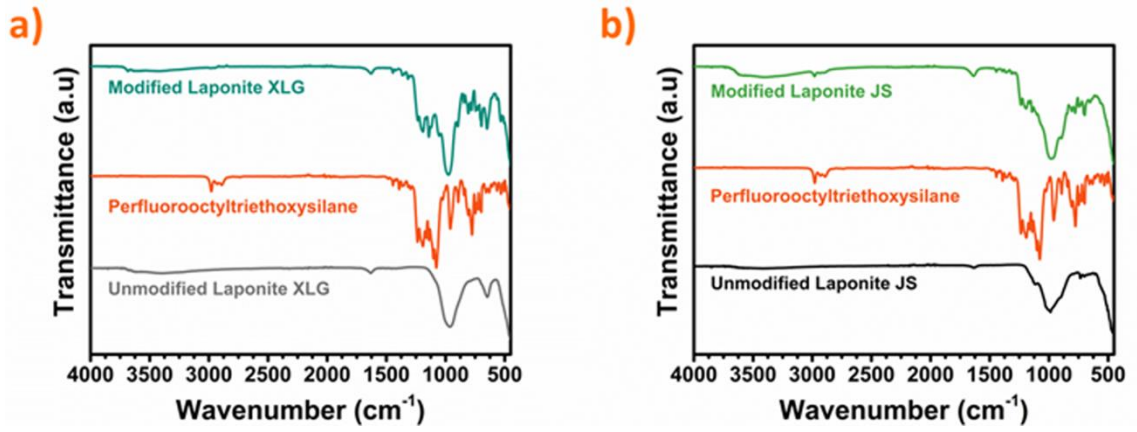

Figure 4.2. Infrared spectra of a) Laponite XLG (grey), 1H, 1H, 2H, 2H-perfluorooctyltriethoxysilane modified laponite XLG (cyan) and 1H, 1H, 2H, 2H-perfluorooctyltriethoxysilane for comparison (orange). b) Laponite JS (black), 1H, 1H, 2H, 2H-perfluorooctyltriethoxysilane modified laponite JS (green) and 1H, 1H, 2H, 2H-perfluorooctyltriethoxysilane for comparison (orange).

To gain more insight into the covalent modification process, TGA was used to determinate the amount of silane anchored on the laponite nanodisks. **Figure 4.3** shows the TGA curves before and after the covalent laponite modification with the silane reagent. The samples were subjected to continuous heat up to 700 °C at 10 °C/min. The thermogram of modified XLG laponites (**Figure 4.3a**,**b**) exhibits three main decomposition regions. The first region ranges from room temperature up to 250 °C, which likely corresponds to water elimination and hydroxyl decomposition. A third region from 550 °C to 700 °C, where no major processes seem to occur can also be detected. However, a

second region between 250 and 550 °C, which corresponds to the thermal decomposition of the covalently attached silane moiety, was only considered for quantitative determination of the laponite modification. It is very remarkable to notice the high degree of organic functionalization achieved, circa 60% of the overall particle weight. This high degree of functionalization is of great interest due to the potentially large omniphobic characteristics provided by these particles, which will be later explained at this study. The silane modification ratio exhibited by these particles goes even further than a similar modification of laponite RD nanodisks previously reported in the literature reaching approximately 13% between grafted and adsorbed perfluorooctylsilane.[28] Regarding laponite functionalization, other studies have been carried out employing different silane groups for different purposes.[29,30,33] All of them with an organic functionalization ranging from 5 to 17% of the overall weight. However, similar omniphobic functionalization to the work described in this study over SiO_2[34] or TiO_2[35,36] nanoparticles, has also been demonstrated obtaining 4% and 19% approximately of weight. The large physical surface of laponites described by the producers of about 900 m^2/g,[37] the great nucleophilic character of laponite nanodisks with a large concentration of hydroxyl and oxygen atoms, and the more severe synthesis conditions employed in this study, may be the main origin of these results. TGA was compared to unmodified laponite XLG clay, which as expected, did not show any silane-related feature. However, 10% of weight loss was detected when the unmodified laponite was heated up to 150 °C. This is mainly due to the presence of water molecules. The minimized weight loss detected for functionalized laponite at the same temperature range seems to anticipate some hydrophobic ability. Similar silanisation work was performed over laponite JS (**Figure 4.3c**,**d**) achieving more modest values of about 20% of functionalization. This finding suggests that the absence of pyrophosphate groups in laponite XLG is a key parameter in the quantitative modification of laponites.

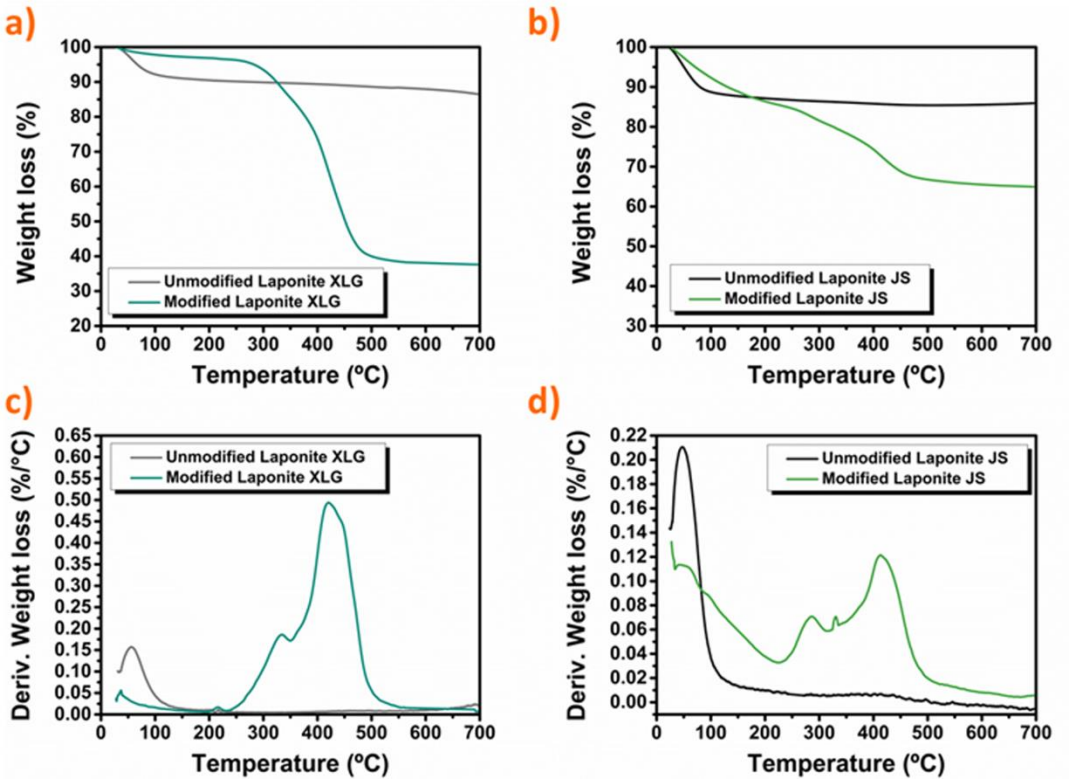

Figure 4.3. a) Thermogravimetric analysis (TGA) of laponite XLG (grey), and laponite XLG modified with silane 1H, 1H, 2H, 2H-perfluorooctyltriethoxysilane (cyan) and b) Changes of weight loss for each laponite XLG seen in the first derivative curve of TGA. c) Thermogravimetric analysis (TGA) of laponite JS (black), and laponite JS modified with silane 1H, 1H, 2H, 2H-perfluorooctyltriethoxysilane (green) and d) Changes of weight loss for each laponite JS seen in the first derivative curve of TGA.

4.3.2 Unmodified and multifunctional laponite coatings

Besides of achieving interesting results when laponites are stabilized in a gel state through colloidal forms,[38,39] unmodified laponites are also known as film forming agents with excellent antistatic and barrier coating applications by simply dispersing laponite powder into water. Examples of laponite films are found in the literature by just slow evaporation of the water dispersion[22,24] or as additive into resin emulsion binders.[28,40,41] The 4% (w/v) ethanolic-aqueous gel mixture obtained from the synthesis of modified XLG laponite nanoparticles was processed into films using a bar-coating application with a 100 µm cylindrical bar. The resulting films had a hydrophobic contact angle of 110°. However it was observed that the obtained perfluoroalkylsilanized-modified laponite films were not electrically conductive, likely due to the quantitative functionalization of the laponite clays, blocking the electrical charge transport through distorting the distinctive

continuous interlinked and overlapped arrange of laponites platelets.[26,37] In order to overcome this limitation, which have a negative impact on the dust-repellent functionality, formulations based on the electrically conductive unmodified laponite and perfluoroalkylsilanised-modified laponites were made. Indeed, adding unmodified laponite not only may ensure electrical conductivity and dust-repellence but also, pave the way to a good quality film formation. The rheology of the laponite dispersions in water was quite important in order to fabricate laponite films through a bar-coating methodology. Hence, the rheology of the laponite dispersions in water had to be adjusted, and different mixtures of laponite clays with different viscosities were evaluated. In order to do so, different grades of laponite were employed. As stated by the laponite manufacturer,[37] laponite XLG is a gel forming grade, and as a result, high viscosities unsuitable for direct bar application were obtained. Low viscosity laponite varieties, such as JS, are sol forming grade, resulting in low viscosity dispersions and in consequence, unable to be applied through bar-coating on its own. The suitable composition for the unmodified laponites finally was set to a mixture of laponite XLG and Laponite JS, in a ratio of 7:3 respectively with a total solid amount of 4% (w/v). The unmodified XLG and JS mixture was consequently added to the ethanolic-aqueous dispersion of perfluoroalkylsilanised-modified XLG laponites 4% (w/v) in a proportion of 7:3 (unmodified:perfluoroalkylsilanised modified laponites). This was found to be the most suitable ratio in order to achieve good quality multifunctional films with good antistatics and omniphobic characteristics.

The morphology, optical properties, dust-repellence and omniphobicity performance and mechanical behavior of the films obtained were characterized.

Figure 4.4a displays representative top-view and cross-section FESEM micrographs of the films constituted by unmodified laponites and multifunctional ones. The films obtained from unmodified XLG and JS laponites showed no significant microscale features in the top-view morphology (**Figure 4.4a1**) and a layered stacking structure (**Figure 4.4a2**). A structure conformation, in which some layer stacking may be also inferred although less obviously than in the unmodified laponite film, was also detected for the multifunctional

films (Figure 4.4a3). Furthermore, some microscale feature size at the surface was detected (Figure 4.4a4). It is noted that films deposited from suspensions prepared with only functionalized laponite XLG show larger density of microscale features and porous structures (Figure 4.4b), probably resulting from swelling and bubble formation occurred during ethanol evaporation from the laponite dispersion.

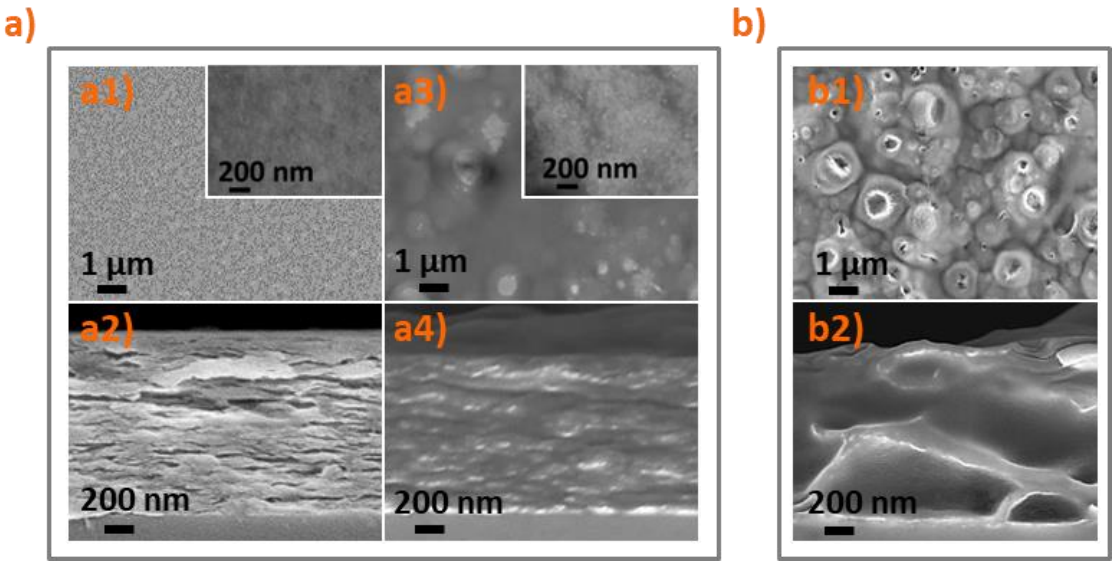

Figure 4.4. a) Top view and b) cross-section of unmodified XLG and JS laponites in a 7:3 ratio mixture coating. c) Top view and d) cross-section of the multifunctional coating (mixture of unmodified and modified laponites). a) Top view and b) cross-section of a film made with fully functionalised laponite XLG.

Because very often self-cleaning coatings require some degree of transparency due to their final applications (e.g. aesthetics products,[42,43] and solar cells[18]) the UV/visible light transmittance was characterized (Figure 4.5a). Two different coatings (unmodified laponites and multifunctional laponites) were applied over a transparent glass substrate through bar-coating and their transparency measured. At the first sight, for the transmittance mode, there are not big differences in the visible region (approx. 380 - 750 nm) between the two laponite coatings and the bare glass substrate. Nevertheless, having a closer look, samples including the multifunctional coating exhibited slightly smaller transmittance. However, a significant increase occurs in the UV range (i.e. below 380 nm). It is noted that samples including multifunctional coating exhibited the lowest reflectance (Figure 4.5b), suggesting some changes in the effective refractive index. The latter may be due to the different chemical nature of the coating, but also from the

changes in morphology. It is indeed worth to highlight that significant light scattering may occur in multifunctional coatings (i.e. micro/nanoscale morphological features) (**Figure 4.5c**).

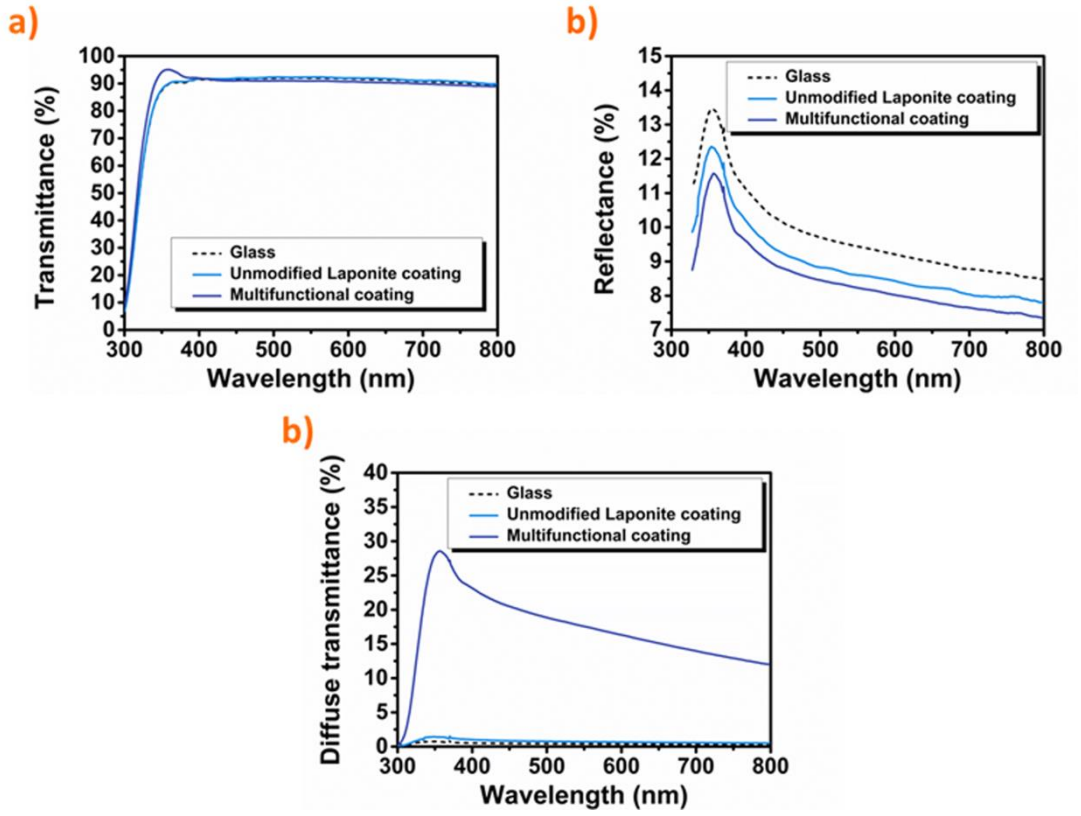

Figure 4.5. Total transmittance (a), reflectance (b) and diffuse transmittance of bare glass (black-dash); unmodified XLG and JS laponites in a 7:3 ratio mixture coating (blue) and multifunctional coating (dark blue).

As mentioned before, one of the characteristics of these coatings is their capacity of acting as antistatic agent due to the laponite intrinsic electrical and ionic conductivities. Therefore, the electrical conductivities of unmodified laponite and multifunctional coatings were measured. In order to avoid any electrical contribution associated to the substrate influence, coatings over blue PVC sheets and glass substrates were prepared. The PVC substrate is characterized as dielectric material prone to static charges. The electrical sheet resistance values are depicted at **Table 4.1**. All coated PVC substrates had a sheet resistance in the rage of 10^6 and 10^7 Ω/□ and the uncoated PVC substrate used as reference had a sheet resistance above 10^{13} Ω/□. It is noted that films with sheet resistance between 10^5 Ω/□ and 10^{12} Ω/□ may allow the dissipation of electrical charges

generally within milliseconds.[44] Therefore, both types of laponite coatings (i.e. those based on unmodified laponites and the multifunctional ones) should have the antistatic characteristics and may be able to perform with a dust-repellence feature.

Table 4.1. Sheet resistance of bare and laponite-coated substrates.

Coating	PVC (Ω/□)	Glass (Ω/□)
Bare substrate	$> 5 \times 10^{13}$	$2.3 \pm 0.3 \times 10^{10}$
Unmodified laponite	$9.0 \pm 1.0 \times 10^{6}$	$3.5 \pm 0.5 \times 10^{7}$
Multifunctional	$3.0 \pm 0.2 \times 10^{7}$	$1.2 \pm 0.1 \times 10^{8}$

The dust attraction test confirmed these results. **Figure 4.6a** shows photographs of bare PVC substrates and coated PVC substrates with both laponite mixtures: XLG:JS unmodified laponite and modified multifunctional laponite coating. The coated and uncoated samples were placed inside a holed lid box with carbon black dust and blown with a pressurized air gun through the orifice in order to generate a carbon black cloud inside the box. After air blowing for 30 seconds, the samples were removed and examined. The two laponite coatings (from unmodified and multifunctional ones) exhibited a similar behavior, with very little amount of carbon black dust deposited over the surface, in contrast to the bare PVC sample, which was significantly covered by carbon black dust. These results show how the coated samples, with a lower electrical sheet resistance are more favorable to evade the dust accumulation.

The static contact angles of the uncoated PVC sample, unmodified laponite and multifunctional-coated samples were measured as a qualitative method to evaluate the liquid repellence functionality (**Table 4.2**). The bare uncoated PVC sample shows very oleophilic contact angles, with modest values against organic and mineral oils and hexadecane; however, as expected and due to its polymeric nature, it has a hydrophobic contact angle of 90°. The unmodified laponite coating does not improve the oleophobic character of the bare PVC substrate, but also a quite important reduction of the water contact angle is observed. As expected, the ionic nature of laponite clays increases its water affinity. The multifunctional coatings show contact angle values with a significant improvement of their performance.

Table 4.2. Static contact angles observed for bare PVC, unmodified XLG and JS laponites in a 7:3 ratio mixture coating, and multifunctional coating (mixture of unmodified and functionalized laponites) for various liquids.

Liquid	Bare PVC	Unmodified laponites	Multifunctional coating
Water	90 ± 1°	19 ± 1°	106 ± 1°
PAO 9	28 ± 2°	27 ± 1°	93 ± 2°
Mineral Oil (GIII)	26 ± 1°	25 ± 3°	88 ± 3°
Hexadecane	25 ± 2°	< 10°	64 ± 1°

Laponite coated PVC substrates with $–CF_2–$ and $–CF_3$ groups enhance the omniphobic character by reducing the SFE (**Table 4.3**) and increasing CA_s (**Table 4.2**).[45,46]

In light of these results, good repellence towards polar solvents such as water, non-polar and organic oils such as polyalphaolefin (PAO 9) are obtained. For other organic solvents, such as hexadecane, CA_s are more discrete, and this can be justified by the low surface tension of hexadecane (27.4 mN/m) versus water (72.8 mN/m).[47] However, hexadecane contact angles obtained through the multifunctional modified laponite coatings are in good agreement with other literature values shown for fluorinated bulk materials,[48] or even significantly higher than other approaches with non-hierarchical morphology surfaces modified with low SFE[47,49,50] or infused liquid surfaces.[51] The evidence shows that the presence of unmodified laponites in the multifunctional coating formulation has no negative impact on the CAs measured. This behavior is also supported by the determined SFE of the different surfaces and coatings; thus, as expected, multifunctional coating showed the lowest determined value (12.05 mN/m) in contrast to the antistatic laponite coating of 64.08 mN/m or PVC coating (39.03 mN/m).

Table 4.3. Surface free energy of different substrates and coatings.

Substrate	SFE (mN/m)
Bare PVC	39.03
Unmodified laponite	64.08
Multifunctional	12.05
Glass	66.23

To assess the self-cleaning performance of both laponite coatings, the bare PVC sample and the two coated PVC samples (XLG:JS unmodified laponite and multifunctional laponite) were placed in two oil tanks. The first oil tank was composed by tinted PAO 9 oil

(Figure 4.6.b) and the second tank was prepared with mineral oil (GIII) stained with a carbon black dust suspension to simulate a used oil condition composed by oil and solid particles (Figure 4.6.c). The excellent self-cleaning response of the multifunctional coating can be observed when the coating is subjected to both oils.

Despite showing modest dynamic contact angles and hysteresis results (Table 4.4), multifunctional coating results almost free of any oil stain on the order of few seconds time, in contrast to bare PVC and unmodified laponite coating, which remained stained by the oil during the test life.

Table 4.4. Water dynamic contact angles and hysteresis angles of multifunctional other similar coatings and for comparison.

Substrate	$CA_{(7\mu L)}$	CA_{adv}	CA_{rec}	CA_{hys}
Multifunctional	110	131	81	50
***Silanized glass**	97	106	66	40
****** **Silanized laponites**	78	100	59	41

* Glass substrate Deltalab S.L. with reference D100001 silanised with 1H,1H,2H,2H-perfluorooctyltriethoxysilane

** Glass substrate Deltalab S.L. with reference D100001 coated with a laponite mixture of unmodified XLG and JS laponites in a 7:3 ratio and treated with 1H,1H,2H,2H-perfluorooctyltriethoxysilane.

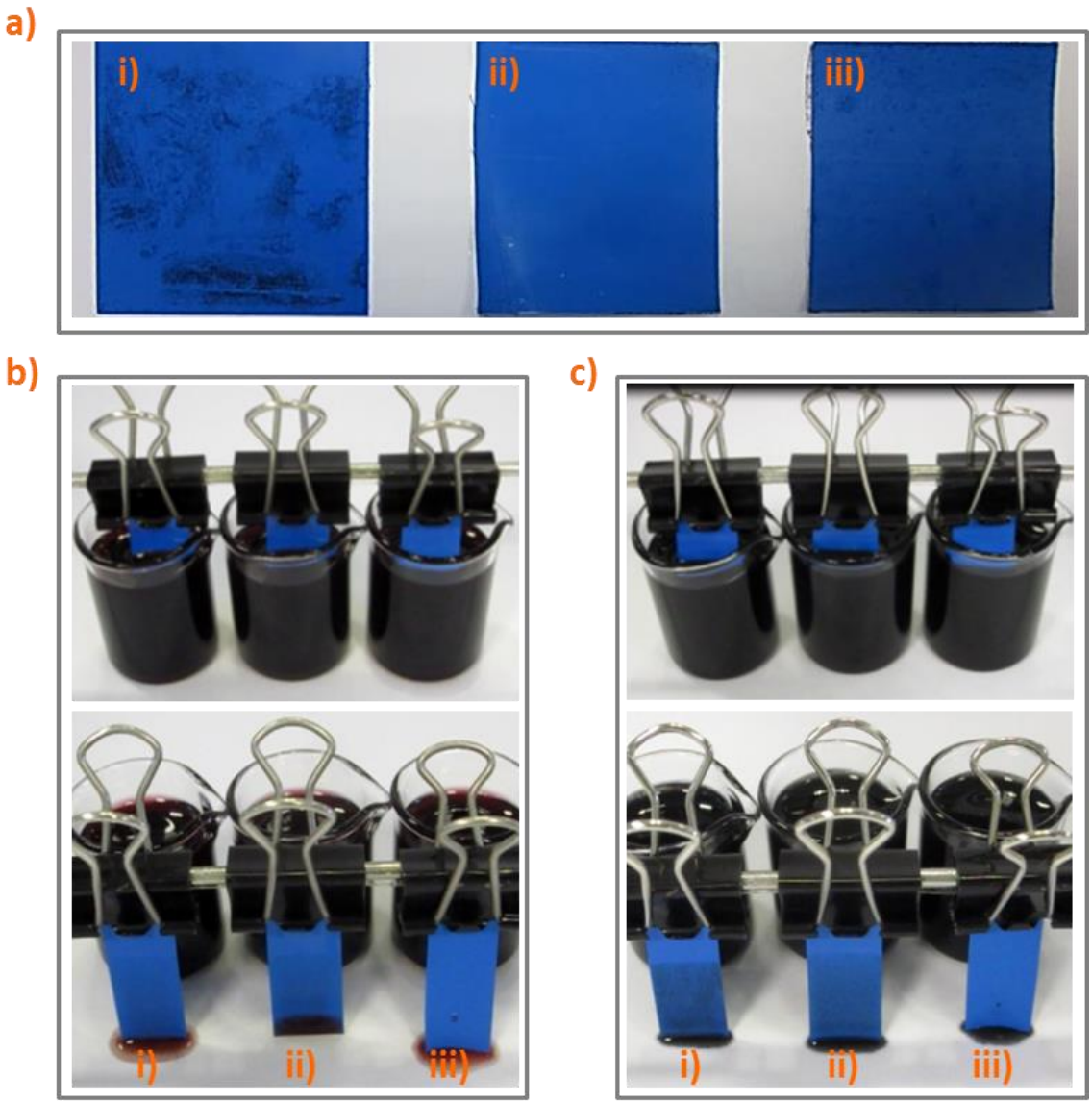

Figure 4.6. a) Dust attraction tests against carbon black powder of i) bare PVC; ii) unmodified XLG and JS laponites in a 7:3 ratio mixture coating and iii) multifunctional coating. b) Oil self-cleaning of i), ii) and iii). c) Mixture of carbon black dust and oil self-cleaning of i), ii) and iii).

Dust-repellence and liquid-repellence holistic functionality indicate that modified multifunctional coatings are suitable to be used as self-cleaning coatings since avoids the accumulation of dirt of any kind, in the form of dust particles, liquids of different nature and combination of everything. This is actually an advantage against other systems, where self-cleaning concept is based exclusively upon liquid repellence, by allowing water droplet carry the dirt away of its surface through the droplet path.[52,53]

In order to evaluate the durability of the coatings, mechanical stability of the flexible coated PVC samples against bending tests and their liquid-repellence behaviour was investigated. As seen in **Table 4.5**, water CAs for both coatings (unmodified XLG:JS laponite and multifunctional ones) were kept unaffected after the bending cycles. However, the surface coating after the bending tests was studied more in depth by electron microscopy and the damage occurred during bending evaluated. As it can be observed in **Figure 4.7**, the unmodified laponite coating shows clear fissures. However, the multifunctional coating does not show any fissures; but shows some folding lines along the bending axis. It is clear that the less ordered stacking character of the multifunctional coating, as seen at the cross-section picture in **Figure 4.4**, helps to avoid any fractures during its manipulation, increasing its plasticity and lasting time of the coating.

Table 4.5. Water static angle values for unmodified laponite and multifunctional coatings after a series of bending tests over a PVC flexible substrate.

Coating	0 bending cycles	2 bending cycles	20 bending cycles	100 bending cycles
Unmodified laponite	20 ± 1°	19 ± 2°	20 ± 1°	20 ± 2°
Multifunctional	106 ± 1°	108 ± 2°	107 ± 2°	105 ± 3°

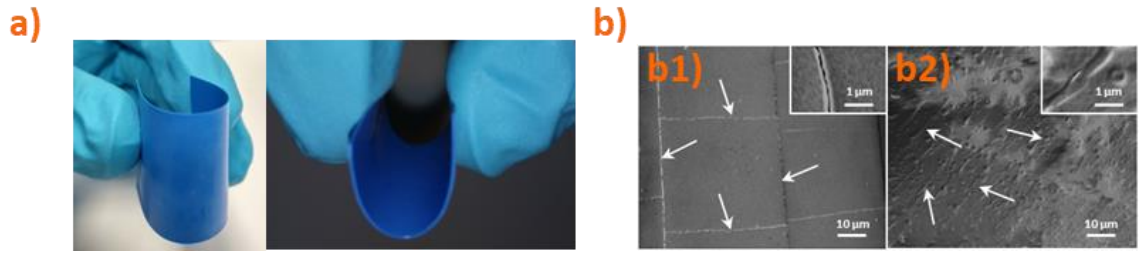

Figure 4.7. a) Bending of 100 µm thick multifunctional coating deposited over a blue PVC flexible substrate. b) FESEM images of unmodified laponite and multifunctional coatings after being put through 100 bending cycles, showing fissures b1) and folding lines b2).

4.4 CONCLUSIONS

Innovative coatings with dual-action, anti-dust accumulation and liquid repellence, are proposed for a holistic approach with a triple active self-cleaning response against liquids, solids and liquid-solid mixtures. We have demonstrated how a hydrophilic material such a laponite can be processed into omniphobic films simply by blending with

a certain amount (e.g. 3:7) of a highly perfluoroalkylsilanised laponite clay. The incorporation of functionalized laponite into a raw laponite matrix allows to deposit multifunctional coatings with holistic self-cleaning functionality based on omniphobic and dust-reduced attraction properties. This is one step further than classical omniphobic approaches, which only show repellence towards liquids. The low processing temperature and the water-based formulation have been successfully demonstrated in order to obtain such holistic self-cleaning functionality coatings, which open wide opportunities for applications in numerous sectors, such electronics, automotive, architecture, furniture protection or decoration.

4.5 References

(1) Halvey, A. K.; Macdonald, B.; Dhyani, A.; Tuteja, A. Design of Surfaces for Controlling Hard and Soft Fouling. *Philos. Trans. R. Soc. Math. Phys. Eng. Sci.* **2019**, *377* (2138), 20180266. https://doi.org/10.1098/rsta.2018.0266.

(2) Eduok, U.; Faye, O.; Szpunar, J. Recent Developments and Applications of Protective Silicone Coatings: A Review of PDMS Functional Materials. *Prog. Org. Coat.* **2017**, *111*, 124–163. https://doi.org/10.1016/j.porgcoat.2017.05.012.

(3) Nayshevsky, I.; Xu, Q. F.; Barahman, G.; Lyons, A. M. Fluoropolymer Coatings for Solar Cover Glass: Anti-Soiling Mechanisms in the Presence of Dew. *Sol. Energy Mater. Sol. Cells* **2020**, *206*, 110281. https://doi.org/10.1016/j.solmat.2019.110281.

(4) Yang, S.; Xia, Q.; Zhu, L.; Xue, J.; Wang, Q.; Chen, Q. Research on the Icephobic Properties of Fluoropolymer-Based Materials. *Appl. Surf. Sci.* **2011**, *257* (11), 4956–4962. https://doi.org/10.1016/j.apsusc.2011.01.003.

(5) He, M.; Gao, K.; Zhou, L.; Jiao, Z.; Wu, M.; Cao, J.; You, X.; Cai, Z.; Su, Y.; Jiang, Z. Zwitterionic Materials for Antifouling Membrane Surface Construction. *Acta Biomater.* **2016**, *40*, 142–152. https://doi.org/10.1016/j.actbio.2016.03.038.

(6) Ladd, J.; Zhang, Z.; Chen, S.; Hower, J. C.; Jiang, S. Zwitterionic Polymers Exhibiting High Resistance to Nonspecific Protein Adsorption from Human Serum and Plasma. *Biomacromolecules* **2008**, *9* (5), 1357–1361. https://doi.org/10.1021/bm701301s.

(7) Kendall, K. The Adhesion and Surface Energy of Elastic Solids. *J. Phys. Appl. Phys.* **1971**, *4* (8), 1186–1195. https://doi.org/10.1088/0022-3727/4/8/320.

(8) Dove, A.; Devaud, G.; Wang, X.; Crowder, M.; Lawitzke, A.; Haley, C. Mitigation of Lunar Dust Adhesion by Surface Modification. *Planet. Space Sci.* **2011**, *59* (14), 1784–1790. https://doi.org/10.1016/j.pss.2010.12.001.

(9) Wang, P.; Xie, J.; Ni, L.; Wan, L.; Ou, K.; Zheng, L.; Sun, K. Reducing the Effect of Dust Deposition on the Generating Efficiency of Solar PV Modules by Super-Hydrophobic Films. *Sol. Energy* **2018**, *169*, 277–283. https://doi.org/10.1016/j.solener.2017.12.052.

(10) Sarver, T.; Al-Qaraghuli, A.; Kazmerski, L. L. A Comprehensive Review of the Impact of Dust on the Use of Solar Energy: History, Investigations, Results, Literature, and Mitigation Approaches. *Renew. Sustain. Energy Rev.* **2013**, *22*, 698–733. https://doi.org/10.1016/j.rser.2012.12.065.

(11) Tian, X.; Verho, T.; Ras, R. H. A. Moving Superhydrophobic Surfaces toward Real-World Applications. *Science* **2016**, *352* (6282), 142–143. https://doi.org/10.1126/science.aaf2073.

(12) Wang, S.; Liu, K.; Yao, X.; Jiang, L. Bioinspired Surfaces with Superwettability: New Insight on Theory, Design, and Applications. *Chem. Rev.* **2015**, *115* (16), 8230–8293. https://doi.org/10.1021/cr400083y.

(13) Samaha, M. A.; Gad-el-Hak, M. Polymeric Slippery Coatings: Nature and Applications. *Polymers* **2014**, *6* (5), 1266–1311. https://doi.org/10.3390/polym6051266.

(14) Hensel, R.; Neinhuis, C.; Werner, C. The Springtail Cuticle as a Blueprint for Omniphobic Surfaces. *Chem. Soc. Rev.* **2016**, *45* (2), 323–341. https://doi.org/10.1039/C5CS00438A.

(15) Wu, L. Y. L.; Shao, Q.; Wang, X. C.; Zheng, H. Y.; Wong, C. C. Hierarchical Structured Sol–Gel Coating by Laser Textured Template Imprinting for Surface Superhydrophobicity. *Soft Matter* **2012**, *8* (23), 6232–6238. https://doi.org/10.1039/C2SM25371B.

(16) Yu, M.; Chen, S.; Zhang, B.; Qiu, D.; Cui, S. Why a Lotus-like Superhydrophobic Surface Is Self-Cleaning? An Explanation from Surface Force Measurements and Analysis. *Langmuir* **2014**, *30* (45), 13615–13621. https://doi.org/10.1021/la5041272.

(17) Lai, Y.; Tang, Y.; Gong, J.; Gong, D.; Chi, L.; Lin, C.; Chen, Z. Transparent Superhydrophobic/Superhydrophilic TiO2-Based Coatings for Self-Cleaning and Anti-Fogging. *J. Mater. Chem.* **2012**, *22* (15), 7420–7426. https://doi.org/10.1039/C2JM16298A.

(18) Narushima, D.; Takanohashi, H.; Hirose, J.; Ogawa, S. Antistatic Effect of Power-Enhancement Coating for Photovoltaic Modules. **2011**, *8112*, 811208. https://doi.org/10.1117/12.892440.

(19) Baytekin, H. T.; Baytekin, B.; Hermans, T. M.; Kowalczyk, B.; Grzybowski, B. A. Control of Surface Charges by Radicals as a Principle of Antistatic Polymers Protecting Electronic Circuitry. *Science* **2013**, *341* (6152), 1368–1371. https://doi.org/10.1126/science.1241326.

(20) Greason, W. D. Review of the Effect of Electrostatic Discharge and Protection Techniques for Electronic Systems. *IEEE Trans. Ind. Appl.* **1987**, *2* (IA-23), 205–216. https://doi.org/10.1109/TIA.1987.4504895.

(21) Gibson, N. Static Electricity — an Industrial Hazard under Control? *J. Electrost.* **1997**, *40–41*, 21–30. https://doi.org/10.1016/S0304-3886(97)00010-7.

(22) Lezhnina, M. M.; Grewe, T.; Stoehr, H.; Kynast, U. Laponite Blue: Dissolving the Insoluble. *Angew. Chem. Int. Ed.* **2012**, *51* (42), 10652–10655. https://doi.org/10.1002/anie.201203236.

(23) Nobel, M. L.; Picken, S. J.; Mendes, E. Waterborne Nanocomposite Resins for Automotive Coating Applications. *Prog. Org. Coat.* **2007**, *58* (2), 96–104. https://doi.org/10.1016/j.porgcoat.2006.08.017.

(24) Le Luyer, C.; Lou, L.; Bovier, C.; Plenet, J. C.; Dumas, J. G.; Mugnier, J. A Thick Sol–Gel Inorganic Layer for Optical Planar Waveguide Applications. *Opt. Mater.* **2001**, *18* (2), 211–217. https://doi.org/10.1016/S0925-3467(01)00111-2.

(25) Wu, W.; Dong, Z.; He, J.; Yu, J.; Zhang, J. Transparent Cellulose/Laponite Nanocomposite Films. *J. Mater. Sci.* **2016**, *51* (8), 4125–4133. https://doi.org/10.1007/s10853-016-9735-8.

(26) Li, Y.-C.; Schulz, J.; Grunlan, J. C. Polyelectrolyte/Nanosilicate Thin-Film Assemblies: Influence of PH on Growth, Mechanical Behavior, and Flammability. *ACS Appl. Mater. Interfaces* **2009**, *1* (10), 2338–2347. https://doi.org/10.1021/am900484q.

(27) Santana, I.; Pepe, A.; Schreiner, W.; Pellice, S.; Ceré, S. Hybrid Sol-Gel Coatings Containing Clay Nanoparticles for Corrosion Protection of Mild Steel. *Electrochimica Acta* **2016**, *203*, 396–403. https://doi.org/10.1016/j.electacta.2016.01.214.

(28) Swartz, N. A.; Price, C. A.; Clare, T. L. Minimizing Corrosion of Outdoor Metalworks Using Dispersed Chemically Stabilized Nanoclays in Polyvinylidene Fluoride Latex Coatings. *ACS Omega* **2016**, *1* (1), 138–147. https://doi.org/10.1021/acsomega.6b00091.

(29) Wu, Y.; Guo, R.; Wen, S.; Shen, M.; Zhu, M.; Wang, J.; Shi, X. Folic Acid-Modified Laponite Nanodisks for Targeted Anticancer Drug Delivery. *J. Mater. Chem. B* **2014**, *2* (42), 7410–7418. https://doi.org/10.1039/C4TB01162G.

(30) Wheeler, P. A.; Wang, J.; Baker, J.; Mathias, L. J. Synthesis and Characterization of Covalently Functionalized Laponite Clay. *Chem. Mater.* **2005**, *17* (11), 3012–3018. https://doi.org/10.1021/cm050306a.

(31) Cummins, H. Z. Liquid, Glass, Gel: The Phases of Colloidal Laponite. *J. Non-Cryst. Solids* **2007**, *353* (41), 3891–3905. https://doi.org/10.1016/j.jnoncrysol.2007.02.066.

(32) Fatnassi, M.; Solterbeck, C.-H.; Es-Souni, M. Clay Nanomaterial Thin Film Electrodes for Electrochemical Energy Storage Applications. *RSC Adv.* **2014**, *4* (87), 46976–46979. https://doi.org/10.1039/C4RA04330H.

(33) Negrete; Letoffe, J.-M.; Putaux, J.-L.; David, L.; Bourgeat-Lami, E. Aqueous Dispersions of Silane-Functionalized Laponite Clay Platelets. A First Step toward the Elaboration of Water-Based Polymer/Clay Nanocomposites. *Langmuir* **2004**, *20* (5), 1564–1571. https://doi.org/10.1021/la0349267.

(34) Livi, S.; Giannelis, E. P. An Improved Process for the Surface Modification of SiO2 Nanoparticles. *Green Chem.* **2012**, *14* (11), 3013–3015. https://doi.org/10.1039/C2GC36369K.

(35) Pazokifard, S.; Mirabedini, S. M.; Esfandeh, M.; Farrokhpay, S. Structure and Properties of Fluoroalkylsilane Treated Nano-Titania. *Chemeca 2011 Eng. Better World Syd. Hilton Hotel NSW Aust. 18-21 Sept. 2011* **2011**, 2155.

(36) Chen, L.; Guo, Z.; Liu, W. Biomimetic Multi-Functional Superamphiphobic FOTS-TiO2 Particles beyond Lotus Leaf. *ACS Appl. Mater. Interfaces* **2016**, *8* (40), 27188–27198. https://doi.org/10.1021/acsami.6b06772.

(37) BYK_B-RI21_LAPONITE_EN.Pdf.

(38) Angelini, R.; Ruzicka, B.; Zaccarelli, E.; Zulian, L.; Sztucki, M.; Moussaïd, A.; Narayanan, T.; Sciortino, F. Observation of Empty Liquids and Equilibrium Gels in a Colloidal Clay. *AIP Conf. Proc.* **2013**, *1518* (1), 384–390. https://doi.org/10.1063/1.4794601.

(39) Wang, Q.; Mynar, J. L.; Yoshida, M.; Lee, E.; Lee, M.; Okuro, K.; Kinbara, K.; Aida, T. High-Water-Content Mouldable Hydrogels by Mixing Clay and a Dendritic Molecular Binder. *Nature* **2010**, *463*, 339–343. https://doi.org/10.1038/nature08693.

(40) Zengeni, E.; Hartmann, P. C.; Pasch, H. Encapsulation of Clay by Ad-Miniemulsion Polymerization: The Influence of Clay Size and Modifier Reactivity on Latex Morphology and Physical Properties. *ACS Appl. Mater. Interfaces* **2012**, *4* (12), 6957–6968. https://doi.org/10.1021/am302110c.

(41) Wheeler, P. A.; Wang, J.; Mathias, L. J. Poly(Methyl Methacrylate)/Laponite Nanocomposites: Exploring Covalent and Ionic Clay Modifications. *Chem. Mater.* **2006**, *18* (17), 3937–3945. https://doi.org/10.1021/cm0526361.

(42) Martin, S.; Bhushan, B. Transparent, Wear-Resistant, Superhydrophobic and Superoleophobic Poly(Dimethylsiloxane) (PDMS) Surfaces. *J. Colloid Interface Sci.* **2017**, *488*, 118–126. https://doi.org/10.1016/j.jcis.2016.10.094.

(43) Brown, P. S.; Bhushan, B. Mechanically Durable, Superomniphobic Coatings Prepared by Layer-by-Layer Technique for Self-Cleaning and Anti-Smudge. *J. Colloid Interface Sci.* **2015**, *456*, 210–218. https://doi.org/10.1016/j.jcis.2015.06.030.

(44) An Introduction to Anti-Static, Dissipative, and Conductive Plastics - Craftech Industries - High-Performance Plastics - (518) 828-5001. *Craftech Industries*, 2014.

(45) Chaudhury, M. K.; Whitesides, G. M. Correlation Between Surface Free Energy and Surface Constitution. *Science* **1992**, *255* (5049), 1230–1232. https://doi.org/10.1126/science.255.5049.1230.

(46) Katasho, Y.; Liang, Y.; Murata, S.; Fukunaka, Y.; Matsuoka, T.; Takahashi, S. Mechanisms for Enhanced Hydrophobicity by Atomic-Scale Roughness. *Sci. Rep.* **2015**, *5* (1), 1–12. https://doi.org/10.1038/srep13790.

(47) Wang, L.; McCarthy, T. J. Covalently Attached Liquids: Instant Omniphobic Surfaces with Unprecedented Repellency. *Angew. Chem. Int. Ed.* **2016**, *55* (1), 244–248. https://doi.org/10.1002/anie.201509385.

(48) Rabnawaz, M.; Liu, G. Rücktitelbild: Graft-Copolymer-Based Approach to Clear, Durable, and Anti-Smudge Polyurethane Coatings (Angew. Chem. 22/2015). *Angew. Chem.* **2015**, *127* (22), 6752–6752. https://doi.org/10.1002/ange.201503955.

(49) Rabnawaz, M.; Liu, G.; Hu, H. Fluorine-Free Anti-Smudge Polyurethane Coatings. *Angew. Chem. Int. Ed.* **2015**, *54* (43), 12722–12727. https://doi.org/10.1002/anie.201504892.

(50) Chen, W.; Fadeev, A. Y.; Hsieh, M. C.; Öner, D.; Youngblood, J.; McCarthy, T. J. Ultrahydrophobic and Ultralyophobic Surfaces: Some Comments and Examples. *Langmuir* **1999**, *15* (10), 3395–3399. https://doi.org/10.1021/la990074s.

(51) Miranda, D. F.; Urata, C.; Masheder, B.; Dunderdale, G. J.; Yagihashi, M.; Hozumi, A. Physically and Chemically Stable Ionic Liquid-Infused Textured Surfaces Showing Excellent Dynamic Omniphobicity. *APL Mater.* **2014**, *2* (5), 056108. https://doi.org/10.1063/1.4876636.

(52) Nine, M. J.; Cole, M. A.; Johnson, L.; Tran, D. N. H.; Losic, D. Robust Superhydrophobic Graphene-Based Composite Coatings with Self-Cleaning and Corrosion Barrier Properties. *ACS Appl. Mater. Interfaces* **2015**, *7* (51), 28482–28493. https://doi.org/10.1021/acsami.5b09611.

(53) Yan, W.; Liu, H.; Chen, T.; Sun, Q.; Zhu, W. Fast and Low-Cost Method to Fabricate Large-Area Superhydrophobic Surface on Steel Substrate with Anticorrosion and Anti-Icing Properties. *J. Vac. Sci. Technol. A* **2016**, *34* (4), 041401. https://doi.org/10.1116/1.4953031.

Chapter 5

Robust omniphobic surfaces by covalent anchored nanoobjects

Paving the way to durable coatings

Patent Application Number: EP20382700.1.

Chapter 6

Summary and conclusions

6.1 CONCLUSIONS

This thesis shows that omniphobic surfaces are promising solutions for a broad range of applications, which could be of interest to many industry sectors. The work here presented was designed with the aim of developing robust omniphobic surfaces with tailor-made properties, seeking to satisfy the industrial interest and the market needs.

This thesis introduces different approaches for the development of omniphobic surfaces focussing on surface structuring and multifunctional solutions. In particular, omniphobic aluminium surfaces with self-cleaning and anti-icing ability have been developed by surface structuring and chemical modification in **Chapter 3**, and, holistic multifunctional coatings capable of reducing surface contamination have been proposed in **Chapters 4** and **5**, giving rise to a disruptive low-adhesion technology based on omniphobic and antistatic properties, which has been patented.

The most relevant findings and conclusions from the present thesis are summarized below:

- PFPE-grafted on micro/nanostructured aluminium surfaces is an effective strategy for obtaining environmentally safe and non-noxious omniphobic surfaces, providing outstanding anti-icing and self-cleaning abilities. In particular, surface structuring positively affects omniphobicity, improving the liquid repellence compared to smooth surfaces with a similar chemistry. Additionally, the effect of surface structuring leads to a 6-fold delay on the freezing time of a water droplet compared to the smooth omniphobic surface, increasing to a 20-fold delay if compared to the pristine one. In the same way, the frost formation from condensed droplets on a structured omniphobic surface subject to low temperatures is notably delayed (85 min) in comparison with both, a smooth omniphobic surface (61 min) and a pristine one (30 min). These results highlight the potential of PFPE-grafted on structured surfaces for applications where anti-icing and self-cleaning capabilities are desired.

The findings of this study have been published in the article: "*Omniphobic Etched Aluminum Surfaces with Anti-Icing Ability". Langmuir 2020. 10.1021/acs.langmuir.0c01324*.

- Conductive laponite nanoparticles are an effective vector to provide antistatic properties, which, in combination with omniphobic perfluorinated-modified laponites, allows the fabrication of multifunctional coatings. This combination of low surface energy and antistatic leads to a holistic self-cleaning solution repelling liquids and reducing the dust attraction. All in all, a new concept, unknown in the state-of-the-art, enables obtaining surfaces suitable for preventing contamination with liquids and dust particles, which can lead to a significant number of industrial applications beyond traditional omniphobic coatings.

  This work has been published in the article: *"Laponite-Based Surfaces with Holistic Self-Cleaning Functionality by Combining Antistatics and Omniphobicity". ACS Appl. Mater. Interfaces 2017, 9 (44), 39078–39085. 10.1021/acsami.7b13535.*

- The functionalization of laponite nanoparticles with an omniphobic precursor with functional groups at the ends of the chain (PFPE S10) allows the fabrication of robust multifunctional coatings with omniphobic and antistatic properties. This double PFPE S10 functionalization enables its simultaneous anchoring to both the laponite nanoparticles and the substrate, improving the durability and mechanical resistance of the resulting coatings. The ability of these coatings to repel liquids and to reduce the adhesion of dust particles along its good adhesion to the substrates, offers a potential solution for a broad range of current and future industrial applications.

  The main outcomes of this work have been protected by the *Patent Application Number: EP20382700.1*.

Following findings were obtained from both strategies: The surface structuring and the incorporation of nanoparticles, as vectors to provide additional functionalities, highlight the advantages of combining nanotechnology with chemical grafting.

In view of the work detailed in **chapters 3**, **4** and **5**, which achievements are above summarized, it can be concluded that this thesis represents a significant contribution to the field of repellent surfaces. The published work and patented technology open the door to durable multifunctional coatings, paving the way to transfer full self-cleaning solutions from the lab to industrial applications.

Contributions

Publications

1. **Laponite-Based Surfaces with Holistic Self-Cleaning Functionality by Combining Antistatics and Omniphobicity**. (Chapter 4).
   Fenero, M.; Palenzuela, J.; Azpitarte, I.; Knez, M.; Rodríguez, J.; Tena-Zaera, R. *ACS Appl. Mater. Interfaces* **2017**, *9* (44), 39078–39085.
   https://doi.org/10.1021/acsami.7b13535.

2. **Omniphobic Etched Aluminum Surfaces with Anti-Icing Ability**. (Chapter 3).
   Fenero, M.; Knez, M.; Saric, I.; Petravic, M.; Grande, H.; Palenzuela, J.
   Langmuir **2020**, 36 (37), 10916–10922.
   https://doi.org/10.1021/acs.langmuir.0c01324.

Patents

1. **Multifunctional coating exhibiting omniphobic and antistatic properties**.
   (Chapter 5).
   Marta Fenero, Jesús Palenzuela, Ana Viñuales, Germán Cabañero, Estíbaliz Medina.
   Application number: **EP20382700.1**.
   Date: 30 July **2020**.

Congress communications

1. **Development of omniphobic aluminum surfaces**.
   Marta Fenero; Jesús Palenzuela; Mato Knez; Hans Grande; Ramón Tena-Zaera.
   Wetting on Soft or Microstructured Surfaces. 11-13 April **2019**. Wilhelm und Else Heraeus Foundation. Bad Honnef, Germany.
   Poster.

2. **Laponite-based multifunctional surfaces: repellence to solids and liquids**.
   Marta Fenero; Jesús Palenzuela; Itxasne Azpitarte; Mato Knez; Javier Rodríguez; Ramón Tena-Zaera.
   32nd International Conference on Surface Modification Technologies (SMT32). 27-29 June **2018**. San Sebastián, Spain.
   Poster.

3. **Omniphobic surfaces: overview and recent progresses**.
   Ramón Tena-Zaera; Jesús Palenzuela; Eneko Azaceta; Marta Fenero; Hans Grande.
   32nd International Conference on Surface Modification Technologies (SMT32). 27-29 June **2018**. San Sebastián, Spain.
   Keynote.

4. **Ionogel-based omniphobic surfaces**.
   Ramón Tena-Zaera; Eneko Azaceta; Jesús Palenzuela; Marta Fenero; Hans Grande.
   Superhydrophobicity and Wetting Symposium. 16-17 May **2018**. Aalto University. Helsinki, Finland.
   Oral communication.


cidetec
surface engineering
CIC
nanoGUNE
nanoscience cooperative research center